SEQUENTIAL HIGH-IMPACT, FREE-FALL LOADING AND ZOLEDRONIC ACID AS A NOVEL PRE-TREATMENT FOR DISUSE-INDUCED BONE LOSS

A Dissertation

by

RAMON DALE BOUDREAUX

Submitted to the Office of Graduate and Professional Studies of
Texas A&M University
in partial fulfillment of the requirements for the degree of

DOCTOR OF PHILOSOPHY

Chair of Committee,	Harry A. Hogan
Co-Chair of Committee,	Susan A. Bloomfield
Committee Members,	Elizabeth M. Cosgriff-Hernández
	Alvin T. Yeh
Head of Department,	Gerard A. Cote

May 2014

Major Subject: Biomedical Engineering

ABSTRACT

The purpose of our investigation was to evaluate the efficacy of prophylactic interventions consisting of simulated exercise (high-impact, free-fall loading) and/or a bisphosphonate (zoledronic acid), to counter disuse-induced bone loss of adult male rats (6 months old) subjected to 28 days of hindlimb unloading. Furthermore, we aimed to define the effects of these treatments on mechanical strength properties and bone turnover. We hypothesized that monotherapy would mitigate adverse alterations in bone mass, microarchitecture, and strength, while the combined sequential treatment would completely prevent them. Animals were assigned to one of six groups (n=12 each): baseline control (BC, euthanized on study day 0), cage control (CC), hindlimb unloading (HU), zoledronic acid treatment plus hindlimb unloading (ZA+HU), simulated exercise treatment plus hindlimb unloading (Ex+HU), and simulated exercise and zoledronic acid treatments plus hindlimb unloading (Ex+ZA+HU). Ex animals were dropped 25 times (five drops from 30 cm followed by 20 drops from 60 cm) three times per week for the first five weeks of the study. ZA (60 μg/kg body weight) was administered on day 36, immediately following Ex and just prior to HU. HU began on day 37 and persisted for four weeks.

At the distal femur metaphysis (DFM), proximal tibia metaphysis (PTM), and femoral neck (FN), HU caused declines in cancellous bone volume fraction (BV/TV, -25%) and total volumetric bone mineral density (vBMD, -4.7% and -14%), respectively, compared to CC. Mechanical strength and bone turnover were also impaired due to unloading. Individually, Ex and ZA attenuated HU-induced changes in mass,

microarchitecture, and strength, but when given sequentially, Ex+ZA fully rescued them. While HU caused an uncoupling of bone remodeling, ZA treatment successfully reduced bone degradation without affecting bone formation. Treatment with Ex followed by ZA resulted in enhanced DFM BV/TV (+20%) and trabecular thickness (Tb.Th, +5%), and PTM total vBMD (+13%). Also, FN ultimate force was highest with combination treatment. While Ex and ZA alone attenuated the deleterious effects of disuse on bone quality, when the two were administered in sequence adult male rats were fully protected against HU-induced alterations in bone mass, microarchitecture, strength, and turnover.

DEDICATION

I gratefully dedicate this work to my fiancé Jackie Perticone. Jackie and I first met as collaborators – she in the Muscle Biology Lab and I in the Bone Biomechanics/Biology Lab. She began by collecting muscle tissue for my study and ended by stealing my heart. She has been an integral part of my dissertation work, both in and out of the lab. Jackie is the love of my life and my best friend. For her, I am forever thankful.

ACKNOWLEDGEMENTS

I would like to thank my committee chairs, Dr. Harry Hogan and Dr. Susan Bloomfield, and my committee members, Dr. Elizabeth Cosgriff-Hernández and Dr. Alvin Yeh for their guidance and support throughout the course of this research. I also must acknowledge Dr. Nancy Turner for her leadership and tutelage throughout my National Space Biomedical Research Institute (NSRBI) Space Life Sciences fellowship. Through the NSBRI fellowship, I had the great fortune of working at NASA Johnson Space Center (Houston, Tx) and Beth Israel Deaconess, Harvard Medical School (Boston, MA). While at JSC, Dr. Jean Sibonga was instrumental in teaching me the ins-and-outs of the space program and guiding me in decisions I would later make in the design of this dissertation work. Dr. Mary Bouxsein at Harvard generously absorbed me into her lab where I performed many of the analyses presented here. I owe a great deal of thanks to her and her lab, most notably Rachel Ellman, Daniel Brooks, and Layma Karim. Many thanks go out to Dr. Matthew Allen (Indiana University) who kindly provided the zoledronic acid used in this study.

At Texas A&M University, I was blessed with the opportunity to work in collaborative laboratories, namely the Bone Biomechanics Lab (PI: Dr. Harry Hogan) and the Bone Biology Lab (PI: Dr. Susan Bloomfield). Because of this collaboration, I gained a more holistic understanding of bone physiology – from the micro to the macro level. Members of the Bone Biomechanics Lab, including Dr. Yasaman Shirazi-Fard and Scott Lenfest, and the Bone Biology Lab, including Dr. Brandon Macias, Corinne Metzger, Alicia Allen, Peyton McBurnett, and Katie Elmer, have all assisted in

completion of this work. I would also like to thank Sunny Narayanan for his generous assistance with animal husbandry and training.

Throughout my extensive career as a college student, my parents and sisters have shown me unending support and guidance. A huge thank you goes out to them, as none of this would have been possible without them.

I have the great fortune of listing the following funding sources: Sydney and JL Huffines Institute for Sports Medicine and Human Performance, NASA Space Physiology Research Grant from the American College of Sports Medicine Foundation, National Space Biomedical Research Institute (NSBRI) Research Grant, and NSBRI Graduate Fellowship NSBRI-RFP-05-02.

Finally, in the spirit of collaboration, the Muscle Biology Lab has been an instrumental part of my research. Graduate student Jackie Perticone, my labmate and fiancé, along with her advisor Dr. James Fluckey, have given me unwavering support throughout my graduate career.

TABLE OF CONTENTS

Page

LIST OF FIGURES

LIST OF TABLES

CHAPTER I

INTRODUCTION

Composition and Structure of Bone

Bone is a dynamic tissue comprised of various cells and an extracellular matrix. The extracellular, or organic, matrix of bone consists primarily of Type I collagen fibers (90%) and noncollagenous proteins (10%). Along with cells and water, the organic matrix makes up 35% of bone and provides strength and resilience. Minerals, consisting mainly of small needle- or plate-like crystals of hydroxyapatite, make up the remaining 65% of bone, and are fixated on collagen fibers (1). The orientation of hydroxyapatite crystals, normally parallel to collagen fibers, adds rigidity and compressive strength to bone (2). The organization of collagen fibers in mammalian bones gives rise to two main types of bone structure: woven and lamellar. Woven bone, a randomly oriented matrix of collagen fibers, is found mostly during bone development and fracture repair (2). Unlike lamellar bone, which consists of preferentially organized layers of collagen fibers, woven bone is laid down quickly and is structurally weak (3). In humans, woven bone is replaced by lamellar bone within approximately 2 and 3 years of age (1).

The human skeleton is made up of both cortical (compact) and cancellous (spongy) bone. In cortical bone, osteocytes and the extracellular matrix aggregate concentrically around Haversian canals forming cylindrical units called osteons (Figure 1). Densely packed osteons create the compact structure of cortical bone and are preferentially oriented to resist compressive forces (4). Found primarily in the walls of the diaphysis, cortical bone is a solid tissue with only microscopic pores which contain

osteocytes, canaliculi, and blood vessels (Figure 1) (3). Cortical bone makes up approximately 80% of the adult skeleton and serves in both mechanical support and organ protection (1). Cancellous bone also consists of osteocytes and an extracellular matrix but differs from cortical bone in its porosity. Rather than forming dense concentric clusters around a Haversian system (osteon), cancellous bone consists of highly porous irregular networks of plates and rods, called trabeculae (Figure 1) (4). Cancellous bone makes up approximately 20% of the adult skeleton and is located primarily in the regions of the epiphysis (Figure 1) (1). Despite its relatively high degree of porosity, cancellous bone is both strong and mechanically resistant to bending.

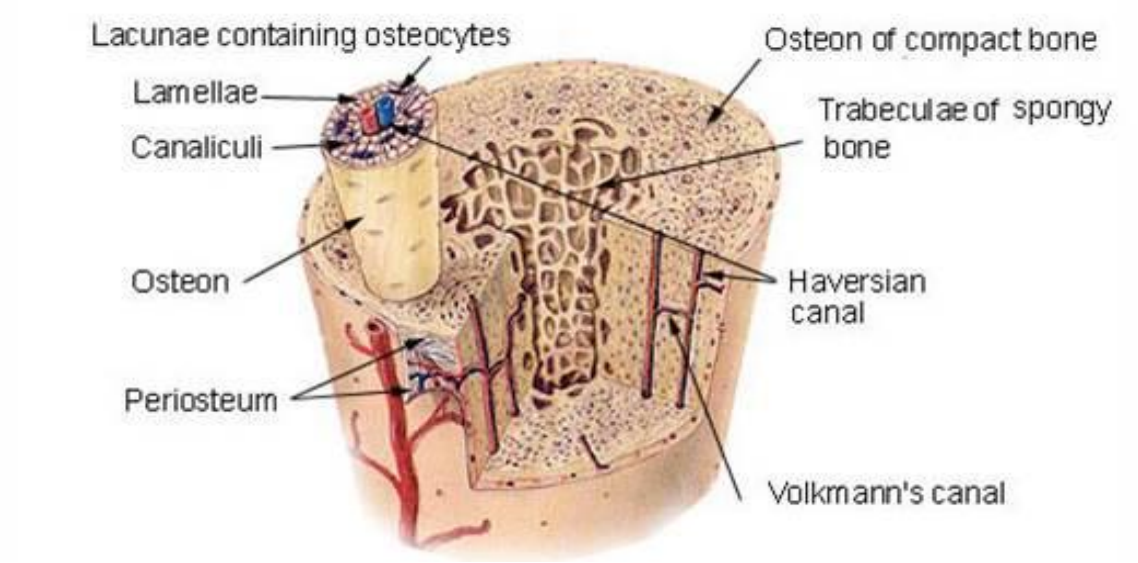

Figure 1. **Cortical and Cancellous Bone: Human Bone Structure**. Public domain image obtained from (5).

The main cellular components of bone are osteoclasts, osteoblasts, lining cells, and osteocytes (1). Osteoclasts are highly differentiated, multinucleated cells, derived from the monocyte/macrophage lineage, which are responsible for the phagocytosis of bone (3). Osteoblasts are responsible for replacing the erosion cavity that was created by the osteoclasts. All of the matrix components of bone are laid down via osteoblasts (3). When osteoblasts are inactive, they become flattened and line the surface of bone. These quiescent osteoblasts are known as lining cells (3). Much like osteocytes, which are trapped osteoblasts in newly formed osteoid, lining cells are influenced by stresses placed upon them, resulting in a release of chemicals which stimulate the activity of the bone remodeling process (1).

Since twenty-four percent of adults in America over the age of fifty will die within one year following a major bone fracture, it is important to understand the relationship between the various cells within bone and the role these cells play in the reconstruction of microcracks throughout the skeleton (6). Although the causes of said microcracks resulting in bone fractures range from decreased estrogen production in postmenopausal women to undesirable levels of mineralization in bone, the underlying problem is often the same: when the activity and balance of the major cellular components of bone remodeling are disrupted, the mechanical properties of bone are affected, ultimately resulting in increased fragility and fracture (7,8).

Bone Remodeling

The first stage of the bone remodeling process is resorption (9). During resorption, osteoclasts degrade bone, creating an erosion cavity within the structure. The

second stage, known as reversal, prepares the bone surface, via mononuclear cells, for the osteoblasts (1). The third stage, therefore, is formation (9). During formation, several osteoblasts are recruited to the erosion site and begin replacing the resorbed bone. Upon completion of the formation phase of the bone remodeling process, osteoblasts secrete the cytokines Receptor Activator of Nuclear-Factor-kappa b Ligand (RANKL) and Osteoprotegerin (OPG). RANKL binds to its receptor, RANK, expressed on the surface of osteoclasts and its precursor cells, stimulating osteoclast differentiation, activation, and bone resorption (10). OPG is a soluble decoy receptor that competitively inhibits RANKL, disallowing RANK/RANKL interaction, ultimately maintaining a healthy balance between osteoclast survival and apoptosis (11). An illustration of the OPG/RANKL secretion from osteoblasts is presented in Figure 2. Since a healthy balance of RANKL/OPG dictates the fate of osteoclasts, and since osteoclasts affect the fate of osteoblasts due to coupling, it is clear how the RANKL/OPG ratio is essential to the overall health of bone.

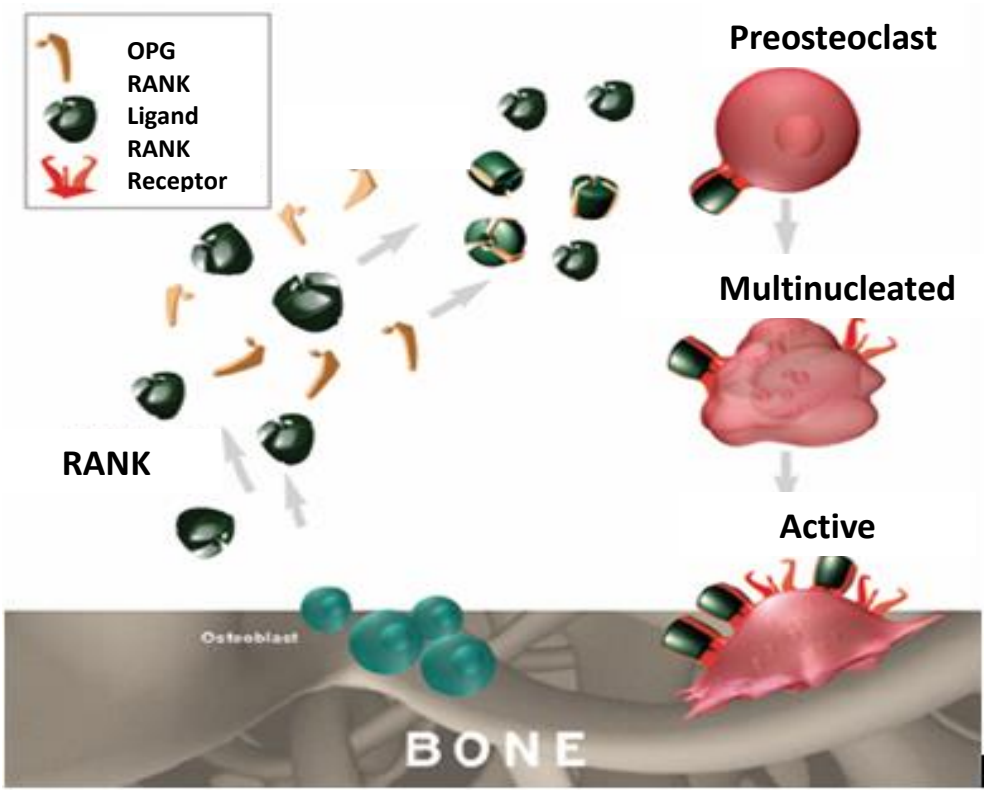

Figure 2. **OGP/RANKL Role in Remodeling.** Image obtained from (12) and used under permission of Fair Use (USC Title 17 SCC 107).

The fourth, and final stage of the bone remodeling process, is resting (1). During this stage of relatively little cellular activity, the bone lining cells await the appropriate signals to initiate another cycle of bone remodeling. Figure 3 illustrates each step of the bone remodeling process and the major cells involved. A tightly balanced relationship between the different stages of the bone remodeling process dictates the health of the bone.

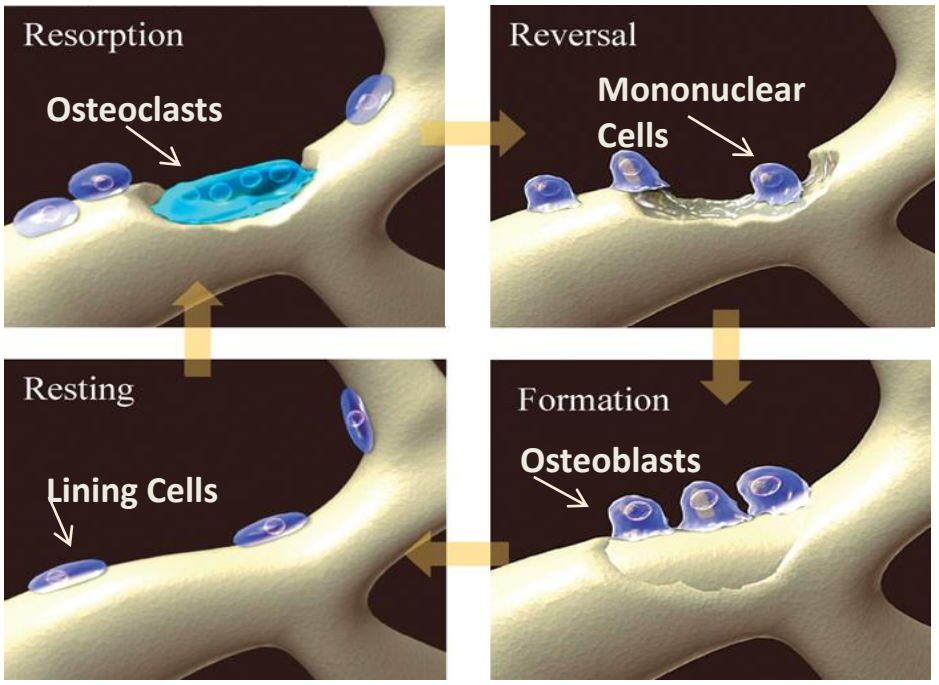

Figure 3. **Normal Bone Remodeling Process.** Reproduced with permission from (13).

In a normal adult bone remodeling process, the activity of osteoblasts and osteoclasts is equal (14). In pathological remodeling, however, an imbalance exists. In osteopetrotic bone, for example, the activity of osteoblasts outweighs that of the osteoclasts, resulting in undesirably thick bones (15). This over-activity of osteoblasts results in increased mineralization, brittleness, and fragility. Conversely, osteoporotic bone experiences an increase in bone resorption and a decrease in bone formation (16). This imbalance leads to increased porosity, decreased bone mass, strength, and resistance to fracture. Therefore, it is imperative that osteoblasts and osteoclasts contribute equally in remodeling to maintain desirable mechanical properties.

Much like the relationship that osteoblast and osteoclast activity has on bone health, the rate at which bone is replaced also plays a significant role. This rate of replacement, known as turnover, is the time it takes osteoclasts to begin resorbing the bone previously laid down by osteoblasts (Figure 4). In the initial, or primary, stage of turnover, the collagen matrix is formed (8). In time, the collagen matrix is allowed to mineralize, providing more rigidity to the bone structure. This mineralization predominates in the secondary phase of turnover. Alterations in bone turnover often result in pathological remodeling (8). In Paget's disease, for example, there exists an increase in bone turnover. As a result, the collagen matrix is not provided adequate time to mineralize, resulting in abnormally soft bones. At the opposite extreme, when bone turnover is decreased, the collagen matrix becomes over mineralized, resulting in increased brittleness. This type of hypermineralization can be found in osteopetrotic bone (14). Changes in remodeling and turnover are also the result of alterations in mechanical environment. Indeed, loads imposed on the skeleton dictate bone mass, geometry, and strength.

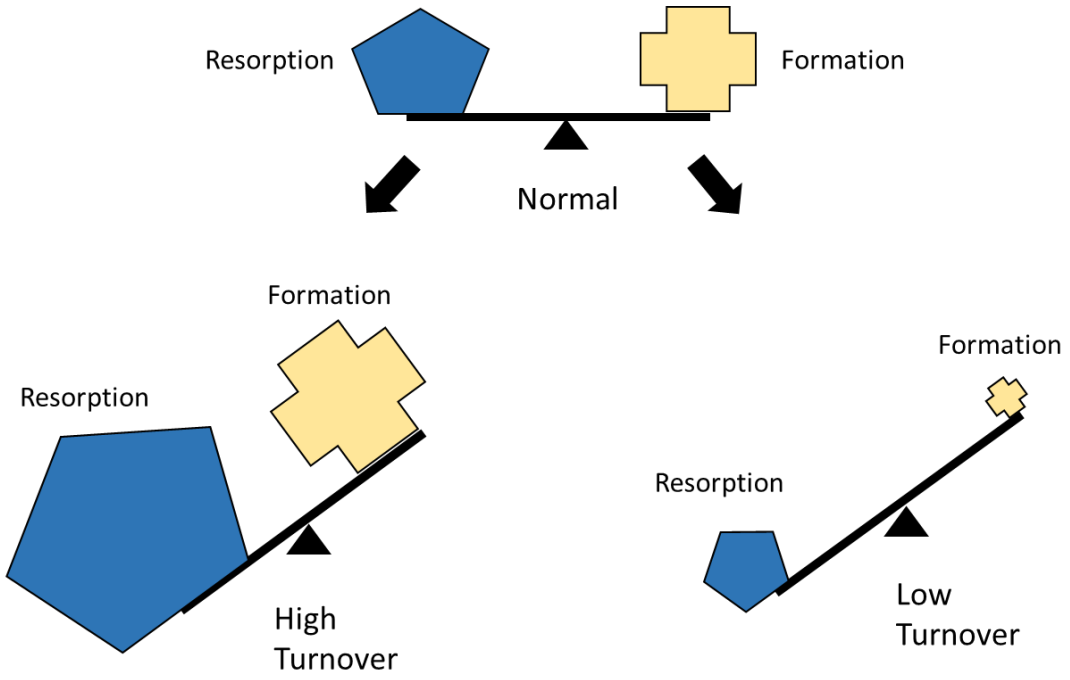

Figure 4. **Bone Turnover**. During stages of high turnover, such as what is experienced post menopause, both resorption and formation increase, with resorption outweighing that of formation. Similarly, during stages of low turnover, both resorption and formation decrease with a net positive effect of resorption.

Wolff's Law to the Mechanostat

In the nineteenth century, Julius Wolff illustrated the interplay between the form and function of bone and its internal architecture. In other words, the mechanical environment of bone dictates bone geometry and development. This novel idea was the foundation of his *Transformationsgesetz* (Transformation Law) (17). Although looked upon by anatomists and orthopaedics for hundreds of years in an effort to answer anatomical and physiological questions of bone health, Wolff's Law was limited as a functional, rather than mechanistic, law and did not translate well into the clinical

setting. Later, and still-evolving, evidence surfaced from live-animal studies conducted in Prof. Lee's laboratory at the University of Utah and helped to resolve the Law's limitations. To wit: *The driving biological mechanisms of healthy, postnatal, load-bearing bones are strongly influenced by the anatomy and physiology of the neuromuscular system* (18). The above Utah Paradigm provides a more clinically relevant proposal for the homeostasis of bone. If muscle and bone are intimately linked by common mechanisms, two questions beg to be answered: *What are the biological mechanisms of the functional muscle-bone unit?* And: *How are these mechanisms monitored and controlled?*

Mechanical stimulation on load-bearing bones causes the skeleton to deform. Osteocytes sense deformations, or changes in mechanical strain, and initiate a cascade of events responsible for determining bone strength and architecture. In 1964, Harold Frost proposed a feedback loop linking biological mechanisms and bone mass (19). At the core of the feedback loop is the mechanostat. As an analogy, consider an automatic thermostat. When temperature values land above or below a predetermined value, or setpoint, the thermostat turns ON. Otherwise, the thermostat remains OFF. The setpoints of the mechanostat are measurements of strain, and the mechanisms turned ON and OFF are modeling and disuse remodeling. When peak strain rises to a value between 1,500 and 2,500 microstrain, modeling is turned ON and cortical mass is increased. By increasing cortical mass, peak strains are consequently lowered towards a threshold range, also known as minimum effective strain (MES). Conversely, when peak strains dip below 100 to 300 microstrain, disuse remodeling is initiated. Thus,

cortical mass is lowered, returning strain values back to MES. It is worth noting that during modeling, bone mass is almost exclusively added to the periosteal surface. During disuse remodeling, however, losses occur solely endocortically, or in the marrow area. In post-menopausal women, the MES is thought to increase 30%, resulting in a mechanostat perception of 30% more bone than actuality (20). With a higher MES, modeling is repressed while disuse remodeling is de-repressed.

Musculoskeletal Disuse

Revisiting Wolff's Law, the size and strength of bone (form) depend on the mechanical environment that it senses it must withstand (function). Therefore, when mechanical loading is removed, the activity of bone resorbing osteoclasts and bone forming osteoblasts becomes uncoupled, skewing the remodeling process in favor of resorption. Data in support of this concept are manifest in spinal cord injury (SCI) patients, head down bed rest (HDBR) subjects, and astronauts. SCI can cause reductions in femoral bone mineral density (BMD) of 25% or more within the first four months of injury (21). Similar, although less dramatic, losses are evident in HDBR subjects, where 12 weeks of bed rest lead to average losses of 3.8% BMD in the proximal femur (22). Twenty-eight days of hindlimb unloading (HU) in the rat model cause reductions of 8% or greater in proximal tibia BMD that persist for up to 112 days of normal ambulation (23). Much like spaceflight, bone loss from SCI, HDBR, and HU is highly variable, site-specific, and well correlated with an increased susceptibility to fracture (24). To counter this inherent limitation to long duration spaceflight, NASA designates considerable attention and effort to in-flight countermeasures. Daily resistance exercise

on the Advanced Resistive Exercise Device (ARED) has provided the greatest protection for bone health to date (25).

Exercise and Skeletal Anabolism

Muscle contraction induced by resistance exercise is a well-documented method of improving bone health (26-30). Forces produced on the skeleton by muscle contractions impart the largest physiological loads, and consequently the highest strains, on the skeleton (31). These muscle-imparted bone strains strongly influence bone architecture and strength. Thus, muscle size and strength are directly related and highly correlated to bone size and strength. Regular physical exercise is highly recommended for both therapeutic and general health benefits. Various types of exercise, such as dynamic versus non-dynamic, will result in different outcomes. Weight-bearing activities, such as weight-lifting, running, dancing, and skiing, stimulate bone cells through muscle contractions and impact loading. Less dynamic exercises, like swimming, cycling, and Tai chi, lack direct mechanical loads, and result in increased muscle balance and strength. Although the precise amount of mechanical loading on the musculoskeletal system needed to promote growth remains unknown, it is largely accepted that a combination of resistance and aerobic, dynamic and non-dynamic activities, leads to improved muscle and bone health. Physically active children, participating in both resistance and aerobic exercise, have been shown to exhibit higher bone accrual and maximum muscle forces compared to non-exercising controls (32,33). Similar exercise programs in adults do not always result in increased bone mass but do, however, help prevent absolute losses (34).

Bisphosphonates as Anti-Catabolic Therapy

Another means of preventing, or slowing, bone loss in adults is through pharmacological interventions. Anti-resorptive bisphosphonate (BP) treatment, for example, is the first-line therapy for prevention and treatment of osteoporosis. Unlike resistance exercise, which increases bone mass and strength (anabolic), BPs slow down bone loss by decreasing the rate of resorption (anti-catabolic). Within hours of administration, oral (alendronate, risedronate, etidronate) and injectable (zoledronic acid, ibandronate, and pamidronate) BPs bind to bone mineral (calcium), preferentially in active resorbing sites (35). During bone resorption, osteoclasts ingest BPs bound to bone crystals, inhibiting their activity via a direct toxic effect and apoptosis (36). Differences in the anti-resorptive potency are dictated by the biochemical activity of the specific bisphosphonate. For example, zoledronic acid's (ZA) high kinetic binding affinity to bone mineral, coupled with its strong inhibition of the farnesyl pyrophosphate synthase enzyme, makes it currently the most potent anti-resorptive bisphosphonate available (37).

In animal studies, both low- (4 – 20 μg/kg body weight) and high-dose (100 – 500 μg/kg body weight) ZA treatment attenuated ovariectomy-induced (OVX , rodent model of postmenopausal osteoporosis) losses in total, cortical, and cancellous bone mass in the proximal tibia of adult virgin rats (38). In fact, high-dose therapy augmented the aforementioned properties beyond baseline values and this effect persisted up to 32 weeks beyond the single intravenous injection. ZA has been shown to reduce the risk of new vertebral fractures by 70% for up to three years following a single injection (39).

As a result of coupling, however, these rapid reductions in bone resorption consequently lead to reductions in bone formation, thus suppressing turnover by reducing the inception of new remodeling units. Unlike other medications, BPs remain bound to bone crystals for many years after cessation of treatment. With a half-life of up to 10 years, BPs are capable of maintaining reduced remodeling rates long after discontinuation (40).

Bone Densitometry and Morphometry

Densitometric parameters obtained from quantitative computed tomography (QCT) and micro computed tomography (μCT) allow for a three-dimensional assessment of bone architecture, structure, and geometry critical for estimating the overall health status of the skeleton. Before discussing how disuse, exercise, and bisphosphonates affect bone densitometry and geometry, it is first worth exploring the basics of QCT and μCT in order to better understand how their derived indices are used to assess bone health.

QCT assesses bone properties based on the interaction between X-ray photons and body tissue (41-43). While dual-energy X-ray absorptiometry (DXA) yields two-dimensional outcomes, such as areal BMD (aBMD), QCT is capable of producing three-dimensional and compartment-specific (cortical and cancellous) properties of bone (e.g., volumetric BMD [vBMD]). The ability of QCT to differentiate between cortical and cancellous bone is important clinically. To begin, cancellous bone is eight times more metabolically active than cortical bone. When assessing the efficacy of pharmacological countermeasures, for example, cancellous bone is likely to be affected before cortical bone. Second, cancellous and cortical bone compartments can separately predict bone

fracture (44). QCT is a measurement of radiographic absorptiometry-derived linear attenuation coefficients (LACs). LACs correspond to the amount of X-rays absorbed by tissue taken at different angles. These absorption measurements are recorded in a computer and combined by filtered back-projection. Briefly, an X-ray source is transmitted through the patient along the length of the scanner to create a thin slice of tissue ranging from a fraction of a millimeter to several millimeters in thickness. The X-ray fan then circumscribes the patient 360° corresponding to a circular matrix of two-dimensional square pixels. Because these cross-sectional pixels correspond with a slice thickness, the picture elements are volumetric in measurement. These volumetric elements, referred to as voxels, may be thought of as a three-dimensional pixel element. Altogether, as the X-ray source and detector rotate around the patient, the detector continuously measures the level of tissue absorption. Absorption measurements are then translated to LACs representative of each voxel. Since LACs vary between different QCT machines (due to different kilovoltage settings), the Hounsfield scale is used for standardization. A Hounsfield unit (HU), which is the gray-scale value of each voxel, is defined as the ratio of the difference of the LAC of a given voxel and the LAC of water to the LAC of water. HUs can be thought of as pixel brightness, and are sometimes reported in that way. HUs are then calibrated to yield values of vBMD which, when combined with structural measures, have been shown to be associated with fracture in the hip, spine, and proximal femur (45-51).

HUs are calibrated with a solid calcium hydroxyapatite phantom and dedicated software. Within the desired region of interest (ROI), linear regression analysis is used

to determine a relationship between mean HU and known concentrations of bone-like material (calcium hydroxyapatite). That is, HUs within an ROI (e.g., vertebra) are converted to a concentration (reported as mg/cm^3) of bone-like material. It is important to note that, unlike DXA areal BMD (aBMD), QCT yields a volumetric measurement of density (vBMD) and is thus independent of bone size. QCT does, however, expose the patient to a relatively larger dose of radiation compared to other diagnostic X-ray exams. An X-ray mammography, for example, imparts an effective dose of approximately 0.6 mSv to the breast (52), while doses from a QCT scan can range from 1 mSv to 6 mSv (53). Although the level of true risk associated with radiation exposure from bone imaging techniques remains largely unknown, the potential risk for carcinogenesis is thought to be very small (53).

Over the past decade, the advantages of QCT in both the clinic and in research are becoming increasingly evident. Although QCT is capable of determining three-dimensional geometric bone properties, differentiating between cortical and cancellous bone, and generating volumetric density measurements, this imaging system is still limited by voxel size and spatial resolution. In cancellous bone, for example, the size of a given voxel may be larger than the dimensions of a single trabecular strut. Consequently, the associated HU value for this voxel will include a combination of cancellous bone, collagen, and marrow. Since the surrounding constituents of the trabecular strut are averaged into the calculation of the HU value, the mass of bone per unit tissue volume may be underestimated. This volume averaging, referred to as the partial volume effect, is the primary source of error in QCT imaging. For analyses

requiring higher resolution, alternative options, such a micro computed tomography (μCT), which has a spatial resolution ranging from 1-100 μm (54), are available for use.

Since the late 1980s, μCT has been used to investigate bone morphology and microarchitecture and is now considered the "gold standard" for *ex vivo* use in small animals. With its increasing popularity for animal and human bone imaging, there is a growing need for standardization of μCT reporting. Bouxsein and colleagues provide an excellent review presenting guidelines for consistent reporting of image acquisition, image evaluation, and outcomes (55).

A standard desktop μCT device operates within a range of 20 - 100 kVp. X-rays emitted from a micro-focus X-ray tube are transmitted through the test specimen at several viewing angels, rendering an attenuation projection onto a detector capable of generating a three-dimensional distribution of mineral density. With its characteristically high resolution (voxel size as low as a few micrometers), individual mouse trabeculae, which can be as small as 30 μm in thickness, can be captured and quantified (56,57). When capturing both trabecular and cortical microarchitecture and morphometry, μCT poses several advantages compared to traditional histomorphometric techniques. First, μCT provides a larger volume of interest versus standard histology. Whereas histology may take several weeks/months to process a few tissues, μCT can produce data at multiple bone sites in a matter of minutes. Thus, μCT permits a much higher throughput than histology. Furthermore, since μCT analysis is nondestructive, subsequent testing can be performed (e.g., mechanical testing) corresponding to scan sites.

μCT is often favored over QCT because of its comparatively high resolution (small voxel size). A tradeoff exists, however, for voxel size and scan time. Smaller voxel sizes require longer scan times, exposing the tissue to higher doses of radiation. Scans lasting approximately 20 minutes (voxel size 10 μm) correspond to about 0.4 Gy of radiation incident upon the object tissue (58). Although single scans are not considered to impart damage to bone cells, longitudinal scanning has been shown to affect trabecular bone volume as much as 8 - 20% (59). When μCT analysis is used to investigate trabecular and cortical morphometry, a minimum set of parameters are considered necessary to report (55). For trabecular bone, the variables include bone volume fraction (BV/TV; %), trabecular number (Tb.N; 1/mm), thickness (Tb.Th; mm), and separation (Tb.Sp; mm). Total cross-sectional area (Tt.Ar; mm^2), cortical bone area (Ct.Ar; mm^2), cortical area fraction (Ct.Ar/Tt.Ar; %), and average cortical thickness (Ct.Th; mm) should be reported for cortical morphometry.

Three-dimensional model-independent algorithms can be used to calculate and quantitatively describe bone microarchitecture (60). This method, referred to as quantitative morphometry, was achieved in the past by two-dimensional stereologic techniques. Since the advent of μCT, however, variables such as Tb.Th and Tb.Sp take advantage of the three-dimensional capabilities of μCT. Figure 5 illustrates how trabecular thickness and separation are determined using a three-dimensional sphere fitting method. Briefly, three-dimensional spheres are fit along trabecular struts or inside marrow space to calculate measurements of Tb.Th and Tb.Sp, respectively. Other trabecular parameters, such as connectivity density (Conn.D) and structure model index

(SMI), also yield important microarchitectural results. Connectivity describes 1) number of objects, 2) number of marrow islands, and 3) number of connections that must be severed to completely cut bone into two separate parts. Since connectivity is dependent on bone size, it is normalized by the volume of the bone to obtain Conn.D. Finally, SMI is an index of trabecular bone structure indicating a perfect plate (0), a perfect rod (3), or a perfect sphere (4). Conventionally, lower values of SMI indicate a more structurally sound tissue. For cortical bone, μCT variables are often used as estimates of mechanical strength. Average cross-sectional area (Tt.Ar), for example, particularly in mid-shaft bone, is associated with elastic modulus (i.e., resistance to a bending moment). Tt.Ar is defined as the volume of interest divided by the number of slices and voxel height. Other important parameters include maximum (I_{max}), minimum (I_{min}), and polar (J) area moments of inertia.

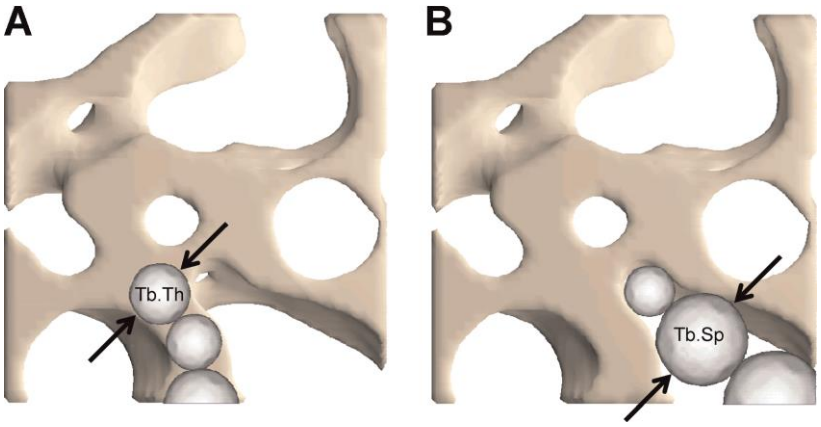

Figure 5. Method used for Calculating μCT Parameters. (A) trabecular thickness (Tb.Th) and (B) separation (Tb.Sp). This direct three-dimensional method uses sphere fitting to obtain object thickness or separation. Image obtained with permission from (55).

Numerous studies have used both QCT and μCT analyses to investigate the role of mechanical disuse on bone health, yet none have explored the sequential treatment of exercise followed by a bisphosphonate prior to unloading (61-68). Furthermore, the potent anti-resorptive effects of ZA have not been explored in the HU rat model. Twenty-eight days of HU caused a 9.7% and 7.4% loss in proximal tibia metaphysis BMC and BMD, respectively (66). Various exercise interventions have been used during and after HU to attempt the prevention of or the recovery from disuse-induced bone loss, yet recovery and prevention are often incomplete (69-80). A head-to-head comparison of jump training versus treadmill running in HU rats concluded that trabecular number and connectivity remained suppressed in rats exercised with jumping while losses in trabecular thickness were not prevented with treadmill running (72). Mechanical stimulation via whole-body vibration treatment during 28-d HU in rats attenuated, but did not prevent, BMD loss in the tibia and femur (79). Furthermore, vibration had zero effect on lumbar spine densitometry measures (79).

Although limited, exercise interventions have proven efficacious to bone health and warrant further research to optimize its anabolic effect on the skeleton. Astronauts aboard the International Space Station (ISS) currently dedicate over 2.5 hours each day to exercise. With exercise alone, however, serial densitometric measurements taken upon return to Earth reveal sustained losses in the hip and spine that may persist for up to 4.5 years (81). Thus, the combined role of exercise and bisphosphonate pharmaceuticals is now being explored on both the ISS and in research. In HU rats, concurrent treatment of a bisphosphonate (alendronate) and exercise (simulated

resistance training [SRT]) has been performed. Independently, alendronate suppressed, while SRT prevented, disuse-induced losses in total and cancellous BMD (82). When combined, however, alendronate and SRT showed no additive benefits to BMD. A similar study concluded that the combination of alendronate and SRT actually dulled the anabolic potential of the exercise intervention (83). A potential explanation for this reaction lies in the anti-resorptive action of bisphosphonates. With exercise and alendronate administered simultaneously, it is possible that the alendronate-induced suppression of bone turnover blunted the osteogenic potential of SRT. That is, with less bone being laid down and removed, exercise was less effective when combined with alendronate at increasing BMD in the proximal tibia metaphysis. Administering bisphosphonate therapy after an exercise intervention, rather than during, may work to sidestep the aforementioned blunting effect of reduced turnover on the anabolism of exercise.

Biomechanical Assessment of Bone

Mechanics may be defined as the behavior of a material when subjected to an applied load. When mechanics methods are employed to study a biological system, such as rat bone, the term biomechanics is often used. Biomechanical testing has been used extensively in research to evaluate skeletal health, to test the efficacy of therapeutic interventions, and to predict fracture risk associated with bone loss. At the core of biomechanical testing, and of which corresponding calculated indices derive, is force and displacement. The relationship between the force applied to a material and the displacement of that material is called the load-deformation curve. Load-deformation

curves provide valuable data, such as flexural rigidity, yield force, and ultimate load, but because they are based on the whole bone structure (i.e., not normalized for bone size and shape), only extrinsic properties can be determined. In order to obtain intrinsic values, such as Young's modulus, load-deformation curves must be converted to stress-strain curves. Stated differently, the rigidity (extrinsic stiffness) of bones of drastically different sizes will be much different, yet their Young's modulus (intrinsic stiffness) will be quite similar. Stress is typically defined as

$$\sigma = \frac{F}{A}, \tag{1-1}$$

where F is the applied load and A is the cross-sectional area. Strain is a change in length over the original length, written as

$$\varepsilon = \frac{\Delta L}{L}, \tag{1-2}$$

and is thus unitless. In order to use these basic, uni-axial equations, some assumptions must first be made. Namely, bone is assumed to be an isotropic, homogenous, linearly elastic material with a uniform cross-sectional area. Although bone is actually an anisotropic, non-homogeneous, viscoelastic, irregularly shaped structure, the aforementioned mathematical assumptions have been shown to be a reasonable approximation and allow for a much less complicated stress analysis (84,85). In fact, these assumptions are considered standard practice in bone biomechanical testing and are used extensively in the literature (43,66,75,86-91).

The stress-strain curve is divided by two regions: the elastic strain region and the plastic strain region. The division of these two regions occurs at a theoretic boundary called the yield point (Figure 6). In the elastic strain region, bone deformation is mostly recoverable. That is, when loading is removed, bone will generally return to its original state. In the plastic strain region, however, permanent deformation has occurred. Once the stress-strain curve enters the plastic region, crack initiation, propagation, and fracture of the bone begins to occur. Thus, the yield point, or yield stress, denotes unrecoverable deformation and damage. Under tensile and compressive loading, the slope of the elastic strain region is called the Young's modulus (E). Ultimate strength is determined as the highest stress achieved by the material during testing. This value often corresponds with the breaking strength but, in the case of bone, is commonly lower. That is, deformation continues beyond the ultimate strength but stress begins to fall just before failure. Absorbed energy, or toughness, is another parameter often used to describe the behavior of materials during mechanical testing. Toughness is defined as the area under the entire stress-strain curve, from the origin to the point of fracture, and describes the material's resistance to fracture. Brittle bone fails just after yielding because of an inherent low resistivity to fracture.

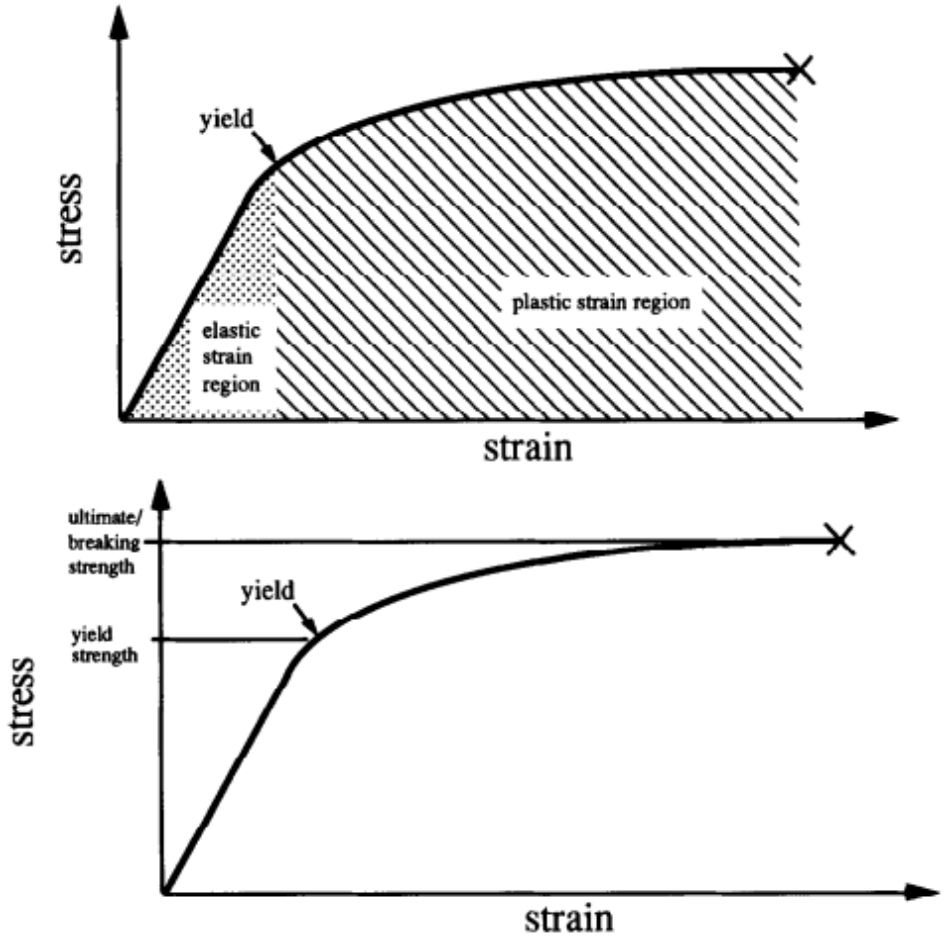

Figure 6. Stress-Strain Curve. Top: Stress-strain curve separated by elastic strain region and plastic strain region. Bottom: Stress-strain curve depicted with yield strength and ultimate/breaking strength. Image obtained with permission from (85).

Several different biomechanical testing procedures can be used to test the overall strength of bone. Basic three-point bending and microindentation testing, along with virtual finite element model (FEM) testing, will be discussed here. The three-point bending technique tests bone strength in bending. Figure 7 illustrates the general setup of a three-point bending test. The span length, *L*, must be long enough to ensure loading

results primarily in bending and not in shear. In mechanics, *L* should be 16 times larger than the thickness of the material. With rodent bones, however, this 16:1 ratio is not practical, so a span ranging from 15-20 mm is conventionally used. Based on the testing setup depicted in Figure 7, the following equations for stress, strain, and Young's modulus, respectively, are obtained:

(1-3) $$\sigma = \frac{FLc}{4I},$$

where *F* is the applied load, *L* is the span length between the bottom supports, *c* is the distance from the center of mass, and *I* is the cross-sectional moment of inertia;

(1-4) $$\varepsilon = \frac{12cd}{L^2},$$

where *d* is the resulting displacement;

(1-5) $$E = \frac{F}{d}\frac{L^3}{48I},$$

where *E* is the ratio of stress to strain in the linear elastic region. The value of *I* can be approximated by the moment of inertia equation for a hollow ellipse, but is more accurately obtained by digital imaging techniques such as QCT. Finally, the ratio *F/d* is often referred to as the extrinsic stiffness, or the slope of the linear elastic region of the force-displacement curve, and can be expressed as a single quantity, *k*.

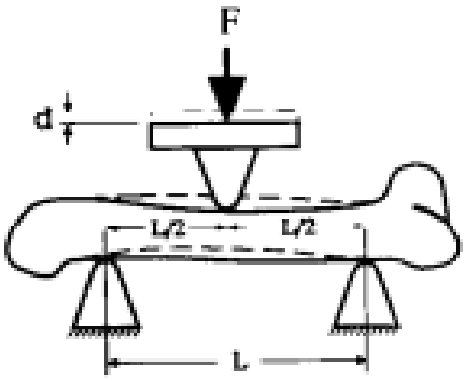

Figure 7. Three-Point Bending Applied to a Rodent Bone. *F* is the applied load. *d* is the displacement of the bone. *L* is the span length between the bottom supports. Image obtained with permission from (85).

Although three-point bending tests provide valuable information about bone strength, it is a destructive test and is thus limited to *ex vivo* use only. In order to obtain material properties from living tissue, non-destructive microindentation, or reference-point indentation (RPI), allows for serial *in vivo* biomechanical tests to be performed and has even proven suitable in the clinical setting (88). As described in Figure 8, the indentation procedure begins by inserting the probe onto the bone surface being testing. Once the periosteum is displaced by the reference probe, 20 indentation cycles are applied via the test probe. The main outcome variable of the RPI test is Indentation Distance Increase (IDI), which is equal to the absolute penetration distance measured from the first cycle to the last cycle. In theory, the less resistant bone is to indentation under loading, the more likely it is to fracture. Thus, larger IDIs correspond to higher fragility and a consequent increased risk of fracture. Although RPI is proving to be a

useful tool capable of quantifying *in vivo* bone material properties at the tissue level, it is limited by its inability to test bone as a composite. That is, RPI can test either cortical or cancellous bone separately, but not together. To non-destructively test composite bone, a computer-based mathematical technique known as finite element modeling (FEM) may be employed.

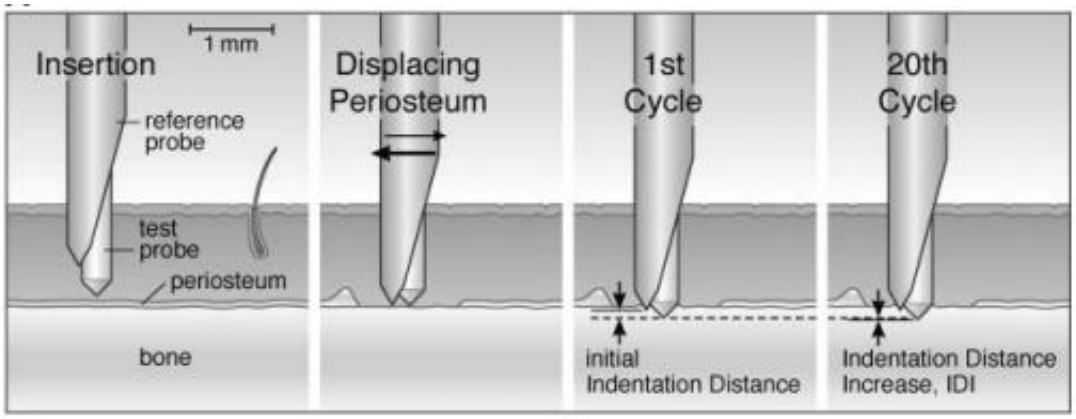

Figure 8. Procedure for Reference-Point Indentation (RPI). RPI test begins by inserting the probe assembly. After the reference probe displaces the periosteum, the test probe cycles 20 times. The major outcome variables are the Initial Indentation Distance and the Indentation Distance Increase which can be converted to parameters related to the material at the tissue level. Image reproduced with permission from (88).

FEM begins by dividing CT-derived scan data into discrete pieces, or "finite elements" (FEs), to form an FE mesh (Figure 9) (92,93). The FE mesh then undergoes three steps: 1) calculations of bone geometry by determining outer boundaries of the specimen, 2) estimates of bone material properties corresponding to each voxel, and 3) determination of failure loads and stress concentrations through simulated applied forces

(94). If 15 or more contiguous elements fail, a fracture is considered to occur. In the instance of a failure, a factor of safety (i.e., strength divided by stress) of less than one is assigned to the tissue. High correlation to measured failure loading (e.g., three-point bending mechanical testing) in both fall ($r = 0.95$) and stance ($r = 0.96$) loading conditions has been demonstrated (95). While CT-derived FEM is most prevalent in research, Keyak and colleagues have developed a clinical application whereby patient-specific FE models of the hip can be generated.

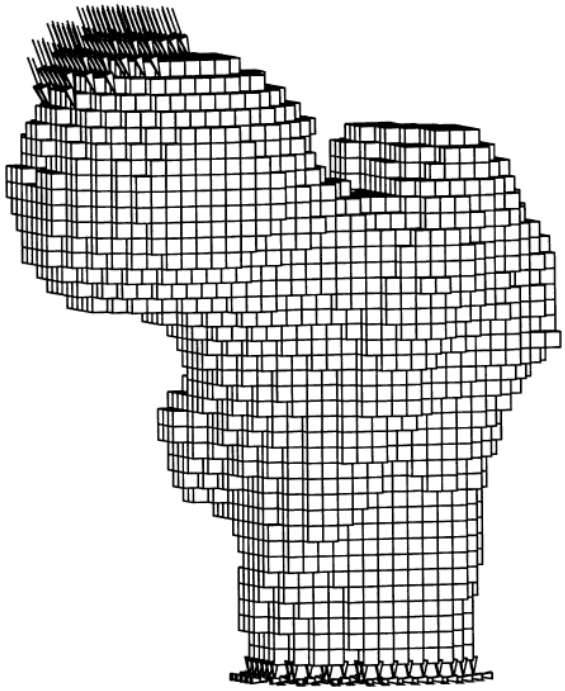

Figure 9. Three-Dimensional Representation of a Finite Element (FE) Mesh. Displacement is being applied to the femoral neck as indicated by arrows applied at the top left corner of the femoral head. Image generated by Keyak and colleagues and reproduced here with permission (96).

Bone Turnover: Relationship between Resorption and Formation

Bone turnover status is a key component in the overall assessment of bone quality. Bisphosphonate therapy, for example, decreases bone resorption because of its potent anti-catabolic effect on osteoclasts. Because of coupling, however, bone formation also declines, with an aggregate result of suppressed bone turnover. In order to determine the rate at which osteoblastic formation occurs, standard bone histomorphometric techniques may be employed. In accordance with the American Society for Bone and Mineral Research (ASBMR) Histomorphometry Nomenclature Committee, the following are the generally agreed upon nomenclature for bone histomorphometry (97).

The term "bone" may take on several meanings. Generally, bone is considered to be an individual organ, or the hard tissue, that makes up the skeletal system. Herein, bone will refer to both the mineralized and not yet mineralized (osteoid) matrix, excluding marrow and other soft tissue. The combination of marrow, soft tissue, and bone matrix (mineralized and osteoid) is referred to as "bone tissue" or "tissue volume" (TV). Other common referents in histomorphometry, along with TV, are bone surface (BS), bone volume (BV), and osteoid surface (OS). Bone volume per tissue volume (BV/TV), for example, is the ratio of cancellous bone volume to tissue volume in a desired ROI. It should be noted, however, that the term "volume" used in standard histomorphometry techniques is not a three-dimensional quantity. Bone volume (BV) is defined as the *area* of bone within a two-dimensional ROI. Along with BV/TV, other

structural indices can be determined from histomorphometry. Trabecular number (Tb.N) is the number, or density, of individual trabeculae within the ROI, and is determined by

(1-6) $$\text{Tb.N} = \frac{\frac{\text{BV}}{\text{TV}}}{\text{Tb.Th}},$$

where Tb.Th represents trabecular thickness, calculated as

(1-7) $$\text{Tb.Th} = \frac{2}{\frac{\text{BS}}{\text{BV}}}.$$

Trabecular separation (Tb.Sp) refers to the distance between edges of individual trabeculae, and is expressed as

(1-8) $$\text{Tb.Sp} = (\text{Tb.N})^{-1} - \text{Tb.Th}.$$

In subjects given label administration, kinetic indices can also be determined.

Dynamic bone histomorphometry yields valuable data from undecalcified sections of bone viewed under fluorescent microscopy. Quickly after tetracycline antibiotics are administered, they become deposited onto sites of active bone formation. Sequential tetracycline injections, separated by a predetermined period of time, permits the measure of mineral apposition rate (MAR). MAR is the linear distance between the midpoints of two labels divided by the time between administration of the labels. Based on data from labeled surface (mineralized surface [MS]), total bone surface (BS), and MAR, bone formation rate (BFR) is computed as

(1-9) $$\text{BFR} = \text{MAR} \times \frac{\text{MS}}{\text{BS}}.$$

BFR is a common parameter used to assess the status of bone formation following anabolic therapy. Eight weeks of treadmill running in rats, for example, caused an increase in BFR of over 30% compared to sedentary control animals (98).

While histomorphometry provides valuable insight for the status of bone formation, bone resorption rate cannot be measured directly from this technique. In order to assess bone resorption, biochemical markers, such as C-terminal cross-linking telopeptides of type I collagen (S-CTX), urinary free deoxypyridinoline (U-DPD), and serum tartrate resistant acid phosphatase (TRAcP) isoform 5b (TRAcP 5b) are often used. Specifically, TRAcP 5b is gaining popularity as an indicator of osteoclast number and has shown to be a predictor of bone fracture in elderly women (99).

TRAcP is an enzyme expressed in inflammatory macrophages, dendritic cells, and osteoclasts. TRAcP has two different isoforms within the blood: 5a, which is derived from macrophages and dendritic cells, and 5b, which is from actively resorbing osteoclasts (100). TRAcP 5b functions as a regulator for the attachment of osteoclasts to bone matrix (101). Transgenic mice exhibiting an overexpression of TRAcP 5b show rapid increases in bone resorption, decreases in cancellous bone, and the onset of a mild osteoporosis (102). Using commercially available immunoassays for serum TRAcP 5b (e.g., BoneTRAP® and MetraTRACP5b®), serum concentrations of TRAcP 5b can be readily assessed in both the lab and the clinic.

Separately, the effect of exercise, bisphosphonate therapy, and unloading on bone turnover has been extensively researched (69,74-76,78,83,86,103-109), yet the combination of exercise and bisphosphonate treatment administered prior to a period of

unloading has not been explored. Furthermore, ZA, which is the most potent suppressor of bone resorption currently available, has not been tested prior to HU in rats. Fourteen days of HU in growing rats caused a 48% decline in periosteal MAR and a 35% increase in urinary bone resorption markers versus control animals (110). Although treatment with a bisphosphonate (pamidronate) was able to reduce bone resorption, since it was unable to prevent declines in formation, losses in cortical mass and strength were not prevented. A similar study conducted in mice revealed that two weeks of HU caused a 45% reduction in total BFR (111). Adding ZA further suppressed total BRF by 42%. Although bisphosphonates act solely on osteoclasts, this reduction in osteoblast activity may be explained by bone coupling. Since osteoclasts and osteoblasts operate in unison, the suppression of one can potentiate the inhibition of the other.

In order to combat declines in bone formation that occur with disuse, exercise interventions are often employed during a period of unloading. Dynamic muscle stimulation in HU rats was evaluated to determine whether disuse osteoporosis could be prevented by daily induced muscle contractions (74). Although losses in cancellous bone were mitigated, daily muscle stimulation did not prevent declines in bone formation. Since exercise and bisphosphonate treatments administered separately yield often incomplete recovery and/or prevention of disuse bone loss, the combination treatment of exercise (SRT) and a bisphosphonate (alendronate) has been explored (82,83). Separately, SRT caused an increase in BFR, while alendronate caused a decrease in serum TRAcP 5b. TRAcP 5b was not further reduced nor was BFR further increased, however, when SRT was used in combination with alendronate. In fact, the

data suggest that alendronate therapy actually impaired the osteogenic response from SRT. It should be noted, however, that SRT and alendronate were administered simultaneously. That is, exercise was performed during a suppressed state of bone turnover. Because turnover was reduced, the skeletal anabolism of exercise may have been blunted. Future research is needed to elucidate the combined role of exercise and bisphosphonates administered sequentially, rather than simultaneously, so exercise is performed prior to a decreased state of turnover.

Combining Simulated Exercise with Zoledronic Acid: Better Together?

Because they have two distinct mechanisms of action, the anabolic potential of exercise, along with the anti-catabolic effect of BPs, may perhaps work in combination when administered together during or prior to a period of mechanical disuse. Although previous studies have aimed to illuminate the additive potential of exercise and BPs on bone health (82,83,112-114), the combined effect of exercise and BP interventions prior to HU in rats has not been investigated. Furthermore, no studies to the author's knowledge have explored the potent anti-resorptive effect of ZA, alone or in combination with exercise, in the HU rat model. A review of the literature reveals an equivocal understanding of the combined effect of exercise and BP treatment. Fuchs et al. demonstrated additive interactions between exercise (treadmill running) and alendronate administration on bone densitometric and strength properties in OVX rats (113). Similarly, BP treatment (risedronate, alendronate, or zoledronate) did not inhibit bone growth in OVX mice when mechanically loaded (112). Compared to BP alone,

bone formation rate was enhanced when BP and loading were used in combination (Figure 10).

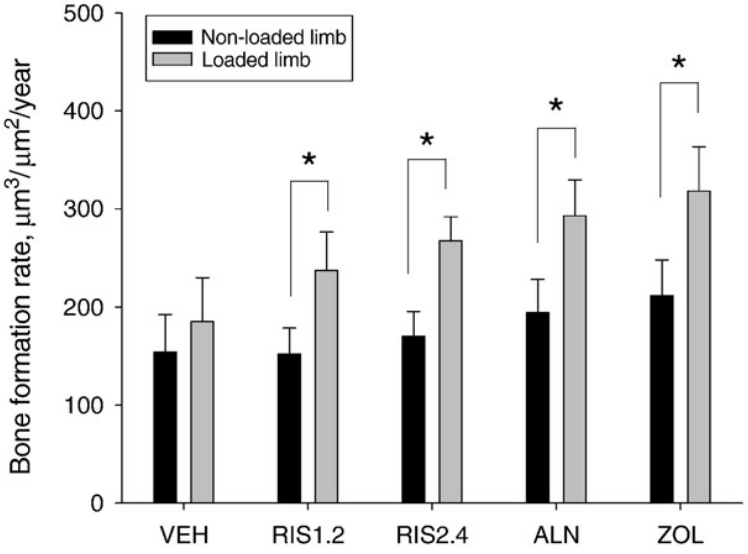

Figure 10. **Periosteal Bone Formation Rate (BFR).** BFR affected by BP Treatment and Loading after OVX. Among groups, no significant differences exist for non-loaded BFR. For all BP groups, loading significantly increased BFR compared to non-loading ($p<0.05$). VEH = placebo treated; RIS1,2 and RIS2,4 = risedronate groups; ALN = alendronate groups; ZOL = zoledronate groups. Image obtained with permission from (112).

Lung transplant recipients (LTR), a population highly susceptible to rapid bone loss and heightened fracture risk (via prolonged glucocorticoid therapy), experienced additive benefits of resistance exercise and BP (alendronate) therapy (Figure 11) (115). As Figure 11 reveals, untreated LTR suffered a decline in BMD (-12.5%) at the lumbar vertebra two months post-transplant. Although BP treatment alone was able to maintain

BMD levels (+1.4%), the combination of BP with once-weekly resistance exercise was osteogenic (+10.3%).

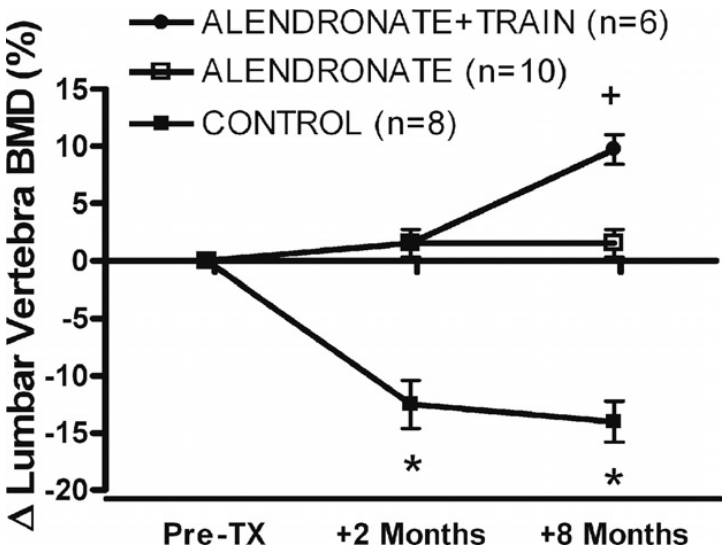

Figure 11. **Change in Lumbar Vertebral BMD.** Data assessed in lung transplant patients**.** BP treatment began seven days after transplantation and prevented BMD losses. Resistance exercise began, with and without BP, at two months post-transplant and ceased at eight months. Combined treatment led to an anabolic response. *indicates significant differences ($p \leq 0.05$) versus pre-transplantation (Pre-TX); +indicates significant differences ($p \leq 0.05$) versus alendronate and control. Image obtained with permission from (115).

Recent data from the International Space Station reveal a promising effect of BPs taken before and during in-flight missions (116). Compared to controls, declines in BMD at the proximal femur and lumbar spine are drastically reduced with BP treatment. Although the data are encouraging, confounding factors in the control groups (i.e., use of the interim Resistive Exercise Device (iRED) in the controls versus the Advanced

Resistive Exercise Device (ARED) in the BP group) exist and make interpretation of these results challenging. Thus, the combined role of BP and exercise remains unclear.

Ground-based animal studies of disuse in HU rodents treated with a BP (alendronate) and exercise (SRT) have been performed in our laboratory. Swift et al. demonstrated a marked increase in bone architectural properties and bone formation rate when SRT, alone or in combination with BP, was administered during HU (Figure 12) (82). This study found that BP treatment, however, blunted the osteogenic effects of SRT. That is, SRT treatment alone yielded higher gains in cancellous bone formation versus SRT combined with BP, although both groups exhibited significant gains in BFR relative to weight bearing controls. Macias et al. found a similar hindrance of bone formation with the SRT and BP combination on periosteal bone surfaces (83).

It is noteworthy to mention, however, that the impact of these treatments on bone resorption remains largely unknown. Since the SRT and BP therapies were introduced after HU was initiated, it can likely be assumed that bone remodeling was uncoupled with HU (before the initiation of treatment). Thus, even though bone formation was greatest in the HU+SRT group, HU+SRT/ALEN may have produced a more favorable balance of osteoclast and osteoblast activity.

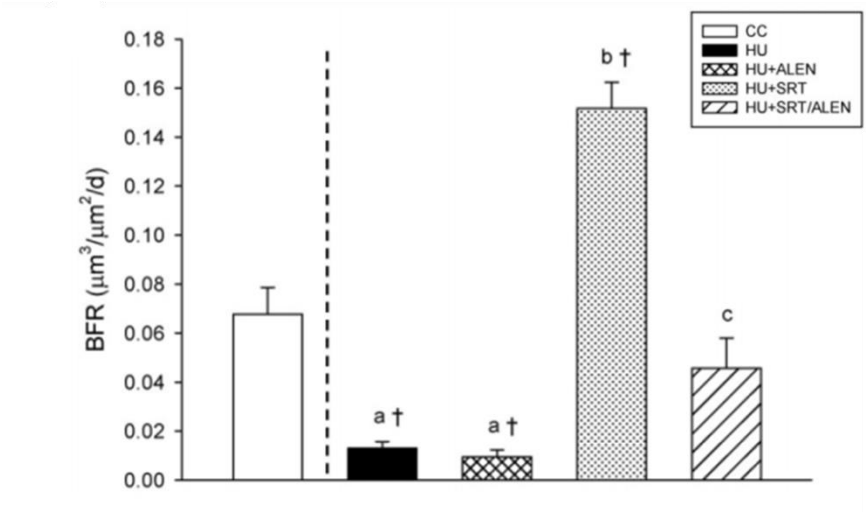

Figure 12. **Cancellous Bone Formation Rate.** BFR assessed with or without alendronate (ALEN) treatment and/or simulated resistance training (SRT) taken at the proximal tibia metaphysis. Groups not sharing the same letter are significantly different ($p<0.05$). †indicates significant difference versus CC ($P<0.05$). Image obtained with permission from (82).

The current study was conceived and developed to seek a better understanding of the interactions between simulated exercise, BPs, and disuse. By administering high-impact, free-fall simulated exercise first, we forecasted that bone formation would be enhanced without interference from ZA. That is, because BPs reduce turnover, they have the potential to reduce the anabolism of exercise. Thus, by incorporating simulated exercise prior to ZA treatment, our first hypothesis was that Ex would increase bone formation and mitigate disuse-induced alterations in bone mass, density, microarchitecture, and strength in the hindlimbs of adult rats subjected to 28 days of musculoskeletal disuse. Similarly, we hypothesized that ZA monotherapy (ZA+HU), because of its potent reduction of bone resorption, would lower bone resorption and

mitigate the aforementioned losses resulting from HU. Our final hypothesis was that the sequential, combination treatment (Ex+ZA+HU) would completely prevent alterations in bone mass, density, microarchitecture, and strength in the hindlimbs of adult rats subjected to 28 days of musculoskeletal disuse.

CHAPTER II

MATERIALS AND METHODS

Animals and Experimental Design

Adult male Sprague-Dawley rats were obtained from Harlan Laboratories (Houston, TX) at 5.5 months of age and singly housed in a temperature-controlled (23 ± 2 ºC) room with a 12-hour light-dark cycle (9PM-9AM) in an AAALAC-accredited animal care facility. Animals were provided standard rodent chow (Harlan Teklad 8640) and water ad-libitum. Animal care and all experimental procedures described in this study were conducted in accordance with the Texas A&M University Institutional Animal Care and Use Committee rules and approvals.

After 14 days of acclimation, animals were block assigned to groups normalized by body weight (Figure 13). Animals (n=72) were assigned to one of six categories (n=12 each): baseline control (BC, euthanized on study day 0), cage control (CC), hindlimb unloading (HU), zoledronic acid treatment plus hindlimb unloading (ZA+HU), free-fall simulated exercise treatment plus hindlimb unloading (Ex+HU), and free-fall simulated exercise and zoledronic acid treatments plus hindlimb unloading (Ex+ZA+HU).

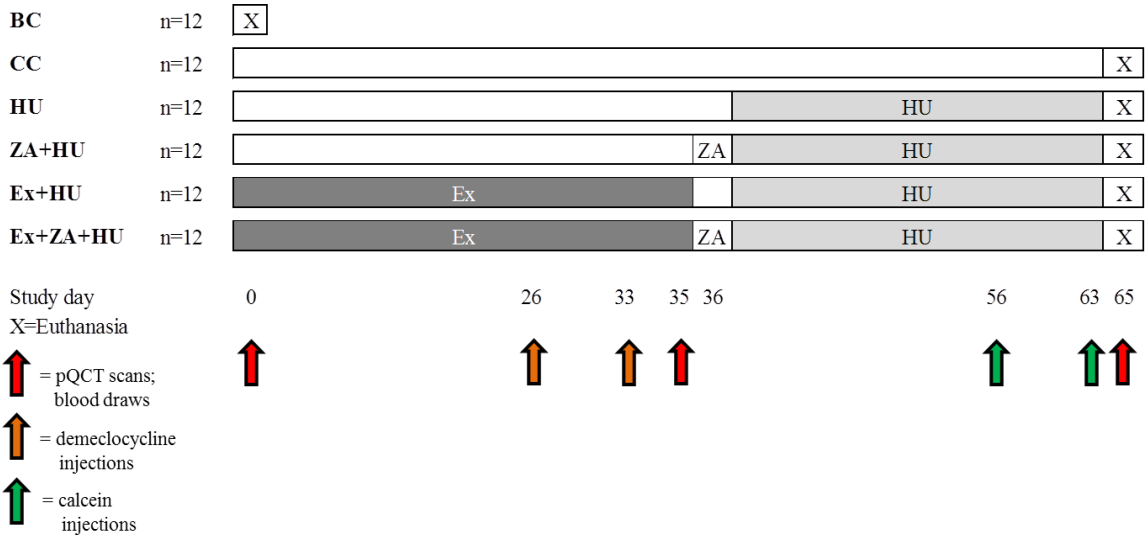

Figure 13. Experimental Design. X = Termination; Ex = high-impact, free-fall simulated exercise; ZA = zoledronic acid treatment; HU = hindlimb unloading

High-Impact, Free-Fall Simulated Exercise (Ex)

Rats performed high-impact, free-fall simulated exercise through a custom-designed drop training protocol. Animals in groups Ex+HU and Ex+ZA+HU were dropped 25 times (five drops from 30 cm followed by 20 drops from 60 cm) thrice weekly (sessions separated by at least 48 hours) for five weeks. Using the basic four-finger scruff hold, Ex animals were dropped, given an 11 sec rest (shown to be an optimal rest period for rat bone growth) (117,118), then picked up and dropped again until all drops were completed. During the rest period, the rats were held in the trainer's arms and lightly petted. After 25 completed drops, which took approximately 5 minutes, rats were put back in their cages to resume normal cage activity for the next 48 hrs. The health of the animals was assessed by project personnel and by the Comparative

Medicine Program (CMP) staff 2-3 times each day. We were looking for: 1) normal cage activity, 2) normal ad-libitum, 3) normal gait, and 4) any signs of general distress, limping, or swelling. If a rat appeared injured based on the aforementioned criteria, they did not perform the following session of jumps. If the rat in question did not improve past the first skipped session, it was removed from the study. We chose high-impact, free-fall simulated exercise based on previous findings which found this type of loading to be osteogenic in rats (117-119). Results from Welch et al. concluded that free-fall impact from heights of 30 and 60 cm generated significant gains in CSA and BMD in both the ends and the shafts of forelimb bones, yet they showed only marginal gains in the hindlimbs (118). According to peak vertical impact force production, the forefeet received over twofold higher loads than the hind feet, likely explaining the ineffectiveness of this type of training at the tibia and femur. To account for this, we adapted our impact training by dropping the rats hind feet first, thus producing greater force production in the tibia and femur relative to the forefeet. Peak ground reaction forces (GRF) experienced in the forelimbs and hindlimbs during Ex in a subset of animals were determined using a force plate (MatScan Evolution, Model 3150, Tekscan, Inc., South Boston, MA) and graphed using MatScan Analysis Software.

Zoledronic Acid (ZA) Treatment

A single 60 μg/kg body weight subcutaneous injection of zoledronic acid [2-(imidazol-1-yl)-hydroxy-ethylidene-1,1-bisphosphonic acid, disodium salt, 4.75 hydrate] was administered to ZA+HU and Ex+ZA+HU groups on day 36 (one day before HU). On a mg/kg basis, our dose of 60 μg/kg body weight equates to a 4 mg dose

administered to a 67 kg human. ZA was kindly donated by Dr. Matthew Allen of Indiana University School of Medicine.

Hindlimb Unloading (HU)

HU was achieved by tail suspension as described previously (120-122). Briefly, while under anesthesia, animal tail was first cleaned then allowed to dry thoroughly. A thin layer of adhesive (Amazing Goop, Eclectic Products, Los Angeles, CA, USA) was then applied to the medial and lateral sides of the tail to secure the custom-made harness. A paperclip was used to attach the harness to a swivel that spans atop the suspension cage (18x18x18 in). Suspension height was set to achieve a 30º head-down tilt. HU animals permitted normal ambulation of the forelimbs, voluntary feeding, and ad-libitum drinking water. Animal health was assessed thrice daily throughout the HU period.

Euthanasia and Tissue Harvest

At each study endpoint (day 0 and day 65), animals were euthanized using a Ketamine/DexaDomitor (3:2) cocktail and killed by decapitation. In HU groups, animals were anesthetized prior to removal from suspension to prevent load bearing on the hindlimbs prior to termination. At necropsy, soleus muscles were excised and wet masses were recorded. Left femora, tibiae, humeri, and right proximal femora and spine were excised, cleaned of soft tissue, wrapped in gauze, soaked in phosphate buffered saline (PBS), and stored at -20 ºC. After excision and extraction of soft tissue, right distal femora and proximal tibiae were fixed with 10% formalin for 24 hours then stored in 70% EtOH at 4 ºC. Right distal tibiae and humeri were excised, cleaned of soft tissue, and stored in 70% EtOH at 4 ºC. Left tibiae were used for 3-piont bending, left femora

for μCT, FEA, and BioDent, right distal tibiae for cortical histomorphometry, and left proximal femora for *ex vivo* pQCT and mechanical testing. The remaining tissues remain stored for future use.

In Vivo Peripheral Quantitative Computed Tomography (pQCT)

At baseline, day 35, and day 65, serial *in vivo* pQCT scans were taken at the proximal tibia metaphysis (PTM, four slices distal to the growth plate) and the tibia diaphysis (TD, two slices at 50% of bone length, 1 mm apart) using a Stratec XCT Research-M device (Norland Corp., Fort Atkinson, WI), using a voxel size of 100 μm and a scanning bean thickness of 500 μm. Daily calibration of the machine was performed with a hydroxyapatite standard cone phantom. Stratec software (version 6.00, Norland Corp., For Atkinson, WI) was used to analyze scan slices at the PTM (contour mode 3, peel mode 4, outer threshold 0.450 g/cm^3, inner threshold 0.800 g/cm^3, and Cortmode 4, outer threshold 0.450 g/cm^3, and inner threshold -0.100 g/cm^3) and at the TD (contour mode 1, peel mode 2, outer and inner threshold 0.650 g/cm^3, and Cortmode 2, outer threshold 0.650 g/cm^3).

Cortical, cancellous, and total volumetric bone mineral density (vBMD), bone mineral content (BMC), bone cross-sectional areas (total, cortical, and marrow), and cortical thickness were averaged across slices at the PTM to yield a mean result. Similarly, values at the TD derived from the average of the two slices taken at that site. Cross-sectional moment of inertia (CSMI) values taken at the TD correspond to the neutral bending axis during three-point bend testing and are used in the calculation of mid-diaphysis material properties. Using pQCT data, calculated strength indices were

derived. Compressive strength index (CSI) and bending strength index (BSI) were determined by an approach similar to Lang et al. (49):

(2-1) $$CSI = vBMD^2 \times CSA_{min},$$

(2-2) $$BSI = \frac{I_X + I_Y}{W},$$

where *vBMD* is total volumetric BMD, CSA_{min} is the minimum cross-sectional area of the total cross-section, I_X and I_Y are geometry-based moment of inertias, and *W* is the diameter of the equivalent circular cross-section, defined as

(2-3) $$W = 2 \times \sqrt{\frac{CSA_{min}}{\pi}}.$$

From manufacturer's data, machine precision is ±9 mg/cm^3 for cortical vBMD and ±3 mg/cm^3 for cancellous vBMD. *In vivo* coefficients of variation determined from repeat scans on six adult male rats are ±0.6% (total vBMD), ±1.6% (total BMC), ±1.9% (total area), and ±2.13% (cancellous vBMD).

Ex Vivo Peripheral Quantitative Computed Tomography (pQCT)

Following euthanasia (day 65), femoral necks were scanned using a Stratec XCT Research-M device (Norland Corp, Fort Atkinson, WI) and a custom-made femoral neck mold (used to align femoral neck with CT scan lines) as previously described (123). Scan speed was set at 2.5 mm/sec with a voxel resolution of 0.07 X 0.07 X 0.5 mm. Three adjacent scan lines were generated using a scout view scan and placed just below the femoral head. Stratec software (version 6.00) was used to analyze scan slices (contour mode 3, peel mode 2, outer threshold 0.700 g/cm^3, inner threshold 1.200

g/cm^3). Values for total bone mineral content (BMC, mg/mm), total, trabecular, and cortical vBMD (mg/cm^3), Ct.Th, and CSMI were averaged across all slices scanned to get a mean value.

Ex Vivo Micro-Computed Tomography (μCT)

Microarchitecture and morphology of femoral cancellous and cortical bone were obtained using high-resolution μCT scans (microCT40 Scanco Medical AG, Bruettisellen, Switzerland) with an isotropic resolution of 16 μm (70 kV, 114 μA, 300 ms integration time). All analyses were performed in accordance with previously published guidelines (55). Scans were analyzed at the distal femur metaphysis and mid-shaft diaphysis. Metaphysis scans began 1.3 mm proximal to the peak of the growth plate and extended 5 mm proximally. Scans of the diaphysis began at 55% of the bone length and extended 1.6 mm distally. Gaussian filtration parameters were $\sigma = 1$, support = 2 for both metaphysis and diaphysis. A semi-automated contouring method was used to define the cancellous bone region. Bone volume fraction (BV/TV, %), trabecular thickness (Tb.Th, mm), trabecular number (Tb.N, mm^{-1}), trabecular separation (Tb.Sp, mm), connectivity density (Conn.D, 1/mm^3), and structure model index (SMI) were assessed for cancellous bone in the metaphysis. Diaphyseal cortical bone parameters include cortical thickness (Ct.Th, mm), total cross-sectional area (Tt.Ar, mm^2), cortical bone area (Ct.Ar, mm^2), bone area fraction (Ct.BA/TA, %), and polar moment of inertia (J, mm^4). Cancellous and cortical bone were segmented from soft tissue using a global threshold of 386 mg HA/cm^3 and 696 mg HA/cm^3, respectively.

Three-Point Bend Mechanical Testing

Mechanical properties from left tibia mid-shaft were evaluated using three-point bending load-to-failure testing. Mid-shaft tibiae sites corresponded to pQCT sampling sites (50% of total bone length). Just before testing, bones were brought to room temperature, hydrated with PBS, and measured (total length, half-length, anterioposterior (AP) and mediolateral (ML) surface diameters) using Absolute Digamatic calipers, (Mitutoyo Corp., Japan). For testing, whole tibiae were placed lateral side down on custom-built metal pin (D=3 mm) supports (L=18 mm). A quasi-static load, using a 1,000 lb load cell (calibrated to 100 lb maximum load), was applied at a rate of 2.54 mm/min to the medial side of the bone until fracture. Raw data was collected at 10 Hz as load versus displacements curves and analyzed using Bluehill software (version 2.14.582, Instron Bluehill) and a custom-written Matlab (version 7.12.0, The MathWorks, Inc.) program. Material properties were calculated as previously mentioned in this chapter. Briefly, structural properties were normalized to bone geometry at the mid-diaphysis tibia using pQCT derived cross-sectional moment of inertia (CSMI), extrinsic stiffness (k, slope of the linear portion of load-displacement curve), and support span distance (L= 18 mm) to obtain ultimate stress (Equation 1-3) and elastic modulus (Equation 1-5).

Femoral Neck Mechanical Testing

Mechanical properties of the femoral neck were assessed via axial loading testing equipment (Instron 3345, Norwood, MA). Right proximal femora were settled vertically into a fitted hole in a custom-made aluminum plate fixture (½-inch think) prior to

testing. Using a 10-mm cylindrical platen, a quasi-static load was applied to the femoral head parallel to the axis of the shaft of the femur. A displacement of the platen was maintained at 2.54 mm/min until fracture occurred. Ultimate force was recorded and absorbed energy was obtained in MatLab similar to the aforementioned left tibia mid-shaft.

Reference Point Indentation

Mechanical properties of the anterior diaphysis femur were analyzed using a cyclic microindentation instrument (BioDent 1000™ Reference Point Indentation, Active Life Scientific, Inc., Santa Barbara, CA) and BP2 probes. A detailed description of BioDent microindentation mechanical testing can be found at (124). Briefly, each microindentation consisted of an applied force of 9 N, cycled 10 times with a frequency of 2 Hz. Up to four indentation measurements per bone were taken 1.5-2 mm apart in the femur diaphysis beginning at a location 75% of the total bone length (approximately 10 mm proximal to the edge of the condyles). Primary outcome variables are shown in Figure 14 and described further by Diez-Perez et al.(88).

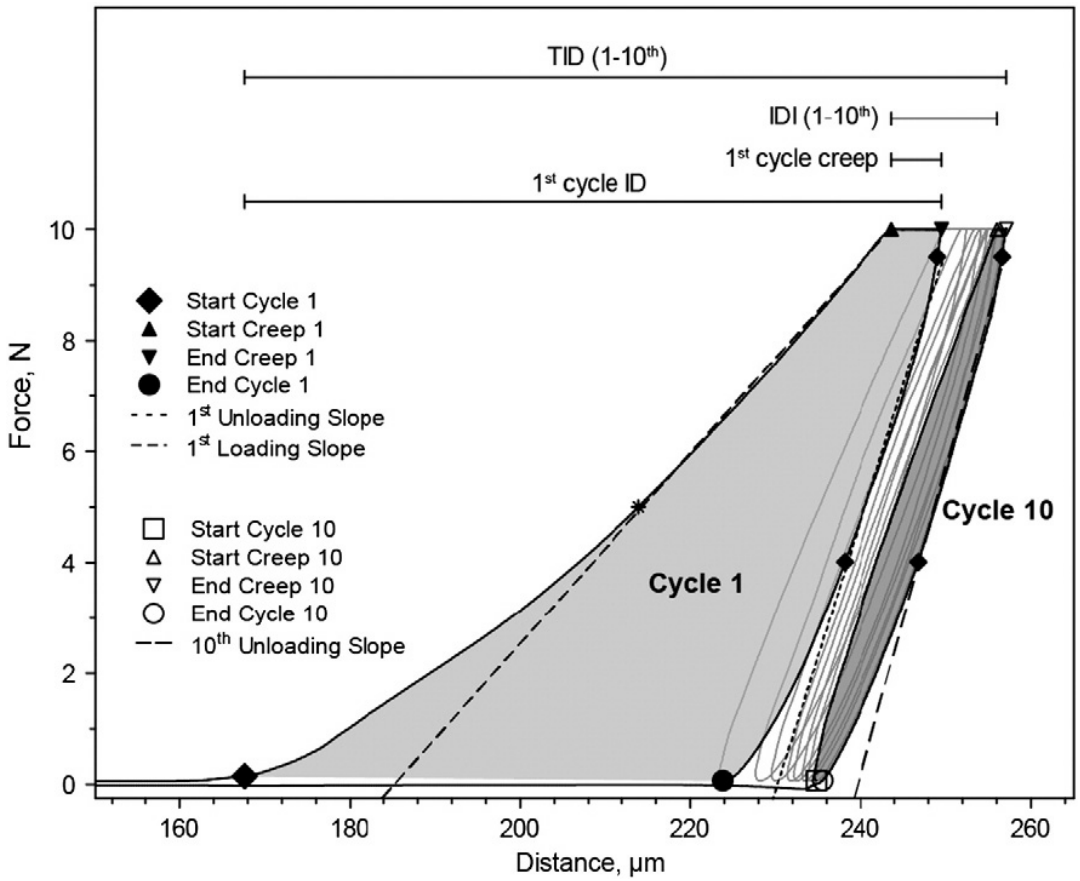

Figure 14. Microindentation Curve. Graph obtained with permission from (125).

Finite Element Analysis

Linear elastic micro-finite element analysis (µFEA) was performed on the distal femur metaphysis to evaluate mechanical properties using manufacturer's software (Scanco Medical AG, Bassersdorf, Switzerland). In order to create the µFEA model, all µCT-derived bone voxels were converted to approximately eight million equally sized brick elements. Both cortical and cancellous bone were assigned an elastic modulus of 10 GPa and Poisson's ratio of 0.3. A high-friction compression test in the z-direction

was then applied, effectively displacing all nodes located on the z_{min} face while holding all nodes in the z_{max} face fixed. Outcome measurements included axial stiffness (N/mm) and percent load carried by the cortex.

Dynamic Histomorphometry

Intraperitoneal fluorochrome injections of demeclocycline (15 mg/kg body weight, Sigma Chemical, St. Louis, MO) and calcein (25 mg/kg body weight, Sigma Chemical, St. Louis, MO) were administered to capture two separate windows of bone formation. First, at nine and two day days before HU, injections of demeclocycline were administered to produce an orange fluorochrome label. Later, at nine and two days prior to termination, calcein was injected to achieve a green fluorochrome label. After termination, undemineralized excised distal right tibia were dehydrated and embedded in methyl-methacrylate (Sigma-Aldrich M5, 590-9, St. Louis, MO). After trimming down the methyl-methacrylate blocks, serial cross sections (150-200 μm thick) were cut using a diamond wafer low-speed saw (Buehler, Lake Bluff, IL) approximately 1 mm from the tibia-fibular junction. OsteoMeasure Analysis Software, version 1.3 (OsteoMetrics, Atlanta, GA) was used to analyze each specimen and determine mineralizing surface/bone surface (MS/BS), mineral apposition rate (MAR), and bone formation rate (BFR = MS/BS · MAR). Histomorphometric analyses follow the standardizations as defined previously (126).

Tartrate-Resistant Acid Phosphatase 5b (TRAcP 5b)

Saphenous vein blood draws were obtained pre- and post-HU. Blood was allowed to clot for 10-15 minutes after extraction then centrifuged at 1500 rpm for 15

minutes. Serum levels of TRAcP 5b were then assessed using the RatTRAP Assay (IDS, Fountain Hills, AZ, USA) and results were analyzed using a DTX 880 microplate reader (Beckman Coulter, Brea, CA, USA). Further details may be found at (82).

Statistical Analyses

All data are reported as means ± standard error of the mean (SE). Data were evaluated for statistical relationships using SigmaPlot 12.5 (Systat Software Inc., San Jose, CA). Comparisons among groups were performed using a one-factor ANOVA. When a significant effect was determined, pairwise comparisons of the means were evaluated by the Student-Newman-Keuls post hoc test. For longitudinal pQCT comparisons, a repeated measure one-factor ANOVA was used to detect differences over time. When a significant time effect was determined, pairwise comparisons of the means were evaluated by the Student-Newman-Keuls post hoc test. Statistical significance was accepted at $p<0.05$.

CHAPTER III

RESULTS

Animals

At baseline, animals averaged 473 ± 9.5 g with no significant differences between groups (Table 1). Body mass declined (-10%) during the first two weeks of simulated exercise (Ex+HU, Ex+ZA+HU) before eventually stabilizing at 7% below baseline. Compared to Day 35 values, HU led to a slight decrease in body mass (-3%) in non-exercised animals (HU, ZA+HU) and a slight increase in body mass (+4%) in animals previously exercised (Ex+HU, Ex+ZA+HU). At the end of the study, CC animals gained 8% in body mass while all other groups ended just slightly below (-0.1 to -3%) baseline. Soleus muscle mass was reduced by over 50% in all HU animals versus CC, with no differences between treatment groups (Table 1); this confirms the efficacy of the unloading treatment.

Table 1. Effects of Ex, ZA, and HU on Body Mass and Soleus Muscle Mass

	Day	CC	HU	ZA+HU	Ex+HU	Ex+ZA+HU
Body Mass (g)	0	471.8 ± 8.49	473.0 ± 11.29	472.8 ± 9.24	473.2 ± 9.31	472.8 ± 9.20
	35	489.9 ± 7.82 α	487.1 ± 9.17 α	487.7 ± 8.76 α	441.3 ± 8.13 α†	435.2 ± 8.72 α†
	65	508.3 ± 9.94 αβ	471.1 ± 8.56 β†	471.4 ± 11.26 β†	459.3 ± 8.61 αβ†	457.4 ± 13.16 αβ†
Soleus Mass (g)	65	0.194 ± 0.005	0.093 ± 0.004 †	0.090 ± 0.004 †	0.089 ± 0.003 †	0.095 ± 0.004 †

Values are presented as mean ± SE

α indicates significant difference from Day 0 value, $p<0.05$

β indicates significant difference from Day 35 value, $p<0.05$

† indicates significant difference from CC at same timepoint, $p<0.05$

High-Impact, Free-Fall Simulated Exercise

One animal did not complete the simulated exercise protocol (Ex+HU group) as he demonstrated an aversion to handling. In the Ex+ZA+HU group, one animal did not wake from tail harnessing anesthesia. All other animals responded to training and unloading with minimal stress. To investigate whether there were differences in ground reaction forces (GRFs) experienced with this training between the different limbs, peak vertical GRFs were compared for the forelimbs and the hindlimbs during landing. Hindlimb GRFs were 69% higher than the forelimb, equating to hindlimb vertical forces of over 3X body weight (Figure 15). Results from a pressure contour of the landing stance in all four limbs illustrate that pressure in the hindlimbs exceeded 25 N/cm^2, whereas the forelimbs peaked at 15 N/cm^2. For the purpose of this study, higher pressure and force in the hindlimbs during landing is critical, as HU unloads the hindlimbs only, thus causing bone loss at that site. To our knowledge, this is the first free-fall training protocol that has documented higher GRFs in the hindlimbs than in the forelimbs

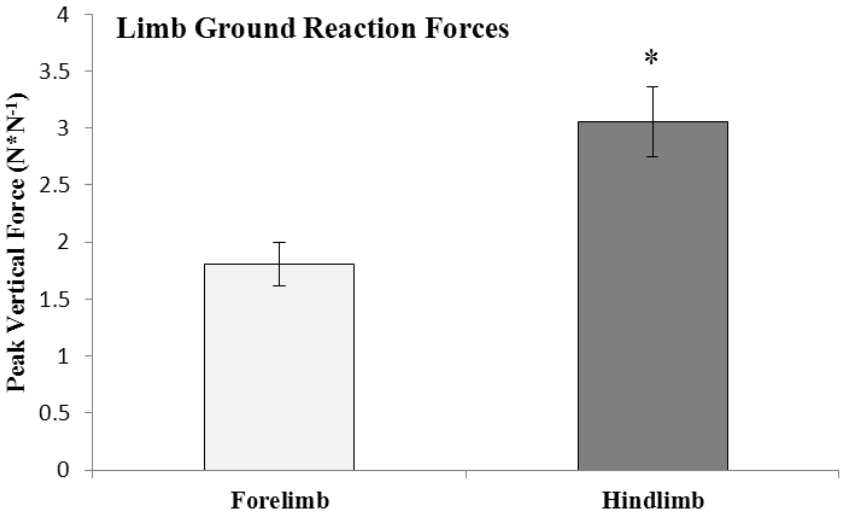

Figure 15. Normalized Peak Ground Reaction Forces. Peak GRFs were normalized to animal body mass and are presented as mean ± SE. * Indicates significant difference from forelimb ($p<0.05$).

In Vivo Longitudinal Peripheral Quantitative Computed Tomography

For longitudinal pQCT results (e.g., PTM and TD), HU-induced losses may be characterized in three ways: relative to baseline (Day 0), relative to Day 35, or relative to CC at Day 65. In this study, we chose to use Day 35 (start of HU) as our reference point. That is, when Day 65 (post-HU) values are significantly different than Day 35 values, we designate these HU-induced changes. Similarly, effectiveness of our treatment regimens may be defined in several ways. Again, we have chosen our primary comparison to be Day 65 versus Day 35. As a secondary reference point, comparisons among groups at Day 65 were made.

Proximal Tibia Metaphysis. Hindlimb unloading caused marked alterations in bone mass, density, and geometry. HU (alone) animals experienced average losses in

total BMC and vBMD of 8.9% and 8.1%, respectively (Table 2). Cancellous vBMD also declined with HU by 7.4%. Both cortical cross-sectional area and cortical thickness were negatively impacted by HU compared to CC (-11 and -12%, respectively). Treatment with ZA completely prevented all HU-induced densitometric losses. Total BMC and vBMD were fully protected with ZA, and actually increased relative to Day 35 values (9.6% and 4.1%), to HU animals (19.4% and 12.8%), and to CC animals (6.5% and 6.8%). Cortical and cancellous vBMD were also protected from losses, while the cortical compartment increased by 2.5% compared to Day 35. Although total area was not altered by HU, ZA heightened it by 8.3%. Furthermore, HU-induced cortical area and thickness losses were prevented with ZA. In contrast to ZA monotherapy, simulated exercise alone did not induce densitometric or structural gains in the PTM. Relative to Day 35, total BMC was 5.3% lower in Ex, yet it was not significantly different than CC, suggesting a protective effect in spite of slight decrements during HU. Total vBMD was unchanged during 28 days of unloading (Ex+HU) relative to Day 35, ending 6.6% higher than HU animals. Similar to ZA monotherapy, sequential treatment with Ex and ZA prevented losses in all measured densitometric parameters and produced gains in total and cortical BMC and vBMD. Ex+ZA increased total and cortical vBMD relative to Day 35 values (5.0% and 4.6%), and to those in HU animals (13.2% and 11.8%), and in CC animals (7.2% and 6.5%). Losses in cortical thickness were prevented with sequential Ex and ZA, ending 14.5% and 20.3% higher than Day 35 values and HU animals, respectively (Figure 16).

Table 2. Longitudinal pQCT Results at the Proximal Tibia Metaphysis

	Day	CC	HU	ZA+HU	Ex+HU	Ex+ZA+HU
Total BMC (mg/mm)	0	10.28 ± 0.21	10.43 ± 0.23	10.08 ± 0.17	10.80 ± 0.18 #†	10.79 ± 0.30
	35	10.34 ± 0.18	10.51 ± 0.19	10.43 ± 0.16	10.49 ± 0.18	10.48 ± 0.20
	65	10.73 ± 0.24 αβ	9.57 ± 0.15 αβ†	11.43 ± 0.23 αβ#†	9.93 ± 0.22 αβ	11.13 ± 0.27 β#†
Cortical BMC (mg/mm)	0	8.10 ± 0.15	8.06 ± 0.11	8.17 ± 0.18	8.42 ± 0.15	8.29 ± 0.24
	35	8.19 ± 0.18	8.18 ± 0.13	8.53 ± 0.17 α	8.40 ± 0.19	8.28 ± 0.20
	65	8.47 ± 0.17 αβ	7.50 ± 0.18 αβ	9.34 ± 0.20 αβ#	7.99 ± 0.18	8.90 ± 0.18 αβ
Cancellous BMC (mg/mm)	0	2.18 ± 0.13	2.37 ± 0.17	1.91 ± 0.13 #	2.37 ± 0.13	2.50 ± 0.15
	35	2.16 ± 0.14	2.33 ± 0.17	1.90 ± 0.15	2.09 ± 0.20	2.20 ± 0.09
	65	2.26 ± 0.10	2.07 ± 0.13	2.08 ± 0.18	1.94 ± 0.16 α	2.23 ± 0.17
Total vBMD (mg/cm^3)	0	586.59 ± 8.62	597.24 ± 10.32	589.66 ± 7.72	597.88 ± 6.79	593.98 ± 8.64
	35	574.27 ± 11.16	587.55 ± 9.81	585.21 ± 9.92	597.07 ± 15.95	582.05 ± 7.85
	65	570.40 ± 7.80	540.12 ± 14.22 αβ	609.26 ± 8.29 αβ#†	575.59 ± 14.23 #	611.28 ± 8.78 β#†
Cortical vBMD (mg/cm^3)	0	1054.6 ± 6.9	1052.9 ± 8.4	1061.6 ± 7.9	1053.7 ± 6.2	1054.1 ± 6.7
	35	1053.1 ± 9.8	1060.5 ± 8.0	1067.5 ± 8.5	1072.3 ± 13.5	1067.6 ± 5.5
	65	1055.8 ± 5.5	1049.0 ± 12.1	1093.9 ± 6.4 αβ#†	1076.1 ± 10.5	1098.7 ± 6.1 αβ#†
Cancellous vBMD (mg/cm^3)	0	215.74 ± 7.76	233.67 ± 11.87	198.15 ± 10.34 #	230.85 ± 11.06	235.46 ± 7.73
	35	203.92 ± 7.94	223.33 ± 10.03	187.21 ± 11.12 #	205.16 ± 9.79 α	210.87 ± 6.27 α
	65	204.16 ± 6.33	189.45 ± 7.40 αβ	197.60 ± 13.25	189.90 ± 10.53 α	213.13 ± 9.05 α#
Total Area (mm^2)	0	17.58 ± 0.38	17.55 ± 0.45	17.15 ± 0.27	18.09 ± 0.36	18.25 ± 0.53
	35	17.32 ± 0.30	17.65 ± 0.43	17.37 ± 0.33	17.49 ± 0.52	17.71 ± 0.464
	65	18.86 ± 0.38 αβ	17.88 ± 0.44	18.82 ± 0.39 αβ	17.37 ± 0.50	18.28 ± 0.55
Cortical Area (mm^2)	0	7.68 ± 0.13	7.67 ± 0.11	7.70 ± 0.14	8.00 ± 0.14	7.88 ± 0.21
	35	7.77 ± 0.13	7.72 ± 0.12	7.99 ± 0.13 α	7.84 ± 0.15	7.75 ± 0.17
	65	8.03 ± 0.15 αβ	7.15 ± 0.13 αβ†	8.55 ± 0..17 αβ#†	7.43 ± 0.14 αβ†	8.11 ± 0.17 αβ#
Marrow Area (mm^2)	0	9.90 ± 0.31	9.88 ± 0.37	9.44 ± 0.23	10.09 ± 0.27	10.37 ± 0.41
	35	10.33 ± 0.39	10.26 ± 0.40	9.93 ± 0.33	9.92 ± 0.62	10.29 ± 0.26
	65	10.84 ± 0.28 α	10.73 ± 0.43	10.27 ± 0.30	9.95 ± 0.47	10.18 ± 0.44
Cortical Thickness (mm)	0	0.66 ± 0.03	0.61 ± 0.03	0.61 ± 0.02	0.65 ± 0.04	0.66 ± 0.01
	35	0.63 ± 0.04	0.63 ± 0.03	0.68 ± 0.02 α	0.67 ± 0.03	0.62 ± 0.03
	65	0.67 ± 0.02	0.59 ± 0.02 †	0.73 ± 0.01 αβ#†	0.64 ± 0.02	0.71 ± 0.02 β#
CSMI (mm^4)	0	31.63 ± 1.27	31.85 ± 1.41	30.72 ± 0.95	33.70 ± 1.18	34.27 ± 1.80
	35	33.58 ± 1.43	33.22 ± 1.52	33.36 ± 1.28	32.88 ± 2.15	33.55 ± 1.18
	65	36.54 ± 1.40 α	32.97 ± 1.42	36.44 ± 1.37 α	32.03 ± 1.54	34.56 ± 1.87

Values are presented as mean ± SE

α indicates significant difference from Day 0 value, $p<0.05$

β indicates significant difference from Day 35 value, $p<0.05$

# indicates significant difference from HU at same timepoint, $p<0.05$

† indicates significant difference from CC at same timepoint, $p<0.05$

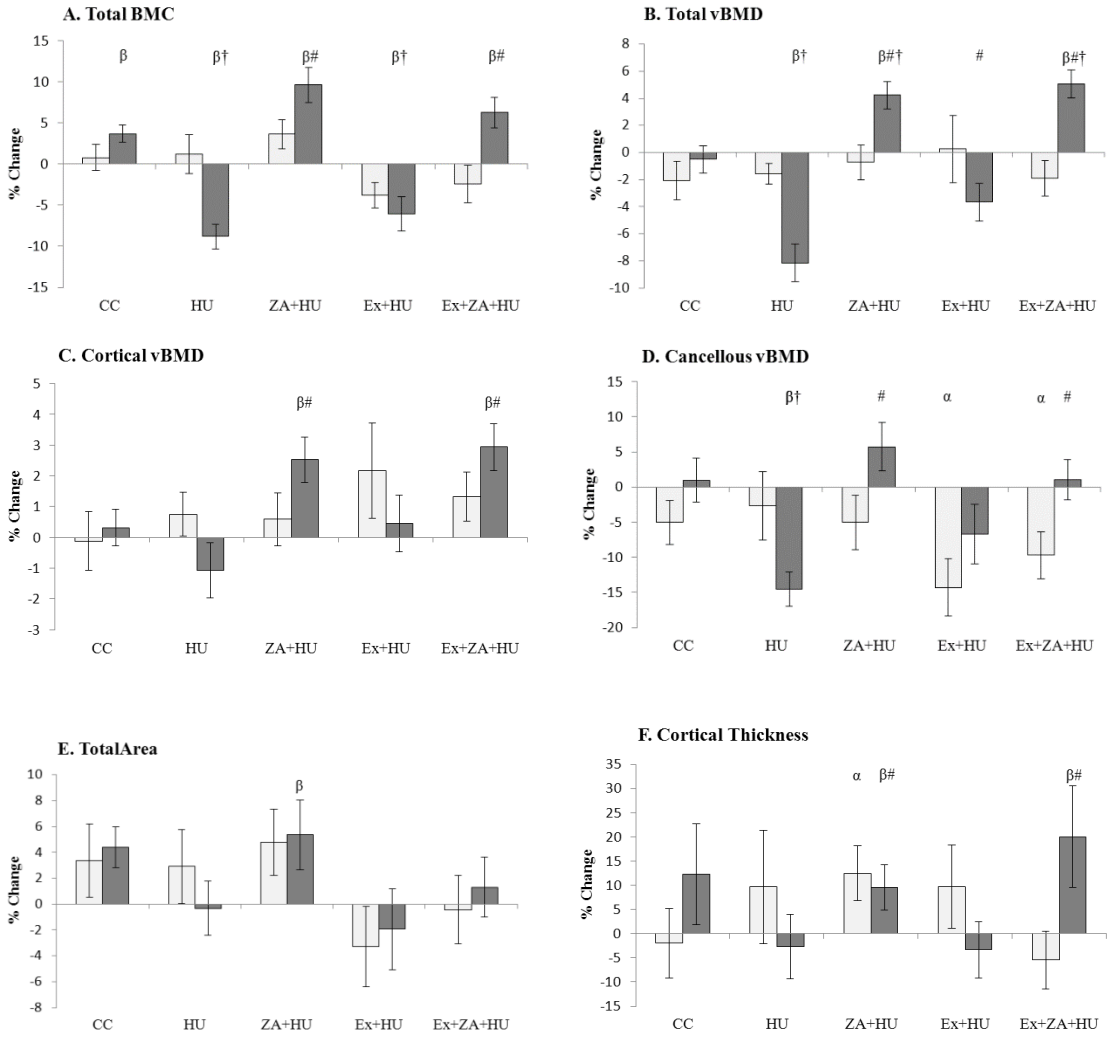

Figure 16. Longitudinal Densitometric/Geometric Changes. Values assessed at the Proximal Tibia Metaphysis. (A) Total BMC, (B) Total vBMD, (C) Cortical vBMD, (D) Cancellous vBMD, (E) Total Area, and (F) Cortical Thickness. Light grey bars represent % change values from Day 0 to Day 35. Dark grey bars represent % change values from Day 35 to Day 65. Values are presented as mean ± SE. α Indicates significant difference from Day 0 ($p<0.05$). β Indicates significant difference from Day 35 to Day 65 ($p<0.05$). # Indicates significant difference from HU ($p<0.05$). † Indicates significant difference from CC ($p<0.05$).

Mid-Diaphysis Tibia. Hindlimb unloading did not result in densitometric or calculated strength losses in tibia diaphyseal bone. Cortical vBMD actually increased slightly during 28 days of unloading by an average of 0.82%. Despite the slight change in cortical vBMD during HU, mid-shaft pQCT values were similar to CC at the end of the study in all groups at every time point.

Table 3. Longitudinal pQCT Results at the Tibia Diaphysis

	Day	CC	HU	ZA+HU	Ex+HU	Ex+ZA+HU
Cortical BMC (mg/mm)	0	8.62 ± 0.14	8.24 ± 0.16	7.89 ± 0.16	8.28 ± 0.13	8.18 ± 0.14
	35	8.64 ± 0.12 α	8.76 ± 0.18 α	8.29 ± 0.15 α	8.64 ± 0.13 α	8.77 ± 0.19 α
	65	8.83 ± 0.12 αβ	8.87 ± 0.15 α	8.45 ± 0.17 α	8.73 ± 0.13 α	8.72 ± 0.17 α
Cortical vBMD (mg/cm^3)	0	1329 ± 4.2	1330 ± 4.1	1327 ± 3.1	1322 ± 2.2	1327 ± 5.1
	35	1339 ± 4.9	1334 ± 1.9	1336 ± 4.9 α	1340 ± 6.1 α	1335 ± 2.7
	65	1351 ± 3.3 α	1345 ± 3.2 αβ	1348 ± 4.5 αβ	1355 ± 4.8 αβ	1350 ± 2.9 αβ
Corticl Area (mm^2)	0	6.22 ± 0.11	6.20 ± 0.13	5.95 ± 0.12	6.26 ± 0.11	6.17 ± 0.11
	35	6.45 ± 0.09 α	6.57 ± 0.14 α	6.21 ± 0.11 α	6.45 ± 0.09 α	6.57 ± 0.14 α
	65	6.54 ± 0.09 α	6.59 ± 0.11 α	6.27 ± 0.13 α	6.44 ± 0.09 α	6.46 ± 0.13 α
Total Area (mm^2)	0	8.89 ± 0.16	8.96 ± 0.22	8.61 ± 0.13	9.05 ± 0.17	8.93 ± 0.22
	35	9.19 ± 0.17	9.59 ± 0.19 α	9.06 ± 0.17 α	9.31 ± 0.21	9.54 ± 0.23 α
	65	9.43 ± 0.16 α	9.55 ± 0.17 α	9.04 ± 0.17 α	9.24 ± 0.21	9.31 ± 0.25 α
Cortical Thickness (mm)	0	0.79 ± 0.012	0.75 ± 0.035	0.76 ± 0.01	0.71 ± 0.044	0.71 ± 0.046
	35	0.79 ± 0.009	0.71 ± 0.045	0.76 ± 0.012	0.77 ± 0.013	0.79 ± 0.013
	65	0.80 ± 0.004	0.80 ± 0.012	0.75 ± 0.030	0.80 ± 0.016	0.79 ± 0.012
CSMI (mm^4)	0	6.21 ± 0.22	6.30 ± 0.31	5.80 ± 0.21	6.47 ± 0.25	6.25 ± 0.27
	35	6.69 ± 0.24	7.25 ± 0.33 α	6.46 ± 0.24 α	6.88 ± 0.31	7.22 ± 0.32 α
	65	6.98 ± 0.22 α	7.18 ± 0.25 α	6.44 ± 0.25 α	6.78 ± 0.29	6.86 ± 0.32 α
SSI (mm^3)	0	6.28 ± 0.16	6.28 ± 0.20	5.87 ± 0.14	6.23 ± 0.15	6.17 ± 0.20
	35	6.63 ± 0.15 α	6.88 ± 0.19 α	6.31 ± 0.15 α	6.60 ± 0.15 α	6.80 ± 0.25 α
	65	6.88 ± 0.15 αβ	6.94 ± 0.16 α	6.44 ± 0.17 α	6.60 ± 0.16 α	6.69 ± 0.25 α
BSI (mm^3)	0	3.68 ± 0.10	3.71 ± 0.14	3.50 ± 0.10	3.80 ± 0.11	3.70 ± 0.12
	35	3.90 ± 0.11	4.14 ± 0.14	3.79 ± 0.10 α	3.98 ± 0.13	4.13 ± 0.13 α
	65	4.02 ± 0.1 α	4.11 ± 0.11 α	3.78 ± 0.11 α	3.94 ± 0.13	3.97 ± 0.14 αβ

Values are presented as mean ± SE
α indicates significant difference from Day 0 value, $p<0.05$
β indicates significant difference from Day 35 value, $p<0.05$
# indicates significant difference from HU at same timepoint, $p<0.05$
† indicates significant difference from CC at same timepoint, $p<0.05$

Ex Vivo Longitudinal Peripheral Quantitative Computed Tomography

Femoral Neck. Relative to CC, HU caused significant reductions in total BMC (-11.0%), total and cancellous vBMD (-5.6 and -13.7%), cortical area (-9.8%), and CSI (-16.1) at the femoral neck (FN) (Table 4). Alone, Ex and ZA mitigated losses in total BMC and cortical area, and completely prevented declines in total and cancellous vBMD and CSI. When applied in sequence, Ex and ZA completely prevented all HU-induced decrements in bone densitometry. Sequential therapy did not, however, appear to provide additive benefits in the femoral neck. That is, Ex+ZA+HU values were not significantly higher than ZA+HU or Ex+HU in any FN variables measured, although combined treatment did protect against BSI, SSI, and BMC losses whereas monotherapy did not.

Table 4. Femoral Neck Imaging Results by pQCT

	CC	HU	ZA+HU	Ex+HU	Ex+ZA+HU
Total BMC (mg/mm)	5.53 ± 0.17	4.92 ± 0.098 †	5.20 ± 0.10	5.26 ± 0.11	5.63 ± 0.15 #
Cortical BMC (mg/mm)	3.71 ± 0.10	3.36 ± 0.10 †	3.62 ± 0.08	3.64 ± 0.10	3.81 ± 0.09 #
Cancellous BMC (mg/mm)	1.83 ± 0.12	1.54 ± 0.10 †	1.58 ± 0.07	1.62 ± 0.08	1.82 ± 0.11 #
Total vBMD (mg/cm^3)	1088 ± 17	1027 ± 24 †	1086 ± 18 #	1096 ± 14 #	1112 ± 14 #
Cortical vBMD (mg/cm^3)	1450 ± 8	1461 ± 6	1456 ± 5	1452 ± 5	1457 ± 4
Cancellous vBMD (mg/cm^3)	715.5 ± 22.4	617.3 ± 13.2 †	682.4 ± 20.7 #	704.1 ± 26.1 #	739.4 ± 15.0 #
Total Area (mm^2)	5.10 ± 0.17	4.83 ± 0.16	4.81 ± 0.13	4.80 ± 0.06	5.08 ± 0.17
Cortical Area (mm^2)	2.56 ± 0.08	2.31 ± 0.06 †	2.48 ± 0.06	2.51 ± 0.07	2.61 ± 0.06 #
Marrow Area (mm^2)	2.54 ± 0.15	2.52 ± 0.18	2.33 ± 0.12	2.29 ± 0.06	2.46 ± 0.15
Cortical Thickness (mm)	0.41 ± 0.050	0.40 ± 0.028	0.45 ± 0.019	0.46 ± 0.013 #	0.47 ± 0.013 #
BSI (mm^3)	1.76 ± 0.08	1.61 ± 0.05	1.79 ± 0.11	1.71 ± 0.04	1.85 ± 0.07 #
CSI (mg^2/mm^4)	6.02 ± 0.21	5.05 ± 0.14 †	5.64 ± 0.13 #	5.77 ± 0.18 #	6.25 ± 0.15 #
SSI (mm^3)	2.62 ± 0.11	2.38 ± 0.11	2.56 ± 0.09	2.60 ± 0.07	2.80 ± 0.11 #

Values are presented as mean ± SE

# indicates significant difference from HU at same timepoint, $p<0.05$

† indicates significant difference from CC at same timepoint, $p<0.05$

Microarchitecture Assessed by Micro-Computed Tomography

Distal Femur Metaphysis. HU resulted in marked alterations in cancellous microarchitecture. Compared to CC, HU rats had lower BV/TV (Figure 17) and Tb.Th, and higher SMI in the distal femur metaphysis (-24%, -15%, and+23%, respectively) (Table 5). Treatment with ZA completely prevented disuse-induced losses in BV/TV (Figure 17) and Tb.Th (Figure 18) and inhibited increases in SMI. Although Conn.D was not reduced with HU, ZA+HU animals ended the study with 20% higher Conn.D than CC. Simulated exercise alone prevented losses with HU in Tb.Th (Figure 18) and increases in SMI but had no effect on BV/TV. Improvements in BV/TV, Conn.D, and SMI were greatest in rats treated with both ZA and Ex. BV/TV in Ex+ZA+HU animals, for example, was 60% greater than HU and 21% higher than CC. Total bone volume (BV) in the distal femur metaphysis was also reduced with HU (-12.2) compared to CC. Treatment with either ZA or Ex alone mitigated total BV losses, while the combined therapy (Ex+ZA) yielded improvements to levels above CC.

Table 5. Cancellous and Cortical Microarchitecture and Morphology Assessed by μCT at the Distal Femur Metaphysis and Femur Diaphysis.

	CC	HU	ZA+HU	Ex+HU	Ex+ZA+HU
Distal Cancellous					
BV/TV (%)	0.20 ± 0.01	0.15 ± 0.008 †	0.22 ± 0.02 #	0.19 ± 0.01	0.24 ± 0.02 †#
Tb.Th (mm)	0.092 ± 0.001	0.078 ± 0.001 †	0.094 ±0.002 #	0.087 ± 0.002 #	0.097 ± 0.003 #
Tb.Sp (mm)	0.35 ± 0.02	0.33 ± 0.02	0.37 ± 0.03	0.35 ± 0.02	0.33 ± 0.02
Tb.N (mm^{-1})	2.85 ± 0.13	2.96 ± 0.11	2.83 ± 0.16	2.85 ± 0.15	3.03 ± 0.13
ConnD (mm^{-3})	47.0 ± 3.1	42.9 ± 3.7	56.2 ± 4.9 #	49.0 ± 4.5	56.4 ± 3.9 †#
SMI	1.81 ± 0.08	2.24 ± 0.09 †	1.66 ± 0.14 #	1.86 ± 0.09 #	1.39 ± 0.13 †#
Diaphysis Cortical					
vBMD (mg/cm^3)	1203.7 ± 3.6	1220.2 ± 2.5	1228.5 ± 1.8	1224.8 ± 0.5	1225.3 ± 1.8
Ct. BA/TA (%)	61.2 ± 1.1	61.2 ± 0.4	61.1 ± 0.4	59.6 ± 1.1	59.4 ± 0.8
Ct.Por (%)	0.081 ± 0.004	0.066 ± 0.005	0.087 ± 0.010	0.071 ± 0.006	0.076 ± 0.005
Ct. Th (mm)	0.79 ± 0.01	0.79 ± 0.01	0.79 ± 0.01	0.77 ± 0.005	0.78 ± 0.01
pMOI (mm^4)	26.9 ± 1.0	25.6 ± 0.6	25.6 ± 0.7	26.4 ± 0.9	28.4 ± 1.4

Values are presented as mean ± SE

# indicates significant difference from HU at same timepoint, $p<0.05$

† indicates significant difference from CC at same timepoint, $p<0.05$

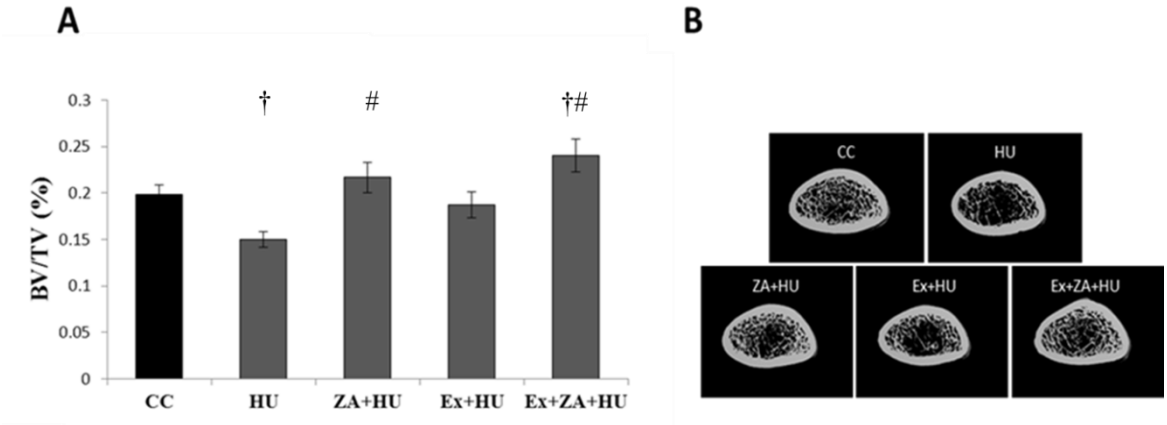

Figure 17. Relative Bone Volume at the Distal Femur. Images expressed (A) graphically and (B) visually. Values are group mean ± standard error of the mean. †vs. CC ($p<0.05$); #vs. HU ($p<0.05$).

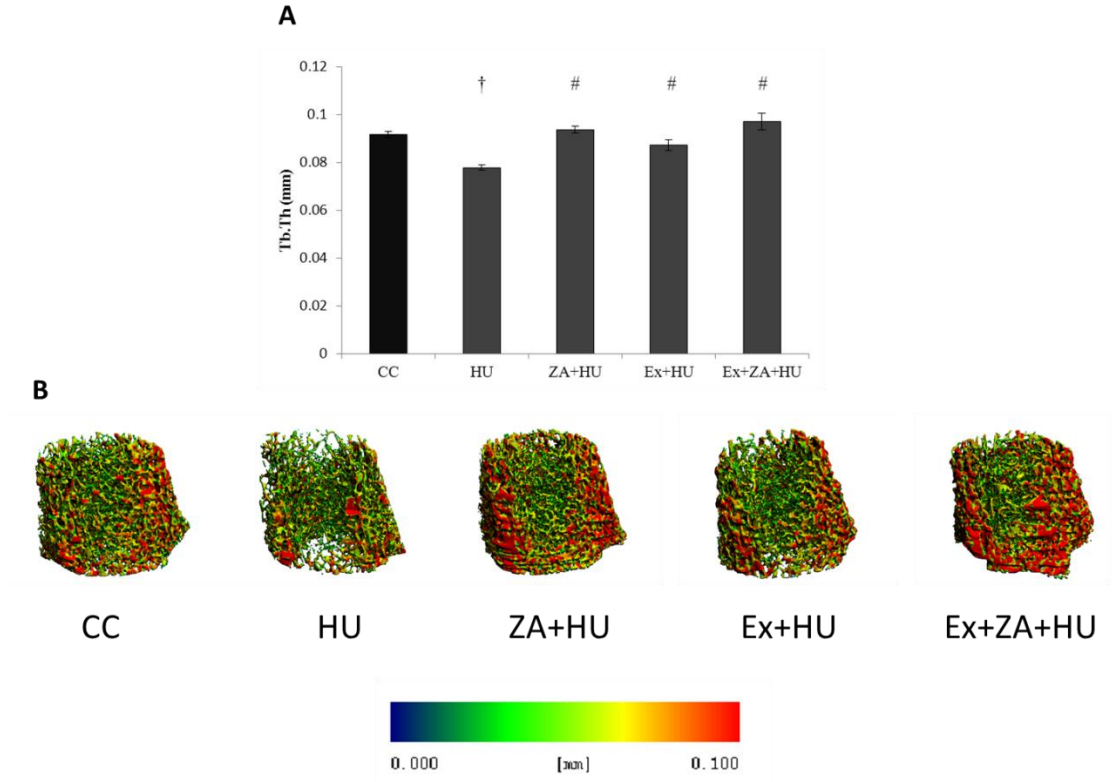

Figure 18. Trabecular Thickness at the Distal Femur Metaphysis. Images expressed (A) graphically and (B) thickness color map. Values are group mean ± standard error of the mean. †vs. CC ($p<0.05$); #vs. HU ($p<0.05$).

Mid-Diaphysis Femur. Unlike at the distal femur metaphysis, none of the µCT parameters measured at the femoral mid-shaft diaphysis were significantly different across groups (Table 4).

Femoral Neck Biomechanical Findings

The ultimate force in axial mechanical testing of the femoral neck in HU animals was 20% lower than CC counterparts (Figure 19A). Compared to total vBMD in the femoral neck (-6% loss versus CC), losses in ultimate force were nearly fourfold higher,

suggesting an underestimation of bone strength by this measure of bone mass. Similarly, energy to ultimate force was drastically reduced with HU (-35%) (Figure 19B). Both monotherapy with either Ex or ZA, as well as sequential treatment, prevented the aforementioned disuse-induced strength losses.

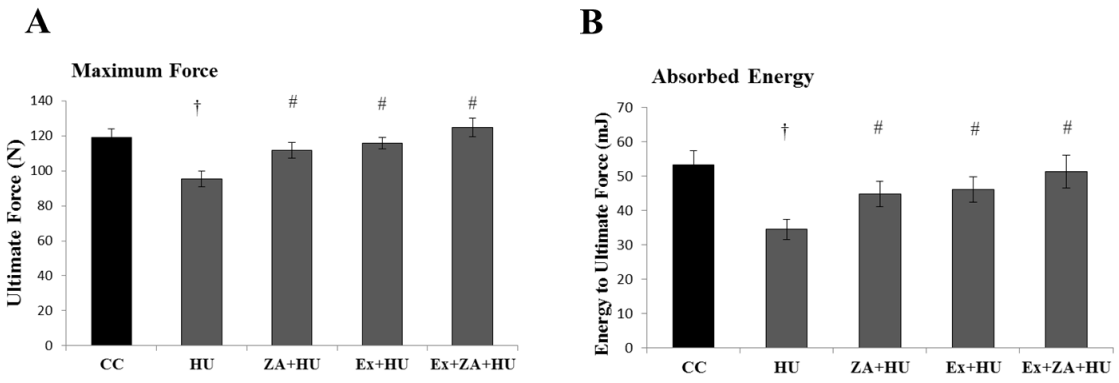

Figure 19. Femoral Neck Biomechanical Testing. (A) Ultimate Force and (B) Energy to Ultimate Force. Values are group mean ± standard error of the mean. †vs. CC ($p<0.05$); #vs. HU ($p<0.05$).

Tibia Mechanical Properties

With the exception of ultimate stress, which was reduced by 13.4% with HU and recovered with treatment, mechanical properties of the mid-tibia diaphysis were generally unaffected by loading status or drug treatment (Table 6).

Table 6. Three-Point Bending Biomechanical Testing at the Tibia Diaphysis

	CC	HU	ZA+HU	Ex+HU	Ex+ZA+HU
Stiffness (N/mm)	367.1 ± 15.6	359.7 ± 14.2	333.8 ± 16.5	343.8 ± 18.7	374.7 ± 16.6
Ultimate Force (N)	140.7 ± 3.3	134.0 ± 3.4	134 ± 4.0	143 ± 2.0	136.8 ± 3.9
Energy to Ultimate Force (mJ)	50.7 ± 3.2	44.3 ± 3.1	43.3 ± 2.6	49.4 ± 3.4	47.4 ± 3.9
Post-Yield Displacement (mm)	0.46 ± 0.054	0.52 ± 0.055	0.62 ± 0.08	0.51 ± 0.078	0.54 ± 0.066
Ultimate Stress (MPa)	178.2 ± 4.8	154.4 ± 7.4 †	181.1 ± 7.9 #	186.6 ± 7.1 #	171.3 ± 6.8
Elastic Modulus (GPa)	6.46 ± 0.33	6.10 ± 0.17	6.40 ± 0.39	6.31 ± 0.35	6.78 ± 0.39

Values are presented as mean ± SE

# indicates significant difference from HU at same timepoint, $p<0.05$

† indicates significant difference from CC at same timepoint, $p<0.05$

Finite Element Derived Estimates of Strength

Compressive stiffness of the combined cortical and cancellous compartments at the distal femur metaphysis was significantly lower in HU (-13%) versus CC animals (Figure 20A). Interestingly, HU-induced reductions in stiffness are 1.7-fold greater than respective losses in total vBMD (-8%), suggesting an underestimation of mechanical properties by total vBMD. Monotherapy with either ZA or Ex improved stiffness back to CC values. Combination therapy, however, heightened stiffness beyond both HU and CC animals (34% and 16%, respectively). Distribution of load sharing between cortical and cancellous bone also was altered with HU. Compared to CC, HU animals experienced 4% higher loads in the cortex (Figure 20B). Alone and in combination, ZA and Ex protected against unfavorable alterations in load sharing.

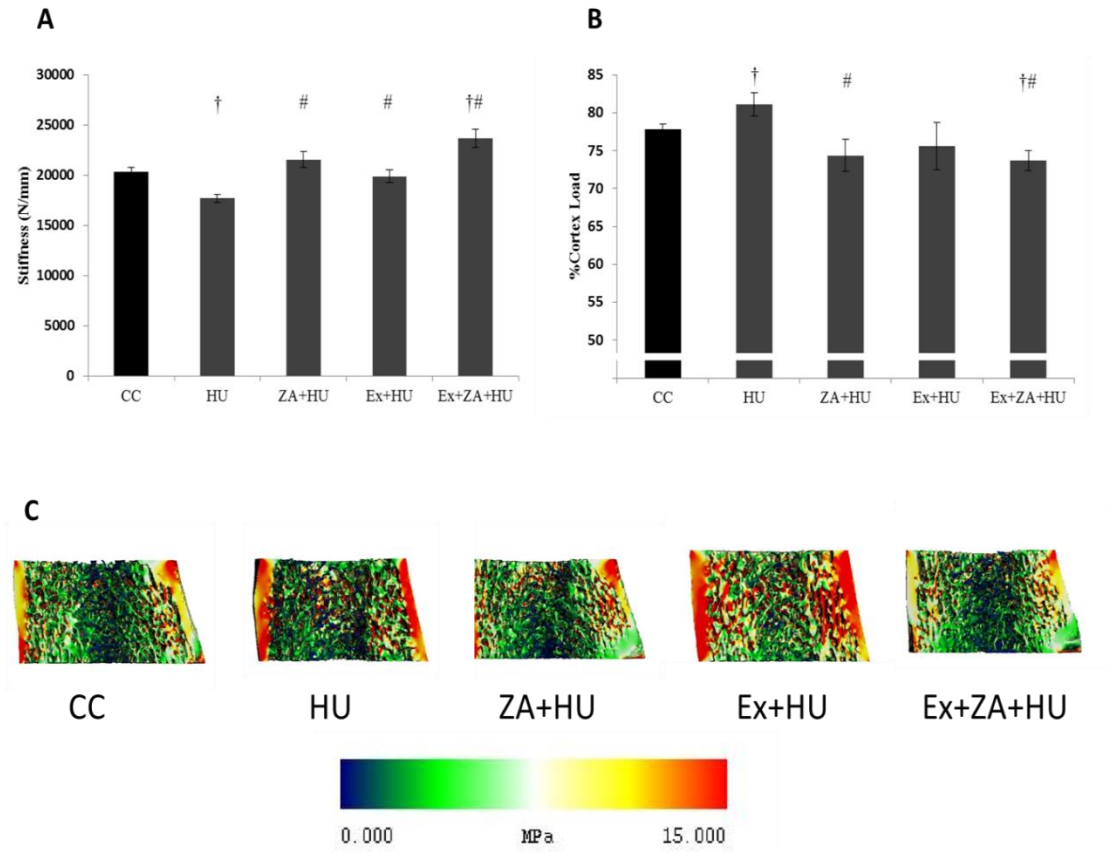

Figure 20. Finite Element Analysis-Derived Mechanical Properties. (A) Stiffness, (B) %Cortex Load, and (C) Cortical-cancellous load sharing color map depicted as von Mises stress distribution. Values are group mean ± standard error of the mean. †vs. CC ($p<0.05$); #vs. HU ($p<0.05$).

Material Properties from Reference Point Indentation

No significant differences in reference point indentation were observed among groups. IDI, ID 1st, TID, nor US was found to be significantly altered with HU or Ex and ZA treatment options (Table 7). Figure 21 illustrates a high resolution µCT image taken post-RPI testing with indentation sites indicated.

Table 7. Reference Point Indentation Results at the Femur Diaphysis

	CC	HU	ZA+HU	Ex+HU	Ex+ZA+HU
IDI (μm)	7.92 ± 0.15	7.88 ± 0.15	8.17 ± 0.17	7.96 ± 0.16	8.36 ± 0.19
ID 1st (μm)	59.3 ± 0.87	59.5 ± 1.15	58.0 ± 0.76	58.2 ± 1.77	59.4 ± 0.81
TID (μm)	63.7 ± 0.91	63.8 ± 1.05	63.0 ± 0.81	62.6 ± 1.49	64.3 ± 0.77
US (N/μm)	0.60 ± 0.015	0.63 ± 0.018	0.62 ± 0.020	0.64 ± 0.018	0.60 ± 0.014

Values are presented as mean ± SE

# indicates significant difference from HU at same timepoint, $p<0.05$

† indicates significant difference from CC at same timepoint, $p<0.05$

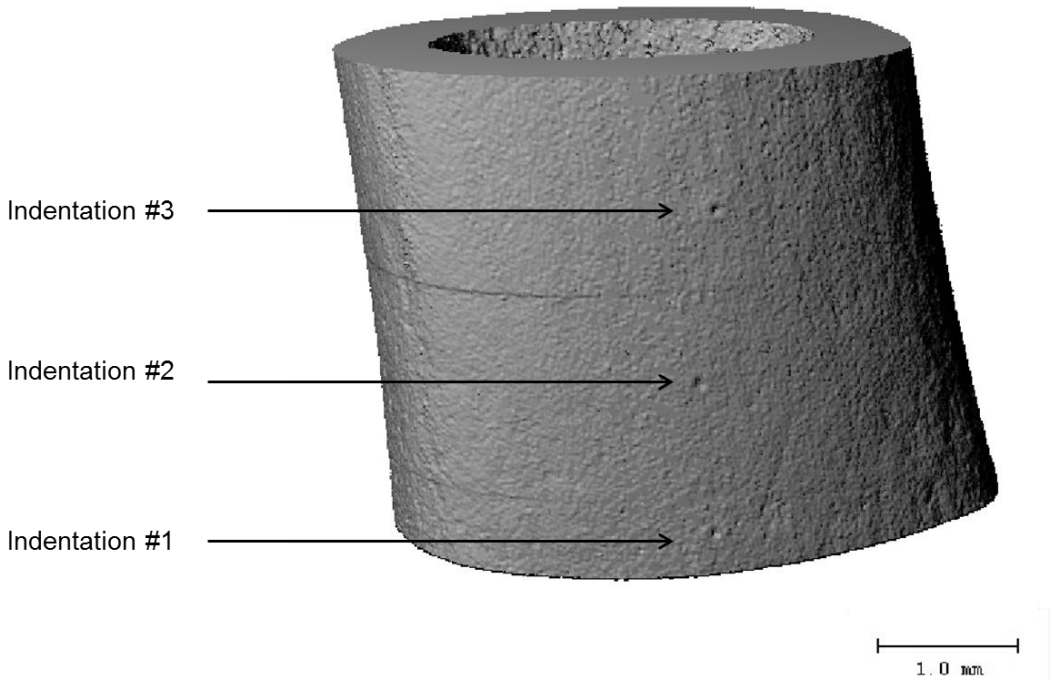

Figure 21. Microindentation Anatomical Sites. μCT illustration of three representative RPI indentations along the femur diaphysis spaced 1-2 mm apart.

Bone Formation Assessed by Dynamic Histomorphometry

Longitudinal assessment of cortical histomorphometry along the periosteal surface via calcein double fluorochrome labels indicate that HU, regardless of treatment status, significantly reduced MS/BS, MAR, and BFR compared to controls (Table 8). In Ex+ZA+HU animals, MS/BS (% change, Figure 22) was significantly higher than HU, while MAR (% change) was significantly lower. Representative images of our two sets of double labels in CC and HU sections are depicted in Figure 23. When samples were missing double labeling, as in the HU group in Figure 23, a minimum MAR of 0.3 μm/day was assigned. Bone formation rate was unaffected by either simulated exercise (as indicated by demeclocycline) or ZA (as indicated by calcein), as percent change differences between HU groups were not statistically different. An alternative method for determining BFR when double label is missing is to designate MAR as "missing data" rather than setting it to 0.3 μm/day. When calculated this way, BFR in CC animals significantly increased (+75%, compared to +63% as previously calculated) while all HU animals significantly decreased by an average of -90%. No labels were found on endocortical surfaces.

Table 8. Periosteal Fluorochrome Label Results

	CC	HU	ZA+HU	Ex+HU	Ex+ZA+HU
End of Ex period					
Double label on periosteum (n)	10/11	11/11	11/11	3/9	10/12
MS/BS (%)	14.20 ± 2.50	16.99 ± 2.85	15.58 ± 1.93	11.94 ± 3.63 #	14.0 ± 3.07
MAR (μm/day)	7.11 ± 2.59	9.00 ± 2.52	5.28 ± 1.13	6.24 ± 3.29	4.33 ± 1.21 #
BFR ($um^3/\mu m^2$/day)	150.6 ± 77.5	179.9 ± 77.7	111.4 ± 30.3	164.8 ± 100.7	101.4 ± 40.3 #
End of HU period					
Double label on periosteum (n)	9/11	2/11	3/11	0/9	6/12
MS/BS (%)	16.87 ± 3.34	3.59 ± 1.46 †	2.60 ± 0.69 †	1.35 ± 0.25 †	3.14 ± 0.54 †
MAR (μm/day)	9.01 ± 3.25	1.08 ± 0.74 †	1.08 ± 0.49 †	0.30 ± 0.04 †	0.32 ± 0.04 †
BFR ($um^3/\mu m^2$/day)	169.8 ± 101.0	10.50 ± 8.98 †	6.75 ± 4.35 †	0.39 ± 0.08 †	0.96 ± 0.21 †

Values are presented as mean ± SE

# indicates significant difference from HU at same timepoint, $p<0.05$

† indicates significant difference from CC at same timepoint, $p<0.05$

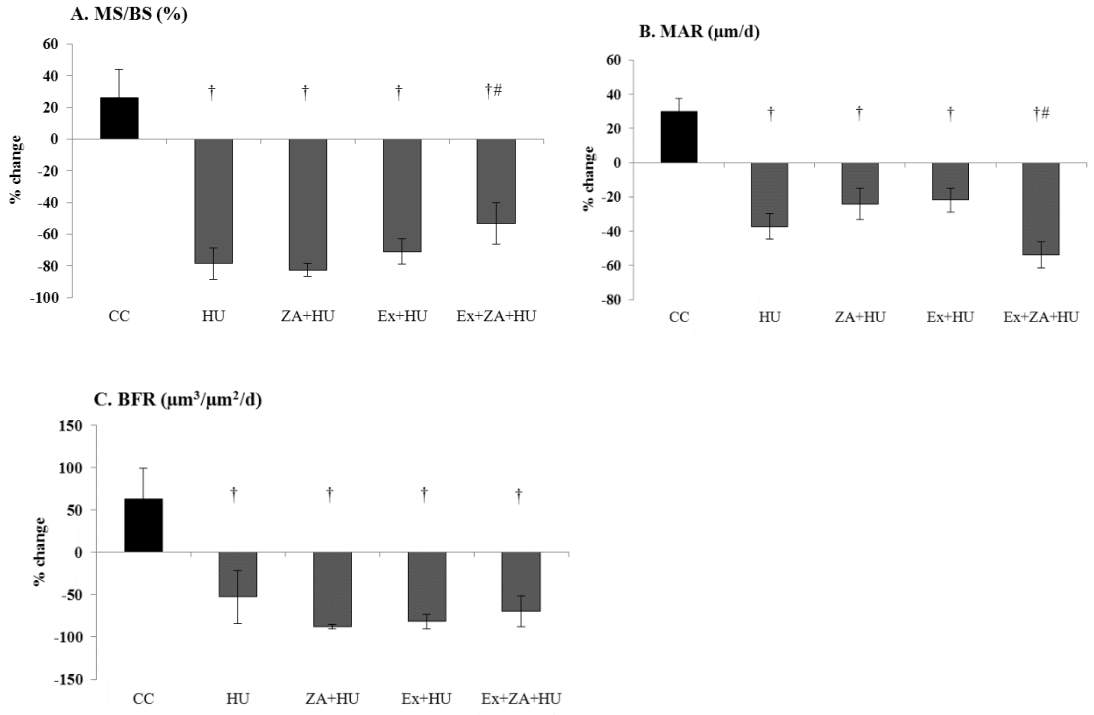

Figure 22. Longitudinal Dynamic Histomorphometry. Data assessed along periosteal cortical bone. (A) MS/BS, (B) MAR, and (C) BFR. Values are group mean percent change (calculated by the percent difference between values obtained via calcein and demeclocycline) ± standard error of the mean. †vs. CC ($p<0.05$); #vs. HU ($p<0.05$).

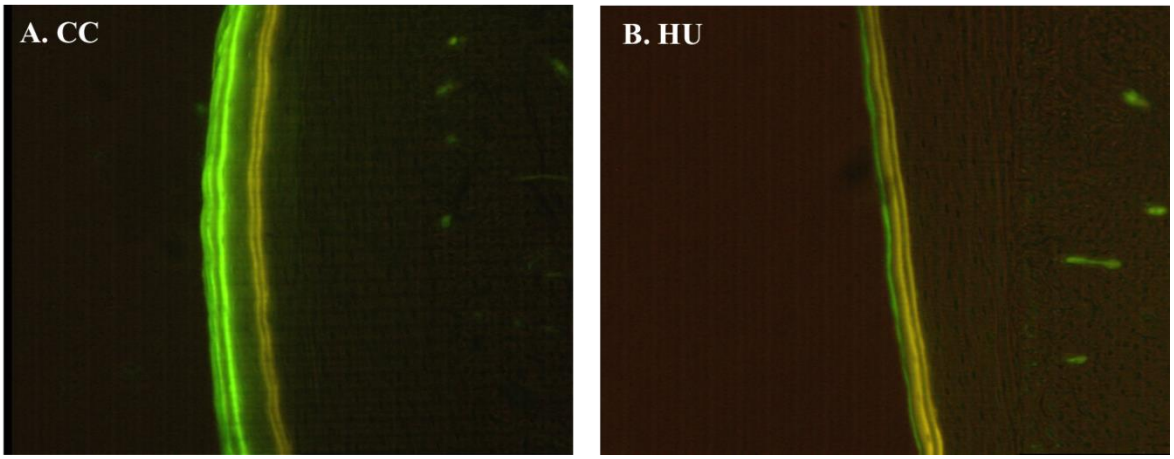

Figure 23. Representative Images of Periosteal Labeling. (A) CC animal and (B) HU animal.

Systemic Resorption: Tartrate-Resistant Acid Phosphatase 5b (TRAcP 5b)

At the end of the study, HU serum TRAcP 5b levels, which provide a systemic-level indicator of active osteoclasts, were 61% higher than in CC animals (Figure 24). ZA administered with and without simulated exercise reduced TRAcP 5b by 87 and 77%, respectively, compared to HU, and 80 and 39%, respectively, compared to CC. Ex alone did not affect TRAcP 5b, as levels were not significantly different than HU or CC at day 65 (Figure 24) or at day 35 (data not shown).

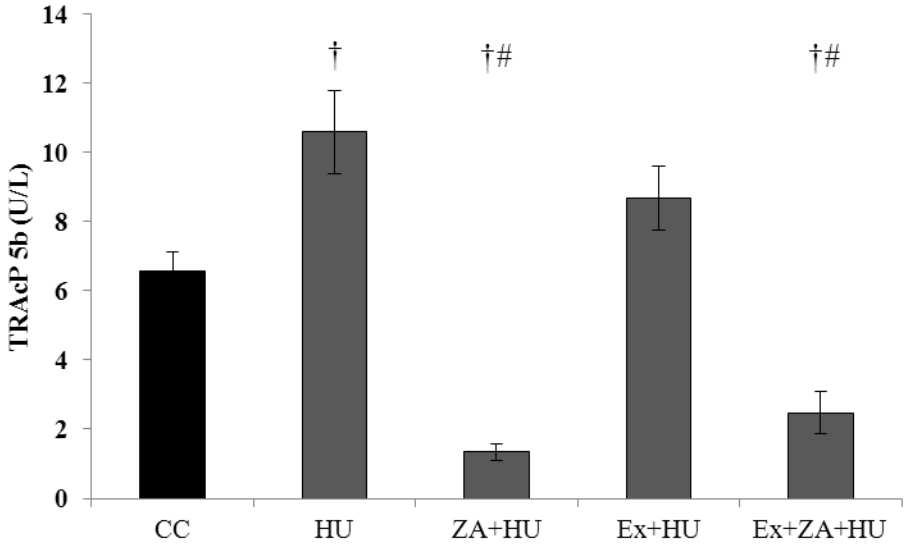

Figure 24. Serum TRAcP 5b Levels at Day 65. Values are group mean ± standard error of the mean. †vs. CC ($p<0.05$); #vs. HU ($p<0.05$).

CHAPTER IV

DISCUSSION

Densitometry, Microarchitecture, and Morphology

The salient densitometric, microarchitectural, and morphological findings of this study were threefold. First, we found that a single injection of ZA (60 μg/kg body weight) administered just prior to 28 days of unloading protected against mass, density, and geometry alterations in the PTM, distal femur metaphysis (DFM), and FN of adult rats. Second, high-impact, free-fall simulated exercise, characterized by thrice weekly drops (25X/session) had a similar effect relative to ZA treatment. Thirdly, when applied in sequence, Ex and ZA completely prevented disuse-induced bone decrements at the PTM and FN and was superior to either treatment alone at the DFM.

Bisphosphonates are currently the frontline class of drugs used to treat osteoporosis and other diseases related to increased bone resorption. Overwhelming evidence demonstrates the efficacy of bisphosphonates in reducing bone loss and fracture risk. A variety of bisphosphonates are available for use, each being characterized by their speed and duration of action as well as their effects on fracture reduction (37). ZA, for example, the most potent of all bisphosphonates, has an extremely high binding affinity for hydroxyapatite and is a major inhibitor of osteoclast-mediated bone resorption (127). Although bisphosphonates primary action is the inhibition of bone resorption, it is generally agreed that bisphosphonate-induced bone gain, rather than simply a suppression of loss, is the result of a reduction in remodeling space by the re-filling of resorption cavities and an increase in secondary mineralization

(128). In a rodent study, prophylactic ZA treatment (20 μg/kg body weight) completely prevented OVX-induced alterations in bone microarchitecture (129).

We cannot strictly compare our results to the latter studies, as our rats were male, were given a different dose of ZA (60 μg/kg body weight), and, most notably, were subjected to disuse rather than to gonadectomy. However, we also saw complete mass, density, and microarchitectural protection with a single dose of ZA. Our dose of 60 μg/kg body weight was chosen because it falls between the generally accepted low- and high-doses used in animal studies and is comparable to the clinical dose of a 4 mg infusion in humans. Furthermore, since bone loss with disuse occurs far more rapidly than with estrogen deficiency, we conjectured that typical low-dose OVX treatment may not suffice for our purposes. To our knowledge, this is the first study to investigate the efficacy of ZA, at any dose, in HU rats. ZA has been used, however, in mice subjected to two weeks of HU (111). Conn.D and BV/TV were both significantly reduced during HU in PBS-treated animals versus loaded controls. A single injection of 45 μg/kg body weight drastically increased Conn.D and BV/TV and blunted declines in cortical area and thickness. Similar to Lloyd et al.(111), the present study demonstrated that ZA therapy prevented unloading-induced alterations in architecture and structure.

Although ZA did improve densitometric and geometric properties beyond aging controls, it is not considered an anabolic therapy. Exercise, on the other hand, is considered anabolic, as it has been shown to be an osteogenic stimulus in both normal- and under-loaded conditions. Eight weeks of resistance exercise (1 hour of jumping every other day) significantly improves L5 and mid-diaphysis femur BMD in normally

loaded young rats (130). Exercise countermeasures applied during and after periods of disuse have also been investigated. Simulated resistance training (SRT) performed during 28 days of HU abolishes disuse-induced deterioration of total, cortical, and cancellous bone mass, density, and area (78). When executed after unloading, 10 jumps per day for two weeks restores cancellous architecture back to baseline levels (71). Our study is unusual in that it employed simulated exercise prior to, rather than during or after, a period of unloading. We conjectured that, by introducing exercise before HU, animals would initiate the unloading period with stronger bones than non-exercising counterparts and would be better protected from skeletal degradation.

According to our peak ground reaction force and pressure contour data, the hindlimbs of our rats during simulated exercise were loaded nearly twice that of the forelimbs, producing higher pressures at that site. Even with these higher loads, however, we failed to show significant gains in bone mass, density, and geometry after 35 days of drop training. These shortcomings are likely the result of declines in body weight in our Ex animals. According to Shapses et al., for every 10% drop in body mass, BMD declines by approximately 1% (131). When normalized to body weight (data not shown), however, total BMD was significantly higher in Ex versus non-Ex animals. Regardless of changes in body weight throughout the study, HU-induced bone loss in the PTM, FM, and DFM was mitigated in Ex animals.

While it was an attractive hypothesis to sequentially administer an osteogenic stimulus with an anti-resorptive bisphosphonate, this intervention did not produce additive benefits in all bone sites assessed. At the PTM and FN, for example, Ex+ZA

values were not significantly higher than either intervention alone. However, at the DFM, improvements in BV/TV, Conn.D, and SMI were greatest when Ex and ZA were applied in sequence. This site-specific response may be explained by different strain environments among bone sites. Although we do not have strain gauge data to support this claim, it is possible that deformations at the DFM produced a more favorable environment for osteogenesis. An alternate explanation may be in the imaging technique used. It is possible that the higher sensitivity of the μCT was capable of capturing subtle changes in microarchitecture at the DFM whereas pQCT was unable to detect these differences at the FN and PTM.

Comparisons of the present study with others using combination bisphosphonate and exercise treatments to counter bone loss should be made with caution. To begin, this is the first study to sequentially pre-treat HU rats with simulated exercise and ZA. Furthermore, the use of dissimilar bisphosphonates, exercise type, age/sex of animals, and timing of treatment make direct comparisons across studies hazardous. Nevertheless, it is important to consider these studies as the exercise-bisphosphonate interaction remains unclear. Stadelmann et al. demonstrated that singular treatments with 1) axial loading with no muscle contractions or 2) ZA therapy increased cortical bone area and perimeter, respectively, while loading-ZA combination therapy was additive in most sites (132). In areas of high strain measured at the tibia mid-shaft, however, the combined effect was significantly lower than the sum of the effects, suggesting an upper limit of mechanical loading benefits when administered with ZA. Although we do not have strain data, it is possible that during landing our

animals experienced mechanical strains in the PTM and FN beyond the aforementioned upper limit, thus preventing an additive response at those sites. Although we did not show greater rescue from HU-induced bone loss at the PTM and FN with sequential countermeasures compared to monotherapy, DFM bone mass was highest in Ex+ZA animals at the end of the study, suggesting greater protection from disuse than either intervention alone. This site-specific reaction has been shown by others, where regional differences in the response of the tibia and femur to treadmill running and the bisphosphonate etidronate exist (133).

A few clinical studies have also investigated the combined role of exercise and bisphosphonates, yet none have demonstrated combined benefits beyond either treatment alone (134-136). Chilibeck et al. performed a randomized trial investigating the combined effect of moderate intensity resistance training (three times per week for 45 minutes) and etidronate (administered for 12 months at a dose of 400 mg/day over 14 days) on bone health in postmenopausal women (134). Etidronate significantly improved whole body and lumbar spine BMD compared to placebo treated controls, yet no interactive or additive benefits where found in patients also exercising. Similar findings were shown by Uusi-Rasi et al. in a study of 164 postmenopausal women taking a daily dose of alendronate (5 mg) and physical exercise (136). Daily activity consisted of progressive jump exercises for 20 minutes plus 15 minutes of stretching. Alone, alendronate proved an effective countermeasure as it improved bone mass in the lumbar spine and femoral neck. While exercise heightened participants' muscular performance and balance, it had no effect on bone mass. Taken together, exercise did not enhance the

beneficial effects that were gained by alendronate therapy. The lack of interaction between exercise and bisphosphonates in the former two studies may be explained by the timing of interventions. Since bisphosphonates inherently reduce bone turnover, it is likely that the anabolic potential of exercise was blunted by the bisphosphonate, disallowing exercise-induced gains in bone mass. In a postmenopausal population similar in age and health status to those investigated by Uusi-Rasi et al., six months of high-impact jump exercise training significantly increased BMD in the lumbar spine and femoral neck compared to non-exercising controls (137). Thus, it is possible to accrue bone through exercise in osteopenia/osteoporosis patients past menopause. Results from our study advocate for clinical research investigating the sequential rather than concurrent use of exercise and bisphosphonates in patients suffering from low bone mass.

In this study, we focused on countermeasures to disuse-induced bone loss incurred via 28 days of hindlimb unloading in adult male rats. HU caused marked alterations in bone mass, density, and geometry at the PTM, FN, and DFM that was partially recovered with high-impact, free-fall mechanical loading and fully recovered with 60 μg/kg body weight of ZA. When administered sequentially, we saw a site-specific reaction to recovery. Whereas the PTM and FN did not experience additive benefits with Ex+ZA, microarchitecture values were highest at the DFM when exercise preceded ZA.

Biomechanical Properties

The most important biomechanics finding of this study was that our sequential prescription of high-impact mechanical loading followed by ZA protected against disuse-induced mechanical strength losses in adult rats more effectively than either treatment alone. HU caused marked reductions in mechanical properties at the FN and DFM that were partially rescued with monotherapy of Ex and ZA and completed prevented with the combination. Although we did not demonstrate HU- or treatment-induced strength changes at the femur diaphysis, these data are in accordance with μCT results at that site.

As demonstrated here, bone mass (quantity) was decreased with HU and salvaged with Ex and/or ZA treatment. According to the National Institute of Health, however, bone strength, and ultimately its susceptibility to fracture, is a function of both bone quantity and quality (138). While bone mass is intuitively understood and readily measurable using standard imaging techniques, bone quality is much more elusive and remains to be uniquely defined. One may consider bone quality to be a compound term which incorporates all aspects of bone strength apart from bone mass. For example, Felsenberg et al. developed the "bone quality framework," which explains bone quality as an umbrella term characterized by both structural properties (e.g., geometry and microarchitecture) and material properties (e.g., degree of mineralization and microdamage) (139). We have shown that bone geometry (PTM, cortical thickness) and microarchitecture (DFM, BV/TV) were negatively impacted by unloading and positively influenced by treatment. Here, we discuss bone material properties as determined by

estimates (finite element modeling) and by direct measurements (RPI, FN testing, and three-point bending) of bone strength.

Because of their two distinct mechanisms of action, namely the anabolic response that has been demonstrated via mechanical loading and the anti-catabolic characteristics of ZA, we investigated the interaction of these two treatments for the protection of disuse bone loss. We hypothesized that cotreatment would fully rescue HU-induced deteriorations in bone mass, microarchitecture, and strength. A similar concept has been explored clinically, where the anabolic therapy parathyroid hormone (PTH) was used in combination with various anti-resorptive bisphosphonates in postmenopausal women (140-143) and in aging men (144,145). Cosman et al. administered a single intravenous infusion of ZA (5 mg) with daily subcutaneous injections of teriparatide (recombinant human PTH (1-34), 20 μg) in postmenopausal women with osteoporosis and showed that the combination was superior to monotherapy at improving BMD in the hip and the spine (142). These results suggest that increases in bone mass were not disrupted by concomitant use of ZA. Alternatively, studies using alendronate in both men (144) and postmenopausal women (141) have revealed a blunting effect of alendronate when taken with PTH. That is, PTH treatment alone was more successful at augmenting hip and spine BMD than combined therapy. Inconsistences between these studies may be attributed to the type of bisphosphonate used or the timing in which treatments were administered. Since bisphosphonates reduce bone resorption by specifically targeting osteoclasts, bone turnover, because of coupling, reduces as well. Thus, when administered simultaneously, bisphosphonates

have the potential to reduce the anabolism of PTH. This concept was investigated in the PaTH (PTH + alendronate) study (140). Combining alendronate with PTH yielded no clear advantage over PTH alone, yet when taken sequentially, rather than concurrently, the effect was more beneficial than monotherapy, suggesting that anabolic treatment should be followed by an anti-resorptive. These findings are in accordance with ours, as the sequential combination of Ex and ZA rescued losses in mass, density, and microarchitecture beyond singular Ex or ZA.

In a follow-up study to PaTH, Keaveny and colleagues compared the effects of PTH and alendronate combinations on the femoral neck mechanical strength of 162 postmenopausal osteoporotic women (146). To determine strength, QCT images were converted to finite element models and virtually tested in a sideways fall configuration. Because bone strength and, ultimately, fracture risk are biomechanical phenomena, it is important to relate underlying treatment-induced changes in mass, density, and architecture to fracture risk. In this study, similar to previous densitometric PaTH findings, improvements in strength were more beneficial when alendronate followed PTH than in any other combination explored. These strength changes, however, were poorly correlated to BMD ($r^2 = 0.14$), demonstrating the importance of assessing bone quality beyond densitometry alone. Although this study is unique in that it is the first to clinically assess different treatment combinations using FEA, orthopaedic biomechanics research has utilized the finite element technique for decades (147). More recently, cadaver studies consistently demonstrated that FEA accurately predicts bone strength superior to DXA or QCT measurements of BMD (148-150). Another benefit of FEA is

its ability to discriminate between the individual roles of the cancellous and cortical compartments under loading. Twenty-eight days of HU significantly increased the ratio of cortical-cancellous loading in the present study, ultimately subjecting the cortex to higher stresses and a consequent greater probability of fracture at that site. Treatment with Ex or ZA alone returned load sharing values back to control levels while cotherapy surpassed them. Mechanical stiffness followed similar trends as load sharing, where sequential treatment was the most salubrious option tested. It is worth noting that differences in stiffness were largely underrepresented by changes in vBMD. That is, HU reductions in vBMD were half the magnitude of stiffness reductions. Similar findings in sclerostin antibody-treated mice were demonstrated with a comparable FEA load sharing technique (67). While FEA currently provides the best clinical estimation of mechanical strength, it remains limited by the fact that it does not directly incorporate tissue properties beyond radiological density. Thus, direct measurement of bone strength may be an important supplement to CT-derived FEA techniques.

Reference point indentation (RPI) is a direct measurement of bone material properties capable of being employed both *in vivo* and *ex vivo*. In our study, we investigated the *ex vivo* mechanical strength of the diaphysis femur. Neither HU nor treatment resulted in any significant changes in microindentation measurements. That is, we were not able to discriminate between loading status, simulated exercise, ZA, or the combination with RPI. These findings are consistent with cortical μCT results along the femur diaphysis. Since RPI inherently evaluates cortical bone only, it was not entirely surprising, based on the minimal changes in cortical densitometry at that site, that we did

not finding significant changes in any microindentation measurements. It is well known that cortical bone is less metabolically active than its cancellous counterpart. Thus, it is possible that neither HU nor treatment influenced femoral diaphysis cortical bone, even though both significantly affected metaphyseal cancellous bone. An alternative explanation could be that RPI was simply not sensitive enough to capture subtle changes among our groups. Since this is the first study to our knowledge to use *ex vivo* RPI in previously unloaded rats, we do not know if our findings are an aberration or if microindentation is indeed not capable of discriminating against subtle changes in unloaded rat femurs. RPI can, however, detect age-related changes in porcine femoral cortical bone (151). Indentation distance increase (IDI), total indentation distance (TID), and average unloading slope (US) all significantly decreased with age in 1- to 48-month old pigs. Because RPI is a relatively new technique, however, it remains to be determined how these variables relate to material properties as measured by traditional biomechanical testing. Compared to standard three-point bending data, US was found to be positively correlated to material stiffness and IDI to be negatively correlated to material toughness (90). Taking these findings to be accurate, IDI results from the former study conducted in pigs would indicate a decrease in material stiffness and an increase in material toughness with age (151). Whereas we did not find differences in IDI in ZA and non-ZA treated rats, Gallant et al. showed higher IDIs in alendronate versus vehicle treated dogs (90). These findings are consistent with the growing concern that long-term bisphosphonate use may deteriorate bone material properties, including toughness, which could lead to atypical femoral fractures (AFF).

Unlike "typical" femoral fractures, which are common in the femoral neck and intertrochanteric hip, AFFs occur with a short oblique orientation in the subtrochanteric and shaft regions of the femur with the radiographic appearance of a stress or fatigue fracture (152). Although registry studies have not found causation between subtrochanteric and femoral shaft fractures and bisphosphonate usage (153-155), and despite the occurrence of AFFs in bisphosphonate-naïve patients, collective evidence does suggest an association between long-term bisphosphonate use and AFFs. While the etiology of these atypical fractures remains unknown, a number of potential mechanisms have been suggested. To begin, because bisphosphonates reduce bone resorption, they inherently reduce bone turnover as a consequence, which in turn may lead to increased accumulation of skeletal microdamage. Although we did not show a decrease in bone toughness at the femoral neck in the present study, bisphosphonate-associated increases in microcracks can lead to decreased structural performance of bone (e.g., dog ribs), including mechanical toughness (156). Thus, insufficiency subtrochanteric and femoral shaft fractures may be explained by reductions in bone turnover inherent of long-term bisphosphonate treatment. It is worth noting, however, that bone remodeling doubles within 12 months of menopause, triples by age 60, and remains elevated if left untreated (157). Treatment with bisphosphonates reduces remodeling back to values within the range of healthy women prior to menopause (158). Although the occurrence of AFFs is rare, comprising less than 1% of all hip and femur fractures (152), some patients, such as those treated with glucocorticoids (GCs), are at an increased risk of both atypical and

typical femoral fractures (159). In fact, GC treated patients may benefit from a sequential, prophylactic treatment protocol rather than a reactive one.

The American College of Rheumatology estimates that 20% of all osteoporosis cases are due to the chronic (>6 months) use of GC medications (160). In fact, GC-induced osteoporosis is the most common form of drug-induced osteoporosis (161). Within the first five to seven months of GC therapy, bone volume declines by as much as 27% (162). This rapid loss of bone is over 20 times the rate of losses experienced by postmenopausal women, leaving patients at a heightened risk of spontaneous, and often asymptomatic, bone fracture. Bone fractures occur in as many as 30–50% of patients treated with GCs (163,164). Because of the high mortality rate of hip fractures in individuals over the age of 50 (24% within the first year of the fracture), it is critical for bone health to be closely monitored and evaluated for treatment before, during, and after GC therapy (165). However, less than one-half of patients receiving GC therapy are evaluated for osteoporosis and less than 14% actually receive treatment (166,167). Various treatment interventions have been explored in an effort to mitigate GC-induced osteoporosis. Still, over 97% of patients receiving GC therapy may experience significant bone loss and increased fracture risk (168).

Bisphosphonates are the current gold standard treatment option for GC-induced bone loss. Relative successes using bisphosphonate therapy as treatment for GC-induced bone loss have been shown. Use of bisphosphonates reduce the risk of GC-induced bone fracture in post-menopausal women (169). Furthermore, Braith et al. revealed that the combination of resistance exercise and bisphosphonate treatment

mitigated BMD losses in GC-treated lung transplant patients (170). However, treatment interventions (bisphosphonate and bisphosphonate plus resistance exercise) were not started until 3 and12 months after the initiation of GC therapy, respectively. Thomas et al. (169) note that after 3 months of GC therapy, before the initiation of bisphosphonate treatment, patients had already experienced significant bone loss. Patients in the latter study were already at an increased fracture risk as high as 50% at the initiation of bone loss treatment (163,164,170). Currently, there are no clinical pre-treatment prescriptions for GC-induced osteoporosis. Thus, it is imperative to treat GC patients proactively rather than reactively to prevent the consequentially rapid and deleterious bone loss from GC therapy. Although the impetus for bone loss is quite different between GCs and HU, the current study has important clinical implications that could shift the current practice of treating patients for GC-induced bone loss post therapy to a novel prophylactic modality.

We have demonstrated here that monotherapy with ZA or high impact Ex mitigated HU-induced declines in mechanical properties at the femoral neck and femoral metaphysis, while sequential cotreatment completely prevented them. Consistent with CT-derived declines in mass, density, and microarchitecture evaluated at the femur, 28 days of unloading caused marked declines in bone quality, such as stiffness and toughness, whereas pre-treatment with Ex and/or ZA rescued these losses. Our results are consistent with PaTH data suggesting that anabolic treatment should precede an anti-resorptive in order to maximize treatment efficacy. That is, we have shown that the timing of anabolic and anti-catabolic therapies is important for the prevention of bone

loss. This study has profound clinical implications as patients exposed to GCs may benefit from a prophylactic, rather than post-operative, therapy regimen to counter GC-induced fracture risk.

Bone Turnover: Systemic Resorption and Cortical Formation

The primary bone turnover findings in this study are threefold. First, cortical bone formation was drastically reduced with HU while markers of bone resorption were significantly enhanced. Second, ZA treatment did not further reduce formation but it did reduce resorption. Finally, we did not detect any effect of Ex on bone formation or resorption.

Both the structural and material properties of bone are affected by the rate at which bone is turned over. That is, bone remodeling plays an integral role in both the extrinsic and intrinsic characteristics of bone health. Spinal cord injury, long-term bed rest, and spaceflight each negatively alter bone turnover. In December 2001, the launch of 24 ten-week old mice on STS-108 marked an opportunity to investigate spaceflight-induced changes in bone turnover in rodents (171). Bone formation in flight mice, assessed by quantitative histomorphometry, was reduced up to 60% versus controls. Similar to what has been observed in rodents flown on shuttle missions, bone turnover is significantly altered in rodents exposed to HU (82). Twenty-one days of HU in 12-week-old female mice suppressed cancellous MAR (distal femur) by over 50% (67). In adult male rats, 28-day HU produced similar reductions in MS/BS, MAR, and BFR rate in proximal tibia cancellous bone (82). Similar decrements in bone formation on long bone diaphyseal surfaces have been shown in cortical bone on both periosteal and

endocortical surfaces (83). The present study demonstrated similarly drastic reductions in bone formation as a result of 28 days of HU. These BFR reductions, however, did not correspond to subsequent loss of mass, density, shape, or strength at that site. It is likely that if the HU were taken out for a longer period of time, reduced BFR would in turn reduce bone quality as well.

Surprisingly, increased mechanical loading in our Ex animals did not increase MS/BS, MAR, or BFR in mid-shaft tibia, nor did it mitigate HU-induced declines in these variables. We conjecture that the strain environment experienced in the diaphysis tibia of Ex animals surpassed the osteogenic threshold. That is, based on the theory of Harold Frost (172), it is possible that our loading paradigm over-strained the tibia beyond what would be experienced in physiological conditions, rendering it unsuccessful at enhancing bone formation at that site. Future studies may seek to investigate this hypothesis by using strain gauge measurements in drop-trained animals to quantify the precise strains experienced during landing. Our histomorphometric findings are consistent, however, with pQCT and strength measurements in the mid-shaft tibia where BFR was evaluated. BFR was measured in one other study which utilized a similar free-fall, high-impact drop training as in the present study (119). Lin et al. determined that short-term exposure to drop training increased ulna BFR approximately 80%, but hindlimb histomorphometry was not reported. Thus, our results should be considered with caution, as this is the first study to our knowledge to investigate hindlimb BFR in drop trained rodents. While Ex did not inhibit HU-induced losses in bone formation, ZA did not further reduce them. These findings are at odds with others,

as ZA administered to suspended mice further reduced bone formation (111). Differences between our study and Lloyd et al. may explain the conflicting results. To begin, the HU period in our study was twice the length of theirs. Thus, our longer HU regimen may have overpowered our ability to detect subtle ZA-induced BFR changes. Secondly, they used growing mice whereas we studied skeletally mature rats. It is possible that growing mice react differently to ZA and HU coupled treatment than adult rats.

Conflicting results exist for whether bone resorption increases in rodents in response to HU. Some studies report a doubling of the bone resorption marker TRAcP 5b following HU in skeletally mature mice (173), while others using young rats mark no change (75). A potential explanation for these discrepancies may be differences in animal weight changes during unloading. When animals do not gain weight, osteoclast number from HU is no different than controls (174,175). Conversely, when HU causes a gain in animal body weight, osteoclast activity is increased (176,177). Although HU caused a slight decrease in body weight in the present study, serum TRAcP 5b levels were elevated. HU studies consistently report dramatically suppressed bone formation without any corresponding drop in bone resorption. This uncoupling of formation and resorption in response to reduced mechanical loading inevitably leads to a net loss in bone mass and likely declines in bone quality. To combat this uncoupling, ZA treatment significantly reduced bone resorption in ZA+HU and Ex+ZA+HU animals. Uncoupled bone remodeling is of great interest to NASA, as long duration spaceflight has been

shown to increase bone degradation without subsequent increases in bone formation (25).

Addressing Key Concerns of the NASA Bone Summit

Spaceflight-induced bone loss is not a new phenomenon to the space program. In the early 1970s, data from Skylab revealed musculoskeletal losses and increased bone resorption during long-duration missions (178). Even with robust exercise equipment available on Mir, X-ray absorptiometry (DXA) measurements document rapid declines in BMD in the lower limbs, hip, and spine, as well as elevated resorption with nonsignifiant changes in formation (179). These findings extended to the International Space Station (ISS), where added exercise equipment, called the interim Resistive Exercise Device (iRED), was unable to prevent average monthly BMD losses of 2.3% in the total hip and even greater declines in estimated strength (180). To combat these losses, a similar, yet more sophisticated, machine called the Advanced Resistive Exercise Device (ARED) was placed on the ISS in 2008 (181). Unlike iRED, which was only capable of producing up to 300 pounds of resistive force, ARED produced twice that with the added benefit of user-friendly interfacing. With this new technology, spaceflight-induced bone degradation was significantly reduced (25). Concern remained, however, with heightened levels of in-flight markers of resorption. As an adjunctive countermeasure, NASA considered the use of an anti-resorptive bisphosphonate (alendronate) to be taken in conjunction with the 2.5 hours of currently prescribed daily exercise.

Very recent data from LeBlanc et al. show promising protection from almost all measures of bone mass, architecture, and strength losses, along with sustained in-flight levels of bone resorption (182). While encouraging, a major drawback of oral bisphosphonates, such as alendronate, is the adverse upper gastrointestinal (GI) effects that may be exaserbated in microgravity. Twenty percent (n=2 out of 10 astronauts) of the participants in this study were forced to withdraw from treatment because of GI issues. This contraindication was recognized by the NASA Bone Summit, a panel of experts at the Johnson Space Center (JSC), which convened in 2010 to discuss the adverse events of prolonged periods of microgravity and to make recommendations for in-flight treatment and post-flight surveillance based on the current long-duration astronaut database (183). For several listed reasons, the Summit recommended the use of an intravenous (IV) infusion of ZA administered prior to flight. To begin, ZA use is not associated with the adverse GI issues of their oral counterparts. Second, a pre-flight IV infusion of ZA would eliminate the need for weekly oral doses of alendronate while in flight. Finally, since ZA would be administered prior to flight, flight surgeons would be permitted to assess any drug side effects while crew members were still on Earth.

Due to these recommendations, the current study was designed in large part to answer key questions raised by the NASA Bone Summit. Carefully designed animal studies must be completed before NASA will make definitive recommendations for future missions aimed beyond low-Earth orbit. For the first time in the rat model, ZA was shown here to completely rescue disuse-induced alterations in bone mass, geometry, microarchitecture, and strength. Furthermore, it prevented increases in a marker of bone

degradation. Consistent with our hypothesis, sequential high-impact loading and ZA countermeasures completely protected against microarchitectural and strength losses. As NASA aims to embark on missions potentially lasting for up to 30 months (i.e., habitation of Mars), our study provides valuable data that could have large implications for important future treatment options for crew members.

This study is not without limitations. We did not subject fully weight bearing animals to Ex, ZA, or the combination. That is, only unloaded animals were provided treatment. Clinically, it would be beneficial to know whether the additional benefits of our sequential therapy translate to patients not removed from gravitational loading. Furthermore, as mentioned prior, strain on bone induced by our loading protocol was not quantified in this study, making predictions about site-specific strain environments during high-impact landing purely speculatory. Although limited, findings from this study demonstrate that a single injection of ZA was capable of rescuing disuse-induced a in bone mass, density, and strength, while preventing systemic increases in bone resorption without further suppressing cortical bone formation. When coupled with mechanical loading, Ex+ZA not only protected against the aforementioned losses, in some instances it facilitated gains in a site-specific manner.

CHAPTER V

CONCLUSION

In the present study, we found that monotherapy using either high-impact, free-fall simulated exercise or a single injection of ZA rescued adverse densitometric and microarchitectural changes associated with 28 days of HU. When administered together, our sequential regimen completely protected against these disuse-induced alterations in a site-specific manner. In the DFM, for example, combination treatment was superior to either alone. Measurements of bone strength were also assessed. Whereas neither loading status nor drug treatment altered material properties evaluated by RPI and three-point bending, μFE analysis was successful at discriminating against these differences. In terms of bone quality, densitometry appears to underestimate the reaction of bone measurements to unloading, overloading, and drug therapy. While we cannot definitely state which is superior, strength measurements via μFE analysis may be able to capture disuse effects on bone beyond current CT capabilities. Analysis of bone turnover through dynamic histomorphometry and serum TRAcP 5b was investigated to elucidate the effect of HU and treatment combinations on remodeling. HU amplified bone degradation without an associated increase in bone formation, suggesting an uncoupling of these two activities during disuse. ZA treatment effectively prevented inclines in bone resorption without affecting bone formation. Although Ex did not increase bone formation, when combined with ZA, it did provide greater protection at some sites than either treatment alone, suggesting some benefit beyond what was captured by BFR measurements.

Results from this study have both clinical and spaceflight applicability. GC-treated patients, for example, are left at an extremely high risk of bone fracture immediately following treatment. Although the modality of bone loss is quite different between disuse and GCs, our data could shift the current standards of treating GC-patients post-operation to a prophylactic regimen that would aim to prevent, rather than simply treat, GC-induce bone loss. In line with the NASA Bone Summit recommendations for future treatment options for long-duration astronauts, and in response to their call for carefully designed animals experiments to test these options, our study may be used to help guide flight surgeons on the potential use of ZA and exercise to counter spaceflight-induced increased fracture risk and premature osteoporosis.

REFERENCES

1. Cowin SC 2001 Bone Mechancis Handbook. CRC Press, Boca Raton, FL.

2. Favus MJ 2003 Primer on the Metabolic Bone Diseases and Disorders of Mineral Metabolism. John Wiley & Sons, Hoboken, NJ.

3. Currey JD 2002 Bones: Structure and Mechanics. Princeton Press, Princeton, NJ.

4. Shier D 2007 Hole's Human Anatomy & Physiology. McGraw-Hill, New York, NY.

5. SEER Training Module, Structure of Bone Tissue, U. S. National Institutes of Health, National Cancer Institute. Retrieved December 2, 2013 from http://training.seer.cancer.gov/anatomy/skeletal/tissue.html.

6. The National Osteoporosis Foundation, Break Free from Osteoporosis. Retrieved February 13, 2012 from http://nof.org.

7. Bekker PJ, Holloway D, Nakanishi A, Arrighi M, Leese PT, Dunstan CR 2001 The effect of a single dose of osteoprotegerin in postmenopausal women. J Bone Miner Res **16**(2)**:**348-60.

8. Suzuki A, Sekiguchi S, Asano S, Itoh M 2008 Pharmacological topics of bone metabolism: recent advances in pharmacological management of osteoporosis. J Pharmacol Sci **106**(4)**:**530-5.

9. Clarke B 2008 Normal bone anatomy and physiology. Clin J Am Soc Nephrol **3:**S131-9.

10. Lacey DL, Timms E, Tan HL, Kelley MJ, Dunstan CR, Burgess T, Elliott R, Colombero A, Elliott G, Scully S, Hsu H, Sullivan J, Hawkins N, Davy E, Capparelli C, Eli A, Qian YX, Kaufman S, Sarosi I, Shalhoub V, Senaldi G, Guo J, Delaney J, Boyle WJ 1998 Osteoprotegerin ligand is a cytokine that regulates osteoclast differentiation and activation. Cell **93**(2)**:**165-76.

11. Pietschmann P, Rauner M, Sipos W, Kerschan-Schindl K 2008 Osteoporosis: an age-related and gender-specific disease--a mini-review. Gerontology **55**(1)**:**3-12.

12. Amgen Bone Academy, Retrieved June 5, 2009 from http://www.boneacademy.com/bone-loss-conditions/biology-of-bone-loss.html.

13. Coxon JP, Oades GM, Colston KW, Kirby RS 2004 Advances in the use of bisphosphonates in the prostate cancer setting. Prostate Cancer Prostatic Dis **7**(2)**:**99-104.

14. Simonet WS, Lacey DL, Dunstan CR, Kelley M, Chang MS, Luthy R, Nguyen HQ, Wooden S, Bennett L, Boone T, Shimamoto G, DeRose M, Elliott R, Colombero A, Tan HL, Trail G, Sullivan J, Davy E, Bucay N, Renshaw-Gegg L, Hughes TM, Hill D, Pattison W, Campbell P, Sander S, Van G, Tarpley J, Derby P, Lee R, Boyle WJ 1997 Osteoprotegerin: a novel secreted protein involved in the regulation of bone density. Cell **89**(2)**:**309-19.

15. Rikhotso E, Reyneke JP, Ferretti C 2008 Osteopetrosis: literature review and report of three cases. SADJ **63**(5)**:**302-7.

16. Pietschmann P, Rauner M, Sipos W, Kerschan-Schindl K 2009 Osteoporosis: an age-related and gender-specific disease--a mini-review. Gerontology **55**(1):3-12.

17. Frost HM 1998 From Wolff's law to the mechanostat: a new "face" of physiology. J Orthop Sci **3**(5):282-6.

18. Frost HM 2000 The Utah paradigm of skeletal physiology: an overview of its insights for bone, cartilage and collagenous tissue organs. J Bone Miner Metab **18**(6)**:**305-16.

19. Frost HM 1964 The Laws of Bone Structure. CC Thomas, Springfield, MI.

20. Frost HM 1987 Bone "mass" and the "mechanostat": a proposal. Anat Rec **219**(1)**:**1-9.

21. Garland DE, Stewart CA, Adkins RH, Hu SS, Rosen C, Liotta FJ, Weinstein DA 1992 Osteoporosis after spinal cord injury. J Orthop Res **10**(3)**:**371-8.

22. Zerwekh JE, Ruml LA, Gottschalk F, Pak CY 1998 The effects of twelve weeks of bed rest on bone histology, biochemical markers of bone turnover, and calcium homeostasis in eleven normal subjects. J Bone Miner Res **13**(10)**:**1594-601.

23. Shirazi-Fard Y 2013 Discordant recovery of bone mass and mechanical properties during prolonged recovery from disuse. Bone **52:**433-443.

24. Giangregorio L, Blimkie CJ 2002 Skeletal adaptations to alterations in weight-bearing activity: a comparison of models of disuse osteoporosis. Sports Med **32**(7)**:**459-76.

25. Smith SM, Heer MA, Shackelford LC, Sibonga JD, Ploutz-Snyder L, Zwart SR 2012 Benefits for bone from resistance exercise and nutrition in long-duration spaceflight: Evidence from biochemistry and densitometry. J Bone Miner Res **27**(9)**:**1896-906.

26. Allen MR, Hogan HA, Bloomfield SA 2006 Differential bone and muscle recovery following hindlimb unloading in skeletally mature male rats. J Musculoskelet Neuronal Interact **6**(3)**:**217-25.

27. Daly RM, Saxon L, Turner CH, Robling AG, Bass SL 2004 The relationship between muscle size and bone geometry during growth and in response to exercise. Bone **34**(2)**:**281-7.

28. Qin YX, Lam H, Ferreri S, Rubin C Dynamic skeletal muscle stimulation and its potential in bone adaptation. J Musculoskelet Neuronal Interact **10**(1)**:**12-24.

29. Swift JM, Nilsson MI, Hogan HA, Sumner LR, Bloomfield SA Simulated resistance training during hindlimb unloading abolishes disuse bone loss and maintains muscle strength. J Bone Miner Res **25**(3)**:**564-74.

30. Colletti LA, Edwards J, Gordon L, Shary J, Bell NH 1989 The effects of muscle-building exercise on bone mineral density of the radius, spine, and hip in young men. Calcif Tissue Int **45**(1)**:**12-4.

31. Turner CH 2000 Muscle-bone interactions, revisited. Bone **27**(3)**:**339-40.

32. Bass SL, Naughton G, Saxon L, Iuliano-Burns S, Daly R, Briganti EM, Hume C, Nowson C 2007 Exercise and calcium combined results in a greater osteogenic effect than either factor alone: a blinded randomized placebo-controlled trial in boys. J Bone Miner Res **22**(3)**:**458-64.

33. Linden C, Ahlborg HG, Besjakov J, Gardsell P, Karlsson MK 2006 A school curriculum-based exercise program increases bone mineral accrual and bone size in prepubertal girls: two-year data from the pediatric osteoporosis prevention (POP) study. J Bone Miner Res **21**(6)**:**829-35.

34. Engelke K, Kemmler W, Lauber D, Beeskow C, Pintag R, Kalender WA 2006 Exercise maintains bone density at spine and hip EFOPS: a 3-year longitudinal study in early postmenopausal women. Osteoporos Int **17**(1)**:**133-42.

35. Papapoulos SE 2008 Bisphosphonates: how do they work? Best Pract Res Clin Endocrinol Metab **22**(5)**:**831-47.

36. Rogers MJ 2003 New insights into the molecular mechanisms of action of bisphosphonates. Curr Pharm Des **9**(32)**:**2643-58.

37. Russell RG, Watts NB, Ebetino FH, Rogers MJ 2008 Mechanisms of action of bisphosphonates: similarities and differences and their potential influence on clinical efficacy. Osteoporos Int **19**(6)**:**733-59.

38. Gasser JA, Ingold P, Venturiere A, Shen V, Green JR 2008 Long-term protective effects of zoledronic acid on cancellous and cortical bone in the ovariectomized rat. J Bone Miner Res **23**(4)**:**544-51.

39. Black DM, Delmas PD, Eastell R, Reid IR, Boonen S, Cauley JA, Cosman F, Lakatos P, Leung PC, Man Z, Mautalen C, Mesenbrink P, Hu H, Caminis J, Tong K, Rosario-Jansen T, Krasnow J, Hue TF, Sellmeyer D, Eriksen EF, Cummings SR, Trial HPF 2007 Once-yearly zoledronic acid for treatment of postmenopausal osteoporosis. N Engl J Med **356**(18)**:**1809-22.

40. Papapoulos SE 2008 Primer on the Metabolic Bone Diseases and Disorders of Mineral Metabolism. John Wiley & Sons, Hoboken, NJ.

41. Cohen A, Lang TF, McMahon DJ, Liu XS, Guo XE, Zhang C, Stein EM, Dempster DW, Young P, Saeed I, Lappe JM, Recker RR, Shane E 2012 Central QCT reveals lower volumetric BMD and stiffness in premenopausal women with idiopathic osteoporosis, regardless of fracture history. J Clin Endocrinol Metab **97**(11)**:**4244-52.

42. Graeff C, Marin F, Petto H, Kayser O, Reisinger A, Pena J, Zysset P, Gluer CC 2013 High resolution quantitative computed tomography-based assessment of trabecular microstructure and strength estimates by finite-element analysis of the spine, but not DXA, reflects vertebral fracture status in men with glucocorticoid-induced osteoporosis. Bone **52**(2)**:**568-77.

43. Liu X, Lei W, Wu Z, Cui Y, Han B, Fu S, Jiang C 2012 Effects of glucocorticoid on BMD, micro-architecture and biomechanics of cancellous and cortical bone mass in OVX rabbits. Med Eng Phys **34**(1)**:**2-8.

44. Adams JE 2012 Advances in bone imaging for osteoporosis. Nat Rev Endocrinol **9**(1)**:**28-42.

45. Black DM, Bouxsein ML, Marshall LM, Cummings SR, Lang TF, Cauley JA, Ensrud KE, Nielson CM, Orwoll ES, Osteoporotic Fractures in Men Research G 2008 Proximal femoral structure and the prediction of hip fracture in men: a large prospective study using QCT. J Bone Miner Res **23**(8)**:**1326-33.

46. Cheng X, Li J, Lu Y, Keyak J, Lang T 2007 Proximal femoral density and geometry measurements by quantitative computed tomography: association with hip fracture. Bone **40**(1)**:**169-74.

47. Gluer CC, Cummings SR, Pressman A, Li J, Gluer K, Faulkner KG, Grampp S, Genant HK 1994 Prediction of hip fractures from pelvic radiographs: the study of osteoporotic fractures. The Study of Osteoporotic Fractures Research Group. J Bone Miner Res **9**(5)**:**671-7.

48. Kang Y, Engelke K, Fuchs C, Kalender WA 2005 An anatomic coordinate system of the femoral neck for highly reproducible BMD measurements using 3D QCT. Comput Med Imaging Graph **29**(7)**:**533-41.

49. Lang T, LeBlanc A, Evans H, Lu Y, Genant H, Yu A 2004 Cortical and trabecular bone mineral loss from the spine and hip in long-duration spaceflight. J Bone Miner Res **19**(6)**:**1006-12.

50. Lang TF, Keyak JH, Heitz MW, Augat P, Lu Y, Mathur A, Genant HK 1997 Volumetric quantitative computed tomography of the proximal femur: precision and relation to bone strength. Bone **21**(1)**:**101-8.

51. Li W, Kezele I, Collins DL, Zijdenbos A, Keyak J, Kornak J, Koyama A, Saeed I, Leblanc A, Harris T, Lu Y, Lang T 2007 Voxel-based modeling and quantification of the proximal femur using inter-subject registration of quantitative CT images. Bone **41**(5)**:**888-95.

52. Damilakis J, Adams JE, Guglielmi G, Link TM 2010 Radiation exposure in X-ray-based imaging techniques used in osteoporosis. Eur Radiol **20**(11)**:**2707-14.

53. Engelke K, Adams JE, Armbrecht G, Augat P, Bogado CE, Bouxsein ML, Felsenberg D, Ito M, Prevrhal S, Hans DB, Lewiecki EM 2008 Clinical use of quantitative computed tomography and peripheral quantitative computed tomography in the management of osteoporosis in adults: the 2007 ISCD Official Positions. J Clin Densitom **11**(1)**:**123-62.

54. Genant HK, Engelke K, Prevrhal S 2008 Advanced CT bone imaging in osteoporosis. Rheumatology (Oxford) **4:**iv9-16.

55. Bouxsein ML, Boyd SK, Christiansen BA, Guldberg RE, Jepsen KJ, Muller R 2010 Guidelines for assessment of bone microstructure in rodents using micro-computed tomography. J Bone Miner Res **25**(7)**:**1468-86.

56. Ellman R, Spatz J, Cloutier A, Palme R, Christiansen BA, Bouxsein ML 2013 Partial reductions in mechanical loading yield proportional changes in bone density, bone architecture, and muscle mass. J Bone Miner Res **28**(4):875-85.

57. Spatz JM, Ellman R, Cloutier AM, Louis L, van Vliet M, Suva LJ, Dwyer D, Stolina M, Ke HZ, Bouxsein ML 2013 Sclerostin antibody inhibits skeletal deterioration due to reduced mechanical loading. J Bone Miner Res **28**(4):865-74.

58. Waarsing JH, Day JS, van der Linden JC, Ederveen AG, Spanjers C, De Clerck N, Sasov A, Verhaar JA, Weinans H 2004 Detecting and tracking local changes

in the tibiae of individual rats: a novel method to analyse longitudinal in vivo micro-CT data. Bone **34**(1)**:**163-9.

59. Klinck RJ, Campbell GM, Boyd SK 2008 Radiation effects on bone architecture in mice and rats resulting from in vivo micro-computed tomography scanning. Med Eng Phys **30**(7)**:**888-95.

60. Laib A, Hildebrand T, Hauselmann HJ, Ruegsegger P 1997 Ridge number density: a new parameter for in vivo bone structure analysis. Bone **21**(6)**:**541-6.

61. Armbrecht G, Belavy DL, Backstrom M, Beller G, Alexandre C, Rizzoli R, Felsenberg D 2011 Trabecular and cortical bone density and architecture in women after 60 days of bed rest using high-resolution pQCT: WISE 2005. J Bone Miner Res **26**(10)**:**2399-410.

62. Ausk BJ, Huber P, Poliachik SL, Bain SD, Srinivasan S, Gross TS 2012 Cortical bone resorption following muscle paralysis is spatially heterogeneous. Bone **50**(1)**:**14-22.

63. Coupaud S, McLean AN, Allan DB 2009 Role of peripheral quantitative computed tomography in identifying disuse osteoporosis in paraplegia. Skeletal Radiol **38**(10)**:**989-95.

64. Manske SL, Boyd SK, Zernicke RF 2010 Muscle and bone follow similar temporal patterns of recovery from muscle-induced disuse due to botulinum toxin injection. Bone **46**(1)**:**24-31.

65. Sheng ZF, Ma YL, Tong D, Fang DY, Liang QC, Liu LH, Zhang J, Liao EY 2012 Strontium ranelate prevents bone loss in a rat model of localized muscle paralysis. Ann Biomed Eng **40**(3)**:**657-65.

66. Shirazi-Fard Y, Kupke JS, Bloomfield SA, Hogan HA 2013 Discordant recovery of bone mass and mechanical properties during prolonged recovery from disuse. Bone **52**(1)**:**433-43.

67. Spatz JM, Ellman R, Cloutier AM, Louis L, van Vliet M, Suva LJ, Dwyer D, Stolina M, Ke HZ, Bouxsein ML 2013 Sclerostin antibody inhibits skeletal deterioration due to reduced mechanical loading. J Bone Miner Res **28**(4)**:**865-74.

68. Swift JM, Lima F, Macias BR, Allen MR, Greene ES, Shirazi-Fard Y, Kupke JS, Hogan HA, Bloomfield SA 2013 Partial Weightbearing Does Not Prevent Musculoskeletal Losses Associated with Disuse. Med Sci Sports Exerc **45**(11):2052-60.

69. Bloomfield SA, Girten BE, Weisbrode SE 1997 Effects of vigorous exercise training and beta-agonist administration on bone response to hindlimb suspension. J Appl Physiol **83**(1)**:**172-8.

70. Fluckey JD, Dupont-Versteegden EE, Montague DC, Knox M, Tesch P, Peterson CA, Gaddy-Kurten D 2002 A rat resistance exercise regimen attenuates losses of musculoskeletal mass during hindlimb suspension. Acta Physiol Scand **176**(4)**:**293-300.

71. Ju YI, Sone T, Ohnaru K, Choi HJ, Choi KA, Fukunaga M 2013 Jump exercise during hindlimb unloading protect against the deterioration of trabecular bone microarchitecture in growing young rats. Springerplus **2**(1)**:**35.

72. Ju YI, Sone T, Ohnaru K, Choi HJ, Fukunaga M 2012 Differential effects of jump versus running exercise on trabecular architecture during remobilization after suspension-induced osteopenia in growing rats. J Appl Physiol **112**(5)**:**766-72.

73. Ju YI, Sone T, Okamoto T, Fukunaga M 2008 Jump exercise during remobilization restores integrity of the trabecular architecture after tail suspension in young rats. J Appl Physiol **104**(6)**:**1594-600.

74. Lam H, Qin YX 2008 The effects of frequency-dependent dynamic muscle stimulation on inhibition of trabecular bone loss in a disuse model. Bone **43**(6)**:**1093-100.

75. Li Z, Tan C, Wu Y, Ding Y, Wang H, Chen W, Zhu Y, Ma H, Yang H, Liang W, Jiang S, Wang D, Wang L, Tang G, Wang J 2012 Whole-body vibration and resistance exercise prevent long-term hindlimb unloading-induced bone loss: independent and interactive effects. Eur J Appl Physiol **112**(11)**:**3743-53.

76. Midura RJ, Dillman CJ, Grabiner MD 2005 Low amplitude, high frequency strains imposed by electrically stimulated skeletal muscle retards the development of osteopenia in the tibiae of hindlimb suspended rats. Med Eng Phys **27**(4)**:**285-93.

77. Shimano MM, Volpon JB 2009 Biomechanics and structural adaptations of the rat femur after hindlimb suspension and treadmill running. Braz J Med Biol Res **42**(4)**:**330-8.

78. Swift JM, Nilsson MI, Hogan HA, Sumner LR, Bloomfield SA 2010 Simulated resistance training during hindlimb unloading abolishes disuse bone loss and maintains muscle strength. J Bone Miner Res **25**(3)**:**564-74.

79. Yang P, Jia B, Ding C, Wang Z, Qian A, Shang P 2009 Whole-body vibration effects on bone before and after hind-limb unloading in rats. Aviat Space Environ Med **80**(2)**:**88-93.

80. Yarrow JF, McCoy SC, Ferreira JA, Pingel JE, Conrad BP, Wronski TJ, Williams AA, Borst SE, Brown M 2012 A rehabilitation exercise program induces severe bone mineral deficits in estrogen-deficient rats after extended disuse. Menopause **19**(11)**:**1267-76.

81. Carpenter RD 2010 Long-term changes in the density and structure of the human hip and spine after long-duration spaceflight. Acta Astronautica **67:**71-81.

82. Swift JM, Swift SN, Nilsson MI, Hogan HA, Bouse SD, Bloomfield SA 2011 Cancellous bone formation response to simulated resistance training during disuse is blunted by concurrent alendronate treatment. J Bone Miner Res **26**(9)**:**2140-50.

83. Macias BR, Swift JM, Nilsson MI, Hogan HA, Bouse SD, Bloomfield SA 2012 Simulated resistance training, but not alendronate, increases cortical bone formation and suppresses sclerostin during disuse. J Appl Physiol **112**(5)**:**918-25.

84. Bronzino JD, Neuman MR, Onaral B, Webster J 1995 The Biomedical Engineering Handbook. CRC Press, Boca Raton, FL.

85. Turner CH, Burr DB 1993 Basic biomechanical measurements of bone: a tutorial. Bone **14**(4)**:**595-608.

86. Allen MR, Chen NX, Gattone VH, 2nd, Chen X, Carr AJ, LeBlanc P, Brown D, Moe SM 2013 Skeletal effects of zoledronic acid in an animal model of chronic kidney disease. Osteoporos Int **24**(4)**:**1471-81.

87. Brouwers JE, Ruchelsman M, Rietbergen B, Bouxsein ML 2009 Determination of rat vertebral bone compressive fatigue properties in untreated intact rats and zoledronic-acid-treated, ovariectomized rats. Osteoporos Int **20**(8)**:**1377-84.

88. Diez-Perez A, Guerri R, Nogues X, Caceres E, Pena MJ, Mellibovsky L, Randall C, Bridges D, Weaver JC, Proctor A, Brimer D, Koester KJ, Ritchie RO, Hansma PK 2010 Microindentation for in vivo measurement of bone tissue mechanical properties in humans. J Bone Miner Res **25**(8)**:**1877-85.

89. Fonseca H, Moreira-Goncalves D, Esteves JL, Viriato N, Vaz M, Mota MP, Duarte JA 2011 Voluntary exercise has long-term in vivo protective effects on osteocyte viability and bone strength following ovariectomy. Calcif Tissue Int **88**(6)**:**443-54.

90. Gallant MA, Brown DM, Organ JM, Allen MR, Burr DB 2013 Reference-point indentation correlates with bone toughness assessed using whole-bone traditional mechanical testing. Bone **53**(1)**:**301-5.

91. Voor MJ, Brown EH, Xu Q, Waddell SW, Burden RL, Jr., Burke DA, Magnuson DS 2012 Bone loss following spinal cord injury in a rat model. J Neurotrauma **29**(8)**:**1676-82.

92. Macintyre NJ, Lorbergs AL 2012 Imaging-Based Methods for Non-invasive Assessment of Bone Properties Influenced by Mechanical Loading. Physiother Can **64**(2)**:**202-15.

93. Winter W, Klein D, Karl M 2013 Effect of model parameters on finite element analysis of micromotions in implant dentistry. J Oral Implantol **39**(1)**:**23-9.

94. Lang TF 2010 Quantitative computed tomography. Radiol Clin North Am **48**(3)**:**589-600.

95. Keyak JH, Kaneko TS, Tehranzadeh J, Skinner HB 2005 Predicting proximal femoral strength using structural engineering models. Clin Orthop Relat Res (437)**:**219-28.

96. Keyak JH, Falkinstein Y 2003 Comparison of in situ and in vitro CT scan-based finite element model predictions of proximal femoral fracture load. Med Eng Phys **25**(9)**:**781-7.

97. Dempster DW, Compston JE, Drezner MK, Glorieux FH, Kanis JA, Malluche H, Meunier PJ, Ott SM, Recker RR, Parfitt AM 2013 Standardized nomenclature, symbols, and units for bone histomorphometry: a 2012 update of the report of the ASBMR Histomorphometry Nomenclature Committee. J Bone Miner Res **28**(1)**:**2-17.

98. Iwamoto J, Yeh JK, Aloia JF 2000 Effect of deconditioning on cortical and cancellous bone growth in the exercise trained young rats. J Bone Miner Res **15**(9)**:**1842-9.

99. Gerdhem P, Ivaska KK, Alatalo SL, Halleen JM, Hellman J, Isaksson A, Pettersson K, Vaananen HK, Akesson K, Obrant KJ 2004 Biochemical markers of bone metabolism and prediction of fracture in elderly women. J Bone Miner Res **19**(3)**:**386-93.

100. Rissanen JP, Suominen MI, Peng Z, Halleen JM 2008 Secreted tartrate-resistant acid phosphatase 5b is a Marker of osteoclast number in human osteoclast cultures and the rat ovariectomy model. Calcif Tissue Int **82**(2)**:**108-15.

101. Lamp EC, Drexler HG 2000 Biology of tartrate-resistant acid phosphatase. Leuk Lymphoma **39**(5-6)**:**477-84.

102. Angel NZ, Walsh N, Forwood MR, Ostrowski MC, Cassady AI, Hume DA 2000 Transgenic mice overexpressing tartrate-resistant acid phosphatase exhibit an increased rate of bone turnover. J Bone Miner Res **15**(1)**:**103-10.

103. Allen MR, Burr DB 2011 Bisphosphonate effects on bone turnover, microdamage, and mechanical properties: what we think we know and what we know that we don't know. Bone **49**(1)**:**56-65.

104. Recker RR, Delmas PD, Halse J, Reid IR, Boonen S, Garcia-Hernandez PA, Supronik J, Lewiecki EM, Ochoa L, Miller P, Hu H, Mesenbrink P, Hartl F, Gasser J, Eriksen EF 2008 Effects of intravenous zoledronic acid once yearly on bone remodeling and bone structure. J Bone Miner Res **23**(1)**:**6-16.

105. Honda A, Sogo N, Nagasawa S, Shimizu T, Umemura Y 2003 High-impact exercise strengthens bone in osteopenic ovariectomized rats with the same outcome as Sham rats. J Appl Physiol **95**(3)**:**1032-7.

106. Judex S, Zernicke RF 2000 High-impact exercise and growing bone: relation between high strain rates and enhanced bone formation. J Appl Physiol **88**(6)**:**2183-91.

107. Nagasawa S, Honda A, Sogo N, Umemura Y 2008 Effects of low-repetition jump exercise on osteogenic response in rats. J Bone Miner Metab **26**(3)**:**226-30.

108. Swift JM, Gasier HG, Swift SN, Wiggs MP, Hogan HA, Fluckey JD, Bloomfield SA 2010 Increased training loads do not magnify cancellous bone gains with rodent jump resistance exercise. J Appl Physiol **109**(6)**:**1600-7.

109. Westerlind KC, Fluckey JD, Gordon SE, Kraemer WJ, Farrell PA, Turner RT 1998 Effect of resistance exercise training on cortical and cancellous bone in mature male rats. J Appl Physiol **84**(2)**:**459-64.

110. Kodama Y, Nakayama K, Fuse H, Fukumoto S, Kawahara H, Takahashi H, Kurokawa T, Sekiguchi C, Nakamura T, Matsumoto T 1997 Inhibition of bone resorption by pamidronate cannot restore normal gain in cortical bone mass and strength in tail-suspended rapidly growing rats. J Bone Miner Res **12**(7)**:**1058-67.

111. Lloyd SA, Travis ND, Lu T, Bateman TA 2008 Development of a low-dose anti-resorptive drug regimen reveals synergistic suppression of bone formation when coupled with disuse. J Appl Physiol **104**(3)**:**729-38.

112. Feher A, Koivunemi A, Koivunemi M, Fuchs RK, Burr DB, Phipps RJ, Reinwald S, Allen MR 2010 Bisphosphonates do not inhibit periosteal bone formation in estrogen deficient animals and allow enhanced bone modeling in response to mechanical loading. Bone **46**(1)**:**203-7.

113. Fuchs RK, Shea M, Durski SL, Winters-Stone KM, Widrick J, Snow CM 2007 Individual and combined effects of exercise and alendronate on bone mass and strength in ovariectomized rats. Bone **41**(2)**:**290-6.

114. Grigoriev AI, Morukov BV, Oganov VS, Rakhmanov AS, Buravkova LB 1992 Effect of exercise and bisphosphonate on mineral balance and bone density during 360 day antiorthostatic hypokinesia. J Bone Miner Res **2:**S449-55.

115. Braith RW, Conner JA, Fulton MN, Lisor CF, Casey DP, Howe KS, Baz MA 2007 Comparison of alendronate vs alendronate plus mechanical loading as prophylaxis for osteoporosis in lung transplant recipients: a pilot study. J Heart Lung Transplant **26**(2)**:**132-7.

116. LeBlanc A 2011 Antiresorptive treatment for spaceflight induced bone atrophy: preliminary results from ASBMR 33rd Annual Meeting, San Diego, CA.

117. Welch JM, Turner CH, Devareddy L, Arjmandi BH, Weaver CM 2008 High impact exercise is more beneficial than dietary calcium for building bone strength in the growing rat skeleton. Bone **42**(4)**:**660-8.

118. Welch JM, Weaver CM, Turner CH 2004 Adaptations to free-fall impact are different in the shafts and bone ends of rat forelimbs. J Appl Physiol **97**(5)**:**1859-65.

119. Hsin-Shih Lin T-HH, Shih-Wei Mao, Yuh-Shiou Tai, Hung-Ta Chiu, Kuang-You B. Cheng, Rong-Sen Yang 2011 A short-term free-fall landing enhances boen formation and bone material properties. J. Mech. Med. Biol **11**(5)**:**1125-1139.

120. Morey-Holton E, Globus RK, Kaplansky A, Durnova G 2005 The hindlimb unloading rat model: literature overview, technique update and comparison with space flight data. Adv Space Biol Med **10:**7-40.

121. Morey-Holton ER, Globus RK 2002 Hindlimb unloading rodent model: technical aspects. J Appl Physiol **92**(4)**:**1367-77.

122. Morey-Holton ER, Globus RK 1998 Hindlimb unloading of growing rats: a model for predicting skeletal changes during space flight. Bone **22**(5 Suppl)**:**83S-88S.

123. Bloomfield SA, Allen MR, Hogan HA, Delp MD 2002 Site- and compartment-specific changes in bone with hindlimb unloading in mature adult rats. Bone **31**(1)**:**149-57.

124. Gallant MA, Brown DM, Organ JM, Allen MR, Burr DB 2013 Reference-point indentation correlates with bone toughness assessed using whole-bone traditional mechanical testing. Bone **53**(1):301-5.

125. Aref M, Gallant MA, Organ JM, Wallace JM, Newman CL, Burr DB, Brown DM, Allen MR 2013 In vivo reference point indentation reveals positive effects of raloxifene on mechanical properties following 6months of treatment in skeletally mature beagle dogs. Bone **56**(2)**:**449-53.

126. Parfitt AM, Drezner MK, Glorieux FH, Kanis JA, Malluche H, Meunier PJ, Ott SM, Recker RR 1987 Bone histomorphometry: standardization of nomenclature, symbols, and units. Report of the ASBMR Histomorphometry Nomenclature Committee. J Bone Miner Res **2**(6)**:**595-610.

127. Green JR, Muller K, Jaeggi KA 1994 Preclinical pharmacology of CGP 42'446, a new, potent, heterocyclic bisphosphonate compound. J Bone Miner Res **9**(5)**:**745-51.

128. Gasser JA 2006 The relative merits of anabolics versus anti-resorptive compounds: where our targets should be, and whether we are addressing them. Curr Opin Pharmacol **6**(3)**:**313-8.

129. Brouwers JE, Lambers FM, Gasser JA, van Rietbergen B, Huiskes R 2008 Bone degeneration and recovery after early and late bisphosphonate treatment of ovariectomized wistar rats assessed by in vivo micro-computed tomography. Calcif Tissue Int **82**(3)**:**202-11.

130. Notomi T, Lee SJ, Okimoto N, Okazaki Y, Takamoto T, Nakamura T, Suzuki M 2000 Effects of resistance exercise training on mass, strength, and turnover of bone in growing rats. Eur J Appl Physiol **82**(4)**:**268-74.

131. Shapses SA, Riedt CS 2006 Bone, body weight, and weight reduction: what are the concerns? J Nutr **136**(6)**:**1453-6.

132. Stadelmann VA, Bonnet N, Pioletti DP 2011 Combined effects of zoledronate and mechanical stimulation on bone adaptation in an axially loaded mouse tibia. Clin Biomech (Bristol, Avon) **26**(1)**:**101-5.

133. Tamaki H, Akamine T, Goshi N, Kurata H, Sakou T 1998 Effects of exercise training and etidronate treatment on bone mineral density and trabecular bone in ovariectomized rats. Bone **23**(2)**:**147-53.

134. Chilibeck PD, Davison KS, Whiting SJ, Suzuki Y, Janzen CL, Peloso P 2002 The effect of strength training combined with bisphosphonate (etidronate) therapy on bone mineral, lean tissue, and fat mass in postmenopausal women. Can J Physiol Pharmacol **80**(10)**:**941-50.

135. Rittweger J, Frost HM, Schiessl H, Ohshima H, Alkner B, Tesch P, Felsenberg D 2005 Muscle atrophy and bone loss after 90 days' bed rest and the effects of flywheel resistive exercise and pamidronate: results from the LTBR study. Bone **36**(6)**:**1019-29.

136. Uusi-Rasi K, Kannus P, Cheng S, Sievanen H, Pasanen M, Heinonen A, Nenonen A, Halleen J, Fuerst T, Genant H, Vuori I 2003 Effect of alendronate and exercise on bone and physical performance of postmenopausal women: a randomized controlled trial. Bone **33**(1)**:**132-43.

137. Basat H, Esmaeilzadeh S, Eskiyurt N 2013 The effects of strengthening and high-impact exercises on bone metabolism and quality of life in postmenopausal women: a randomized controlled trial. J Back Musculoskelet Rehabil **26**(4)**:**427-35.

138. Nih Consensus Development Panel on Osteoporosis Prevention D, Therapy 2001 Osteoporosis prevention, diagnosis, and therapy. JAMA **285**(6)**:**785-95.

139. Felsenberg D, Boonen S 2005 The bone quality framework: determinants of bone strength and their interrelationships, and implications for osteoporosis management. Clin Ther **27**(1)**:**1-11.

140. Black DM, Bilezikian JP, Ensrud KE, Greenspan SL, Palermo L, Hue T, Lang TF, McGowan JA, Rosen CJ, Pa THSI 2005 One year of alendronate after one year of parathyroid hormone (1-84) for osteoporosis. N Engl J Med **353**(6)**:**555-65.

141. Black DM, Greenspan SL, Ensrud KE, Palermo L, McGowan JA, Lang TF, Garnero P, Bouxsein ML, Bilezikian JP, Rosen CJ, Pa THSI 2003 The effects of parathyroid hormone and alendronate alone or in combination in postmenopausal osteoporosis. N Engl J Med **349**(13)**:**1207-15.

142. Cosman F, Eriksen EF, Recknor C, Miller PD, Guanabens N, Kasperk C, Papanastasiou P, Readie A, Rao H, Gasser JA, Bucci-Rechtweg C, Boonen S 2011 Effects of intravenous zoledronic acid plus subcutaneous teriparatide [rhPTH(1-34)] in postmenopausal osteoporosis. J Bone Miner Res **26**(3)**:**503-11.

143. Schafer AL, Burghardt AJ, Sellmeyer DE, Palermo L, Shoback DM, Majumdar S, Black DM 2013 Postmenopausal women treated with combination parathyroid hormone (1-84) and ibandronate demonstrate different microstructural changes at

the radius vs. tibia: the PTH and Ibandronate Combination Study (PICS). Osteoporos Int **24**(10)**:**2591-601.

144. Finkelstein JS, Hayes A, Hunzelman JL, Wyland JJ, Lee H, Neer RM 2003 The effects of parathyroid hormone, alendronate, or both in men with osteoporosis. N Engl J Med **349**(13)**:**1216-26.

145. Kurland ES, Heller SL, Diamond B, McMahon DJ, Cosman F, Bilezikian JP 2004 The importance of bisphosphonate therapy in maintaining bone mass in men after therapy with teriparatide [human parathyroid hormone(1-34)]. Osteoporos Int **15**(12)**:**992-7.

146. Keaveny TM, Hoffmann PF, Singh M, Palermo L, Bilezikian JP, Greenspan SL, Black DM 2008 Femoral bone strength and its relation to cortical and trabecular changes after treatment with PTH, alendronate, and their combination as assessed by finite element analysis of quantitative CT scans. J Bone Miner Res **23**(12)**:**1974-82.

147. Huiskes R, Chao EY 1983 A survey of finite element analysis in orthopedic biomechanics: the first decade. J Biomech **16**(6)**:**385-409.

148. Bessho M, Ohnishi I, Matsuyama J, Matsumoto T, Imai K, Nakamura K 2007 Prediction of strength and strain of the proximal femur by a CT-based finite element method. J Biomech **40**(8)**:**1745-53.

149. Buckley JM, Loo K, Motherway J 2007 Comparison of quantitative computed tomography-based measures in predicting vertebral compressive strength. Bone **40**(3)**:**767-74.

150. Imai K, Ohnishi I, Bessho M, Nakamura K 2006 Nonlinear finite element model predicts vertebral bone strength and fracture site. Spine **31**(16)**:**1789-94.

151. Rasoulian R, Raeisi Najafi A, Chittenden M, Jasiuk I 2013 Reference point indentation study of age-related changes in porcine femoral cortical bone. J Biomech **46**(10)**:**1689-96.

152. Khosla S, Bilezikian JP, Dempster DW, Lewiecki EM, Miller PD, Neer RM, Recker RR, Shane E, Shoback D, Potts JT 2012 Benefits and risks of bisphosphonate therapy for osteoporosis. J Clin Endocrinol Metab **97**(7)**:**2272-82.

153. Abrahamsen B, Eiken P, Eastell R 2009 Subtrochanteric and diaphyseal femur fractures in patients treated with alendronate: a register-based national cohort study. J Bone Miner Res **24**(6)**:**1095-102.

154. Kim SY, Schneeweiss S, Katz JN, Levin R, Solomon DH 2011 Oral bisphosphonates and risk of subtrochanteric or diaphyseal femur fractures in a population-based cohort. J Bone Miner Res **26**(5)**:**993-1001.

155. Vestergaard P, Schwartz F, Rejnmark L, Mosekilde L 2011 Risk of femoral shaft and subtrochanteric fractures among users of bisphosphonates and raloxifene. Osteoporos Int **22**(3)**:**993-1001.

156. Mashiba T, Hirano T, Turner CH, Forwood MR, Johnston CC, Burr DB 2000 Suppressed bone turnover by bisphosphonates increases microdamage accumulation and reduces some biomechanical properties in dog rib. J Bone Miner Res **15**(4)**:**613-20.

157. Recker RR, Weinstein RS, Chesnut CH, 3rd, Schimmer RC, Mahoney P, Hughes C, Bonvoisin B, Meunier PJ 2004 Histomorphometric evaluation of daily and intermittent oral ibandronate in women with postmenopausal osteoporosis: results from the BONE study. Osteoporos Int **15**(3)**:**231-7.

158. Eriksen EF, Melsen F, Sod E, Barton I, Chines A 2002 Effects of long-term risedronate on bone quality and bone turnover in women with postmenopausal osteoporosis. Bone **31**(5)**:**620-5.

159. Giusti A, Hamdy NA, Papapoulos SE 2010 Atypical fractures of the femur and bisphosphonate therapy: A systematic review of case/case series studies. Bone **47**(2)**:**169-80.

160. Gudbjornsson B, Juliusson UI, Gudjonsson FV 2002 Prevalence of long term steroid treatment and the frequency of decision making to prevent steroid induced osteoporosis in daily clinical practice. Ann Rheum Dis **61**(1)**:**32-6.

161. Orcel P 2005 Prevention and treatment of glucocorticoid-induced osteoporosis in 2005. Joint Bone Spine **72**(6)**:**461-5.

162. LoCascio V, Bonucci E, Imbimbo B, Ballanti P, Adami S, Milani S, Tartarotti D, DellaRocca C 1990 Bone loss in response to long-term glucocorticoid therapy. Bone Miner **8**(1)**:**39-51.

163. Cohen S, Levy RM, Keller M, Boling E, Emkey RD, Greenwald M, Zizic TM, Wallach S, Sewell KL, Lukert BP, Axelrod DW, Chines AA 1999 Risedronate therapy prevents corticosteroid-induced bone loss: a twelve-month, multicenter, randomized, double-blind, placebo-controlled, parallel-group study. Arthritis Rheum **42**(11)**:**2309-18.

164. Wallach S, Cohen S, Reid DM, Hughes RA, Hosking DJ, Laan RF, Doherty SM, Maricic M, Rosen C, Brown J, Barton I, Chines AA 2000 Effects of risedronate

treatment on bone density and vertebral fracture in patients on corticosteroid therapy. Calcif Tissue Int **67**(4)**:**277-85.

165. National Osteoporosis Foundation, About Osteoporosis, Bone Health Basics, Retrieved July 13, 2012 from http://nof.org.

166. Peat ID, Healy S, Reid DM, Ralston SH 1995 Steroid induced osteoporosis: an opportunity for prevention? Ann Rheum Dis **54**(1)**:**66-8.

167. Bell R, Carr A, Thompson P 1997 Managing corticosteroid induced osteoporosis in medical outpatients. J R Coll Physicians Lond **31**(2)**:**158-61.

168. Muchmore JS, Cooper DK, Ye Y, Schlegel V, Pribil A, Zuhdi N 1992 Prevention of loss of vertebral bone density in heart transplant patients. J Heart Lung Transplant **11**(5)**:**959-63.

169. Thomas T, Horlait S, Ringe JD, Abelson A, Gold DT, Atlan P, Lange JL 2013 Oral bisphosphonates reduce the risk of clinical fractures in glucocorticoid-induced osteoporosis in clinical practice. Osteoporos Int **24**(1):263-9..

170. Braith RW, Magyari PM, Fulton MN, Lisor CF, Vogel SE, Hill JA, Aranda JM, Jr. 2006 Comparison of calcitonin versus calcitonin + resistance exercise as prophylaxis for osteoporosis in heart transplant recipients. Transplantation **81**(8)**:**1191-5.

171. Bateman TA, Countryman S 2002 Osteoprotegerin and bone loss associated with spaceflight. Drug Discov Today **7**(8)**:**456-7.

172. Frost HM 1994 Wolff's Law and bone's structural adaptations to mechanical usage: an overview for clinicians. Angle Orthod **64**(3)**:**175-88.

173. Lloyd SA, Lewis GS, Zhang Y, Paul EM, Donahue HJ 2012 Connexin 43 deficiency attenuates loss of trabecular bone and prevents suppression of cortical bone formation during unloading. J Bone Miner Res **27**(11)**:**2359-72.

174. Machwate M, Zerath E, Holy X, Hott M, Godet D, Lomri A, Marie PJ 1995 Systemic administration of transforming growth factor-beta 2 prevents the impaired bone formation and osteopenia induced by unloading in rats. J Clin Invest **96**(3)**:**1245-53.

175. Machwate M, Zerath E, Holy X, Pastoureau P, Marie PJ 1994 Insulin-like growth factor-I increases trabecular bone formation and osteoblastic cell proliferation in unloaded rats. Endocrinology **134**(3)**:**1031-8.

176. Vico L, Bourrin S, Very JM, Radziszowska M, Collet P, Alexandre C 1995 Bone changes in 6-mo-old rats after head-down suspension and a reambulation period. J Appl Physiol (1985) **79**(5)**:**1426-33.

177. Vico L, Novikov VE, Very JM, Alexandre C 1991 Bone histomorphometric comparison of rat tibial metaphysis after 7-day tail suspension vs. 7-day spaceflight. Aviat Space Environ Med **62**(1)**:**26-31.

178. Smith SM, Nillen JL, Leblanc A, Lipton A, Demers LM, Lane HW, Leach CS 1998 Collagen cross-link excretion during space flight and bed rest. J Clin Endocrinol Metab **83**(10)**:**3584-91.

179. Oganov VS, Grigor'ev AI, Voronin LI, Rakhmanov AS, Bakulin AV, Schneider VS, LeBlanc AD 1992 [Bone mineral density in cosmonauts after flights lasting 4.5-6 months on the Mir orbital station]. Aviakosm Ekolog Med **26**(5-6)**:**20-4.

180. Keyak JH, Koyama AK, LeBlanc A, Lu Y, Lang TF 2009 Reduction in proximal femoral strength due to long-duration spaceflight. Bone **44**(3)**:**449-53.

181. Loehr JA, Lee SM, English KL, Sibonga J, Smith SM, Spiering BA, Hagan RD 2011 Musculoskeletal adaptations to training with the advanced resistive exercise device. Med Sci Sports Exerc **43**(1)**:**146-56.

182. Leblanc A, Matsumoto T, Jones J, Shapiro J, Lang T, Shackelford L, Smith SM, Evans H, Spector E, Ploutz-Snyder R, Sibonga J, Keyak J, Nakamura T, Kohri K, Ohshima H 2013 Bisphosphonates as a supplement to exercise to protect bone during long-duration spaceflight. Osteoporos Int **24**(7)**:**2105-14.

183. Orwoll ES, Adler RA, Amin S, Binkley N, Lewiecki EM, Petak SM, Shapses SA, Sinaki M, Watts NB, Sibonga JD 2013 Skeletal health in long-duration astronauts: nature, assessment, and management recommendations from the NASA Bone Summit. J Bone Miner Res **28**(6)**:**1243-55.

APPENDIX A*

Bone Loss during Partial Weight Bearing (1/6th Gravity) is Mitigated by Resistance and Aerobic Exercise in Mice

RD Boudreaux[1], CE Metzger[2], BR Macias[2], Y Shirazi-Fard[1], HA Hogan[1,3], and SA Bloomfield[2]

[1]Dept of Biomedical Engineering, [2]Dept of Health and Kinesiology, and [3]Dept of Mechanical Engineering, Texas A&M University, College Station, TX 77843

Ramon D. Boudreaux: rdb1116@gmail.com
Corinne E. Metzger: cmetzger@hlkn.tamu.edu
Brandon R. Macias: b1macias@ucsd.com
Yasaman Shirazi-Fard: yasamanshirazi@gmail.com
Harry A. Hogan: hhogan@tamu.edu
Susan A. Bloomfield: sbloom@tamu.edu

Correspondence: Ramon D. Boudreaux
Texas A&M University
RM 217 Old Herman Heep Bldg
Corner of Spence and Lamar
College Station, TX 77843-0001
Email: rdb11162@gmail.com
Phone: 1-337-739-4276

* This section has been reprinted with permission from, "Bone Loss During Partial Weight Bearing (1/6 Gravity) Is Mitigated by Resistance and Aerobic Exercise in Mice" by Boudreaux RD, Metzger Macias BR, Shirazi-Fard, Y, Hogan HA, Bloomfield SA, Acta Astronautica **99**:71-77." 2014 Elsevier

Abstract

Astronauts on long duration missions continue to experience bone loss, as much as 1 – 2% each month, for up to 4.5 years after a mission. Mechanical loading of bone with exercise has been shown to increase bone formation, mass, and geometry. The aim of this study was to compare the efficacy of two exercise protocols during a period of reduced gravitational loading ($1/6^{th}$ body weight) in mice. Since muscle contractions via resistance exercise impart the largest physiological loads on the skeleton, we hypothesized that resistance training (via vertical tower climbing) would better protect against the deleterious musculoskeletal effects of reduced gravitational weight bearing when compared to endurance exercise (treadmill running). Young adult female BALB/cBYJ mice were randomly assigned to three groups: 1/6g (G/6; n=6), 1/6g with treadmill running (G/6+RUN; n=8), or 1/6g with vertical tower climbing (G/6+CLB; n=9). Exercise was performed five times per week. Reduced weight bearing for 21 days was achieved through a novel harness suspension system. Treadmill velocity (12 – 20 m/min) and daily run time duration (32 – 51 min) increased incrementally throughout the study. Bone geometry and volumetric bone mineral density (vBMD) at proximal metaphysis and mid-diaphysis tibia were assessed by *in vivo* peripheral quantitative computed tomography (pQCT) on days 0 and 21 and standard dynamic histomorphometry was performed on undemineralized sections of the mid-diaphysis after tissue harvest. G/6 caused a significant decrease ($P<0.001$) in proximal tibia metaphysis total vBMD (-9.6%). These reductions of tibia metaphyseal vBMD in G/6 mice were mitigated in both G/6+RUN and G/6+CLB groups ($P<0.05$). After 21 days of

G/6, we saw an absolute increase in tibia mid-diaphysis vBMD and in distal metaphysis femur vBMD in both G/6+RUN and G/6+CLB mice ($P<0.05$). Substantial increases in endocortical and periosteal mineralizing surface (%MS/BS) at mid-diaphysis tibia in G/6+CLB demonstrate that bone formation can be increased even in the presence of reduced weight bearing. These data suggest that moderately vigorous endurance exercise and resistance training, through treadmill running or climb training mitigates decrements in vBMD during 21 days of reduced weight bearing. Consistent with our hypothesis, tower climb training, most pronounced in the tibia mid-diaphysis, provides a more potent osteogenic response compared to treadmill running.

Keywords

partial weight bearing; exercise; spaceflight; histomorphometry

1. Introduction

Spinal cord injury, muscle paralysis, and prolonged bed rest have all been shown to elicit increased bone resorption, decreased bone mass, and a consequent increased risk of bone fracture (1, 2, 18). The observed bone loss under these conditions is commonly attributed to reduced mechanical loading to bone tissue (23). During low-Earth orbit, astronauts aboard the International Space Station (ISS) can lose up to 2% bone mineral density (BMD) at the hip per month while in micro-gravity (13). This level of bone loss in astronauts is an order of magnitude greater than the rate of loss in post-menopausal women, a population at high risk of developing osteoporosis on Earth (7). Decreased BMD and altered bone geometry are strongly associated with increased risk of fracture (3). Finite element modeling analyses reveal that femoral neck strength decreases an average of 2.5% each month during long duration ISS missions (12). Upon returning to Earth, femoral neck volume and trabecular BMD (tBMD) remain below pre-flight values for up to 4.5 years, compromising the long-term skeletal health of crew members, especially those selected for repeat ISS missions (4).

The tail suspended hindlimb unloaded (HU) rodent has become a well-established ground-based analogue for investigating the skeletal adaptations of spaceflight (17). The HU model simulates spaceflight conditions by reducing mechanical loads to the hindlimbs and inducing a cephalic shift of fluids, both deleterious to bone (14, 22) With the National Aeronautics and Space Administration's (NASA) growing interest in returning to the Moon, a near-Earth asteroid, or Mars, it is becoming increasingly important to determine if added resistance exercise protects the

musculoskeletal unit during space missions. Results from our lab using a novel partial weight bearing suspension apparatus have demonstrated that partial weight bearing, and in particular 3/8th body weight (Martian gravity) and 1/6th body weight (Lunar gravity), does not protect against bone loss observed with the full unloading of traditional tail suspension (26). As a result, countermeasures must be considered to protect against bone loss in partial gravity environments, but we are not aware of any data testing exercise countermeasures for bone loss in a reduced weight bearing environment such as the Moon.

The aim of this study was to investigate two different exercise programs during a period of reduced mechanical loading as potential countermeasures to bone loss. Exercise, both aerobic and resistive, can be osteogenic and may effectively mitigate or prevent bone loss during partial weight bearing (19). We hypothesized that both aerobic exercise (G/6+RUN) and resistance exercise (G/6+CLB) during 21 days of 1/6th gravity (G/6) would mitigate bone loss in the femur and tibia of adult mice. We further hypothesized that resistance exercise would be more protective than a running regime.

2. Materials and Methods

2.1. Animals and Experimental Design

Twenty-three 10-week old female BALB/cByJ mice were obtained from Jackson Laboratories (Bar Harbor, Maine) and allowed one week of acclimation before the initiation of the study. Throughout the study, animals were singly housed in a temperature controlled room (23 ± 2°C) with a 12:12-h light-dark cycle, provided water

ad libitum, and fed a standard rodent chow diet (Harlan Teklad 8604). Animal care and experimental procedures from this study were approved by Texas A&M University's Institutional Animal Use and Care Committee (IACUC). The health of all animals was monitored daily through frequent standard health checks and body weight logs.

Following acclimation, animals were block assigned to one of three groups by body weight: 1) $1/6^{th}$ weight bearing group to simulate Lunar gravity (G/6, n=6), 2) $1/6^{th}$ weight bearing group with climbing resistance exercise (G/6+CLB, n=9), and 3) $1/6^{th}$ weight bearing group with treadmill running (G/6+RUN, n=8). Intraperitoneal injections of calcein (Sigma Chemical, St. Louis, 15 mg/kg body weight) were administered seven and two days prior to the end of the study to quantify the rate of new bone formation. On day 21, all animals were anesthetized with a cocktail of ketamine (75 mg/kg body weight) and medetomidine (1.0 mg/kg body weight) then euthanized by cardiac puncture exsanguination and cervical dislocation. Femora and tibiae were excised from animals, stripped of soft tissue, and stored in either PBS-soaked gauze at -30°C for mechanical testing or in 70% ethanol at 4°C for histomorphometry analyses.

2.2. Partial Weight Bearing Suspension

A partial weight bearing suspension system was utilized to simulate Lunar ($1/6^{th}$) gravitational loading in mice (26, 27). Briefly, mice were single-housed in 13 in^3 custom built cages made of clear polycarbonate walls with removable polypropylene perforated floors. A stainless steel aluminum rod, settled across the top of the cage, contained a small nylon wheel and low friction bearing that decreased resistance to

movement of the suspended animals. Mice were suspended horizontally in order to reduce weight bearing of the forelimbs and hindlimbs equally. Forelimbs were supported by a shoulder jacket made of moleskin, athletic tape, and Velcro. Jackets were designed to allow for normal activities (e.g., eating, drinking, and grooming). Support for the hindlimbs was achieved by first applying SteriStrip (3M, St. Paul, MN) loosely around the base of the tail to reduce irritation then wrapping athletic tape around the SteriStrip. To minimize stress to the animals, jackets and tail wraps were applied and conducted under isoflurane anesthesia. All mice were weighed and 1/6 weight bearing titrated daily. Full body weight was measured by suspending the whole mouse in a custom made titration frame, built to precisely the same floor-to-rod height as the suspension cages, placed on an electronic scale (Ohaus Corp., Pine Brook, NJ) To adjust for daily changes in body weight, mice were placed in the titration column and, by adjusting the linear tension spring (spring constant of 0.7 N/m) and eye bolt, were titrated to the desired $1/6^{th}$ weight-bearing (± 0.1 g).

2.3. Exercise

Prior to each exercise bout in G/6+RUN and G/6+CLB groups, animals were removed from harness and allowed to exercise at full weight bearing. Upon completion of daily training protocols, which lasted for approximately 45-60 minutes, animals were re-harnessed under brief isoflurane anesthesia to minimize stress and returned to partial weight bearing in the suspension cages.

Animals in G/6+RUN performed moderately intensive aerobic exercise five times/week for three weeks on a six-lane motorized rodent treadmill with rear shock grid (Columbus Instruments, Columbus, OH) as described previously (15). Animals were familiarized with treadmill running on the first two days of training to eliminate training adaptations. Following the acclimation period, treadmill speed and intensity increased throughout the study, peaking at 20 meters/minute for 45 minutes at a 10° incline. All animals were successful at completing the three week training protocol in its entirety.

Voluntary resistance exercise was performed by all G/6+CLB animals by climbing a 1-meter, vertical, wire-meshed tower five times/week for three weeks. The tubular climb tower, designed and built in our laboratory, was made of steel mesh with cross-stripes spaced 5 mm apart. The tower diameter was 5 cm to allow animals to easily fit and climb inside. A 5 cm hole was bored out of the bottom of a standard mouse cage where the tower could be attached and supported. Climb repetitions began by placing the animal at the base of the tower where they were allowed to climb up the length of the tower and motivated, when needed, by a small fishing bobber looped through the tower. Climbs were considered complete when animals reached the base of the attached cage (top of the climb tower) where they could be retrieved by the trainer. Consistent with the treadmill protocol, tower climbing was designed to be a progressive training program to accommodate for daily improvements. Small lead split-shot pellets were wrapped in athletic tape to achieve incremental increases in total weight (up to 175% animal body weight) and loosely bound to the animals at the tail base. Daily climb number decreased (from 50 down to 36 climbs) as attached tail weight increased

(from 0 up to 100% body weight), peaking at 36 climbs with 175% body weight so that total work performed remained constant. Number and duration of completed climbs were observed and recorded. A typical training session lasted for approximately one hour.

2.4. Peripheral Quantitative Computed Tomography (pQCT)

2.4.1. *In vivo* pQCT Densitometric Test

Under isoflurane anesthesia, left tibiae were scanned *in vivo* at baseline (day 0) and at the end of the study (day 21) using an XCT Research-M device (Stratec Corp., Norland, Fort Atkinson, WI). A hydroxyapatite cone phantom was used to calibrate the machine daily. Scan sites included two slices at the mid-diaphysis (50% bone length) and three slices at the proximal metaphysis. Tibiae were scanned with a speed of 2.5 mm/sec, a voxel resolution of 100 μm^2, and a scan thickness of 500 μm. For analysis, proximal metaphysis outer and inner thresholds were set at 400 mg/cm^3 and 750 mg/cm^3, respectively. Diaphyseal threshold was set at 750 mg/cm^3. Machine precision, based on manufacturer data, is ±9 mg/cm^3 (cortical vBMD) and ±3 mg/cm^3 (trabecular vBMD). Measurement parameters, such as total vBMD, were obtained by averaging the three slices at the proximal metaphysis and the two slices at the diaphysis.

2.4.2. *Ex vivo* pQCT Densitometric Test

After termination, excised right femurs stripped of soft tissue were scanned *ex vivo* with a speed of 2.5 mm/sec, a voxel resolution of 70 μm^2, and a scan thickness of

500 μm. Three slices at the proximal metaphysis and two slices at the mid-diaphysis were scanned and the means of these slices were used for analysis. At the diaphysis, cross-sectional moment of inertia (CSMI) was used in combination with three-point bending data (Table 3) as estimates of strength as described previously (22).

2.5. Three-Point Bending Biomechanical Test

Once thawed to room temperature, right femora were tested to failure in three-point bending on an Instron 3345 machine (Norwood, MA; 100 N load cell; Bluehill v. 2.14.582) as described previously (10). Using precision hand calipers, the anterior-posterior and medial-lateral periosteal diameters at the mid-diaphysis were measured and recorded. Each bone was then placed anterior side down on metal pin supports (D= 3.0 mm) spaced 10 mm apart. To perform the test, a quasi-static load of 2.54 mm/minute was applied to the upper part of the diaphysis region corresponding with pQCT diaphysis scan site (50% total bone length). The test proceeded until fracture occurred. Load and displacement data were collected during tests (at 10 Hz) and analyzed using Bluehill software (version 2.14.582, Instron Bluehill) and a custom-written Matlab (version 7.12.0, TheMathWorks, Inc.) program. Later, load-displacement data were analyzed using Matlab (The Mathworks, Inc.; Natick, MA). Stiffness (k, N/mm) was determined by calculating the slope of the load-displacement curve in the elastic region. Ultimate load (N) designated the largest force achieved throughout the test. Energy absorbed (N·mm) was determined as the area under the entire load-displacement curve.

From classical beam bending theory, elastic modulus (E, GPa) was obtained using the equation $E = (k \cdot S^3) / (48 \cdot CSMI \cdot 1000)$, where S = support span distance (10 mm).

2.6. Histomorphometry

Intraperitoneal injections of calcein (15 mg/kg body weight, Sigma Chemical, St. Louis, MO) were administered at seven and two days prior to termination to label mineralizing surfaces. Undemineralized excised distal right tibia were dehydrated and embedded in methyl-methacrylate (Sigma-Aldrich M5, 590-9, St. Louis, MO). Serial cross sections (150-200 μm thick) were cut using a diamond wafer low-speed saw (Buehler, Lake Bluff, IL) starting1 mm proximal to the tibia-fibular junction. OsteoMeasure Analysis Software, version 1.3 (OsteoMetrics, Atlanta, GA) was used to analyze each specimen and determine mineralizing surface/bone surface (MS/BS), mineral apposition rate (MAR), and bone formation rate (BFR = MS/BS · MAR). Histomorphometric analyses follow the standardizations as defined previously (5).

2.7. Statistical Analysis

All data are presented as mean ± standard error of the mean (SE) and were evaluated for differences using SigmaStat, version 3.5 (Systat Software Inc., San Jose, CA). A two factor ANOVA (exercise and time) with repeated measures on time was used to evaluate differences among *in vivo* pQCT data. Post hoc pairwise comparisons were made using the Tukey Test. All other statistical analyses were made using a one

factor ANOVA with the Holm-Sidak method for pairwise comparisons. Statistical significance was determined with $p<0.05$.

3. Results

Body weight in all groups was maintained throughout the 21 days of the study. Slight initial declines in weight (≤ 2 grams) occurred, but were not significant (Figure 1). Overall, mice appeared healthy and exhibited normal drinking and feeding

Partial weight bearing for 21 days caused a decrease in total vBMD at the tibia metaphysis. These losses were attenuated in both exercise groups (Figure 2). At day 21, *in vivo* tibia and *ex vivo* femur metaphysis vBMD were higher in G/6+RUN and G/6+CLB compared to G/6 (Table 1). Marrow area in tibia metaphysis is elevated with partial weight bearing compared to G/6+RUN (P=0.051). Exercise modalities increased tibia diaphysis cortical vBMD by 3.2% in G/6+CLB and by 2.9% in G/6+RUN (Figure 3).

Ex vivo scans at day 21 revealed that femur metaphysis total BMC and total vBMD were significantly higher in exercising G/6 mice than in G/6 animals (Table 2), suggesting a mitigation of bone loss during G/6 at this site. However, at the femoral diaphysis these *ex vivo* measures demonstrate no effect of G/6 or exercise after 21-days.

Tibia diaphysis bone formation was heightened with resistance exercise during partial weight bearing compared to G/6 alone (Figure 4). Percent mineralizing surface (MS/BS) was over 6-fold higher in G/6+CLB mice at the periosteal surface and over 9-fold higher at the endocortical surface versus that observed in G/6. Due to an absence of

double labels in all animals, mineral apposition rate (MAR), and thus bone formation rate (BFR), could not be determined.

Three-point bending biomechanical testing of the tibia diaphysis yielded no significant differences among groups (Table 3). Neither resistance nor aerobic exercise increased bending strength during a period of 21-day partial weight bearing.

4. Discussion

The purpose of this study was to compare two different modalities of exercise during a period of partial weight bearing and to determine their ability to mitigate disuse bone loss. In accordance with Frost's mechanostat theory, we hypothesized that the higher magnitude loading imposed by resistance exercise (climbing protocol) would have a more robust beneficial effect compared to aerobic exercise (treadmill running) (9). Consistent with results from previous studies using partial weight bearing (6, 25) and the full unloading of traditional tail suspension (11) in adult mice, significant bone loss occurred after 3 weeks of 1/6 partial weight bearing (G/6) in the tibia metaphysis, a site sensitive to disuse bone loss. The effect of exercise in mitigating losses, however, appeared to be site-specific. At the metaphysis, neither treadmill running nor tower climbing was able to protect against total vBMD losses. However, vBMD values at the end of the study were higher compared to partial weight bearing in the absence of exercise, suggesting an exercise-induced mitigation of losses. Contrary to the metaphysis, the tibia diaphysis appears to show possible beneficial effects of exercise, but the results are equivocal. Exercise was able to elicit an anabolic response despite

simultaneous exposure to G/6. Even though cortical vBMD increased over 21 days in both G/6+RUN and G/6+CLB, it also increased slightly for G/6 alone. Further, comparing groups at the study end (day 21), there was no difference in cortical BMC or vBMD among all three groups. Site specificity of exercised-induced bone growth in murine tibia has been demonstrated previously (28). Compounded with the site specificity of exercise, disuse bone loss has also been shown to vary by anatomical site (11). Cancellous bone compartments appear to be more pronounced targets of disuse bone loss, as demonstrated in both human astronaut populations and rodent studies (11, 16, 24).

The most important findings of this study were that exercise, both running and climbing, show some beneficial effects at both the tibia and femur metaphyses, a mixed bone site, as well as the tibia diaphysis. Unlike previously published work using the partial weight bearing model, G/6 did not induce bone loss at the femur diaphysis in our study (6). However, comparisons between our study and theirs should be made with caution, as different strains of mice were used.

Consistent with the lack of change in cortical BMC and vBMD at the femur diaphysis, mechanical strength at this site was not affected by loading status. When subjected to a three-point bending test to fracture, no significant differences were found between groups. It is likely that neither the prescribed treadmill running nor tower climbing provided a potent enough stimulus to affect the femur diaphysis. Future studies should investigate the efficacy of a combined program incorporating both a resistance and aerobic component to mitigate or prevent disuse bone loss in the femur.

The largest physiological loads imparted on bone occur via tensile forces produced by contracting muscles during exercise (29). This external stimulus is transduced by osteocytes and, via decreased sclerostin expression, upregulates Wnt signaling (20) which activate osteoblast activity and new bone formation, with a consequent increase in bone mass, geometry, and strength (8). This external relationship between muscle and bone makes up, in part, the functional muscle-bone unit (21). In this study, mineralizing activity (%MS/BS) was highest on the endocortical and periosteal surfaces of the tibia diaphysis of G/6+CLB. This increase in %MS/BS versus G/6+RUN and G/6 may be attributed to the muscle-bone unit, since resistance exercise is known to produce large muscle contractions. Increased mineralized surface of G/6+CLB at the tibia diaphysis (endocortical, +633%; periosteal, +935%; vs. G/6) corresponds with an increase in total vBMD at this site, even in the context of a partial weight bearing environment, suggesting that bone formation rate was higher with resistance exercise. We were not capable of quantifying BFR, however, due to an absence of double label. It is likely that mineralization either began or ended in the window of time between injections of our fluorochrome label.

This study is not without limitations. Unlike the hindlimb unloaded (HU) rodent model, which imparts a cephalic fluid shift, this partial weight bearing model does not alter the distribution of fluids throughout the body. Bone loss in the lower limbs of animals subjected to HU is considered to be partially attributed to decreased fluid flow to those bones. However, even in the absence of a cephalic fluid shift, G/6 animals did experience declines in bone mineral content and in an important index of osteoblast

activity. A second limitation to our study is the lack of ambulatory jacketed controls to test whether or not stress from the apparatus itself was a contributing factor to the deleterious effects on bone. Thirdly, animals in exercise groups were subjected to full weight bearing for approximately one hour each exercise day (5 times/week) and brief anesthesia, whereas non-exercising animals were not. In the future, it may be appropriate to equate the period of full weight bearing ambulation and anesthesia exposure in all groups.

In summary, our hypothesis that resistance and aerobic exercise would mitigate disuse-induced bone loss was satisfied. Furthermore, resistance exercise, because of its ability to significantly increase bone formation in the diaphysis, may perhaps be more favorable than aerobic training in terms of osteogenic responsiveness. With future aspirations of exploring and inhabiting partial gravity planetary surfaces, these results have profound implications for the importance of increased mechanical loading on bone health. The most profound response to exercise in BALB/cByJ mice appears to take place at the tibia diaphysis. Other bone sites, such as the femur diaphysis, may require a more potent stimulus than the ones presented here to protect against bone loss from reduced mechanical loading. Overall, our study has demonstrated that during a period of disuse, both resistance and aerobic exercise can partially mitigate losses in bone.

Acknowledgments

This study was funded by the National Space Biomedical Research Institute (NSBRI) via NASA Cooperative Agreement NCC 9-58. RDB and BRM are supported by the National Space Biomedical Research Institute Graduate Training Fellowship NSBRI-RFP-05-02. The authors would like to thank Kaleigh Camp, Evelyn Yuen, Zachary Brown, and Tiphaine Cecchini for their contributions with animal care and training.

Conflicts of Interest

None

References

1. Ausk BJ, Huber P, Poliachik SL, Bain SD, Srinivasan S, and Gross TS. Cortical bone resorption following muscle paralysis is spatially heterogeneous. *Bone* 50: 14-22.

2. Battaglino RA, Lazzari AA, Garshick E, and Morse LR. Spinal Cord Injury-Induced Osteoporosis: Pathogenesis and Emerging Therapies. *Curr Osteoporos Rep*.

3. Black DM, Bouxsein ML, Marshall LM, Cummings SR, Lang TF, Cauley JA, Ensrud KE, Nielson CM, Orwoll ES, and Osteoporotic Fractures in Men Research G. Proximal femoral structure and the prediction of hip fracture in men: a large prospective study using QCT. *Journal of bone and mineral research : the official journal of the American Society for Bone and Mineral Research* 23: 1326-1333, 2008.

4. Carpenter RD. Long-term changes in the density and structure of the human hip and spine after long-duration spaceflight. *Acta Astronautica* 67: 71-81, 2010.

5. Dempster DW, Compston JE, Drezner MK, Glorieux FH, Kanis JA, Malluche H, Meunier PJ, Ott SM, Recker RR, and Parfitt AM. Standardized nomenclature, symbols, and units for bone histomorphometry: a 2012 update of the report of the ASBMR Histomorphometry Nomenclature Committee. *Journal of bone and mineral research : the official journal of the American Society for Bone and Mineral Research* 28: 2-17, 2013.

6. Ellman R, Spatz J, Cloutier A, Palme R, Christiansen BA, and Bouxsein ML. Partial reductions in mechanical loading yield proportional changes in bone density, bone architecture, and muscle mass. *Journal of bone and mineral research : the official journal of the American Society for Bone and Mineral Research* 28: 875-885, 2013.

7. Finkelstein JS, Brockwell SE, Mehta V, Greendale GA, Sowers MR, Ettinger B, Lo JC, Johnston JM, Cauley JA, Danielson ME, and Neer RM. Bone mineral density changes during the menopause transition in a multiethnic cohort of women. *J Clin Endocrinol Metab* 93: 861-868, 2008.

8. Frost HM. Bone's mechanostat: a 2003 update. *The anatomical record Part A, Discoveries in molecular, cellular, and evolutionary biology* 275: 1081-1101, 2003.

9. Frost HM. The Utah paradigm of skeletal physiology: an overview of its insights for bone, cartilage and collagenous tissue organs. *Journal of bone and mineral metabolism* 18: 305-316, 2000.

10. Hubal MJ, Ingalls CP, Allen MR, Wenke JC, Hogan HA, and Bloomfield SA. Effects of eccentric exercise training on cortical bone and muscle strength in the estrogen-deficient mouse. *Journal of applied physiology* 98: 1674-1681, 2005.

11. Judex S, Garman R, Squire M, Busa B, Donahue LR, and Rubin C. Genetically linked site-specificity of disuse osteoporosis. *J Bone Miner Res* 19: 607-613, 2004.

12. Keyak JH, Koyama AK, LeBlanc A, Lu Y, and Lang TF. Reduction in proximal femoral strength due to long-duration spaceflight. *Bone* 44: 449-453, 2009.

13. LeBlanc AD, Spector ER, Evans HJ, and Sibonga JD. Skeletal responses to space flight and the bed rest analog: a review. *Journal of musculoskeletal & neuronal interactions* 7: 33-47, 2007.

14. Macias BR, Swift JM, Nilsson MI, Hogan HA, Bouse SD, and Bloomfield SA. Simulated resistance training, but not alendronate, increases cortical bone formation and suppresses sclerostin during disuse. *Journal of applied physiology* 112: 918-925, 2012.

15. Massett MP, and Berk BC. Strain-dependent differences in responses to exercise training in inbred and hybrid mice. *Am J Physiol Regul Integr Comp Physiol* 288: R1006-1013, 2005.

16. Milstead JR, Simske SJ, and Bateman TA. Spaceflight and hindlimb suspension disuse models in mice. *Biomedical sciences instrumentation* 40: 105-110, 2004.

17. Morey-Holton ER, and Globus RK. Hindlimb unloading of growing rats: a model for predicting skeletal changes during space flight. *Bone* 22: 83S-88S, 1998.

18. Morgan JL, Skulan JL, Gordon GW, Romaniello SJ, Smith SM, and Anbar AD. Rapidly assessing changes in bone mineral balance using natural stable calcium isotopes. *Proc Natl Acad Sci U S A* 109: 9989-9994.

19. Notomi T, Okazaki Y, Okimoto N, Saitoh S, Nakamura T, and Suzuki M. A comparison of resistance and aerobic training for mass, strength and turnover of bone in growing rats. *European journal of applied physiology* 83: 469-474, 2000.

20. Robling AG, Niziolek PJ, Baldridge LA, Condon KW, Allen MR, Alam I, Mantila SM, Gluhak-Heinrich J, Bellido TM, Harris SE, and Turner CH. Mechanical stimulation of bone in vivo reduces osteocyte expression of Sost/sclerostin. *The Journal of biological chemistry* 283: 5866-5875, 2008.

21. Schoenau E. From mechanostat theory to development of the "Functional Muscle-Bone-Unit". *J Musculoskelet Neuronal Interact* 5: 232-238, 2005.

22. Shirazi-Fard Y, Kupke JS, Bloomfield SA, and Hogan HA. Discordant recovery of bone mass and mechanical properties during prolonged recovery from disuse. *Bone* 52: 433-443, 2013.

23. Sievanen H. Immobilization and bone structure in humans. *Archives of biochemistry and biophysics* 503: 146-152, 2010.

24. Squire M, Donahue LR, Rubin C, and Judex S. Genetic variations that regulate bone morphology in the male mouse skeleton do not define its susceptibility to mechanical unloading. *Bone* 35: 1353-1360, 2004.

25. Swift JM, Hogan HA, and Bloomfield SA. beta-1 Adrenergic Agonist Mitigates Unloading-Induced Bone Loss by Maintaining Formation. *Medicine and science in sports and exercise* 2013.

26. Swift JM, Lima F, Macias BR, Allen MR, Greene ES, Shirazi-Fard Y, Kupke JS, Hogan HA, and Bloomfield SA. Partial Weightbearing Does Not Prevent Musculoskeletal Losses Associated with Disuse. *Medicine and science in sports and exercise* 2013.

27. Wagner EB, Granzella NP, Saito H, Newman DJ, Young LR, and Bouxsein ML. Partial weight suspension: a novel murine model for investigating adaptation to reduced musculoskeletal loading. *Journal of applied physiology* 109: 350-357, 2010.

28. Wallace JM, Rajachar RM, Allen MR, Bloomfield SA, Robey PG, Young MF, and Kohn DH. Exercise-induced changes in the cortical bone of growing mice are bone- and gender-specific. *Bone* 40: 1120-1127, 2007.

29. Zofkova I. Hormonal aspects of the muscle-bone unit. *Physiological research / Academia Scientiarum Bohemoslovaca* 57 Suppl 1: S159-169, 2008.

Table 1. Changes in *In Vivo* Proximal and Mid-Diaphysis Tibia Densitometry

	G/6		G/6+RUN		G/6+CLB	
	Pre (Day 0)	Post (Day 21)	Pre (Day 0)	Post (Day 21)	Pre (Day 0)	Post (Day 21)
Proximal Tibia Metaphysis						
Total BMC (mg)	1.55 ± 0.15	1.40 ± 0.08	1.56 ± 0.05	1.41 ± 0.02	1.67 ± 0.05	1.51 ± 0.03
Total vBMD (mg/cm^3)	714.6 ± 44.0	564.8 ± 12.2 *	666.5 ± 11.9	635.0 ± 8.7 *#	679.5 ± 9.3	630.8 ± 11.7 *#
Total Area (mm^2)	2.26 ± 0.32	2.50 ± 0.17	2.36 ± 0.11	2.22 ± 0.02	2.46 ± 0.09	2.41 ± 0.09
Marrow Area (mm^2)	1.12 ± 0.22	1.45 ± 0.12	1.18 ± 0.08	1.20 ± 0.03	1.22 ± 0.06	1.29 ± 0.07
Cort vBMD (mg/cm^3)	700.4 ± 35.5	578.2 ± 11.0 *	668.4 ± 10.9	641.9 ± 7.2 #	676.1 ± 7.9	636.6 ± 10.4 *#
Tibia Mid-Diaphysis						
Cort BMC (mg)	0.90 ± 0.04	0.93 ± 0.02	0.88 ± 0.02	0.91 ± 0.01	0.90 ± 0.02	0.93 ± 0.02
Cort vBMD (mg/cm^3)	1183.9 ± 12.2	1189.6 ± 12.1	1153.8 ± 9.2	1190.6 ± 3.0 *	1150.4 ± 11.5	1181.5 ± 6.4 *

Values presented as mean ± standard error of the mean (SE). * indicates significant effect of time within group (p<0.05). # indicates significantly different from G/6 post (p<0.05). BMC, bone mineral content; vBMD, volumetric bone mineral density

Table 2. *Ex Vivo* Densitometry at the Proximal and Mid-Diaphysis Femur

	G/6	G/6+RUN	G/6+CLB
Femur Proximal Metaphysis			
Total BMC (mg)	1.44 ± 0.07	1.64 ± 0.02 #	1.60 ± 0.03 #
Total vBMD (mg/cm^3)	570.9 ± 23.5	631.9 ± 11.6 #	637.2 ± 12.6 #
Total Area (mm^2)	2.53 ± 0.11	2.62 ± 0.06	2.53 ± 0.07
Marrow Area (mm^2)	1.44 ± 0.09	1.41 ± 0.06	1.33 ± 0.06
Femur Mid-Diaphysis			
Cort BMC (mg)	1.33 ± 0.06	1.31 ± 0.02	1.35 ± 0.02
Cort vBMD (mg/cm^3)	1312.9 ± 11.2	1324.2 ± 4.1	1326.8 ± 3.7
Cort Area (mm^2)	1.00 ± 0.04	0.99 ± 0.01	1.01 ± 0.01
CSMI (mm^4)	0.19 ± 0.01	0.18 ± 0.00	0.19 ± 0.00

Values are post (Day 21) presented as mean ± SE. # indicates significantly different than G/6 (p<0.05). BMC, bone mineral content; vBMD, volumetric bone mineral density; CSMI= cross-sectional moment of inertia

Table 3. Mid-Diaphysis Femur Mechanical Properties

	G/6	G/6+RUN	G/6+CLB
Femur Mid-Diaphysis			
Ultimate Load (N)	12.18 ± 0.70	12.56 ± 1.15	12.74 ± 0.24
Stiffness (N/mm)	54.61 ± 2.27	53.53 ± 2.27	55.77 ± 2.46
Energy Absorbed (N·mm)	3.63 ± 0.62	3.43 ± 0.48	3.37 ± 0.34
Elastic Modulus (GPa)	6.14 ± 0.38	6.05 ± 0.25	6.16 ± 0.34

Values are post (Day 21) presented as mean ± SE. No significant differences were found.

Figure Legends

Figure 1. Daily body weight of mice throughout 21-day period of partial weight bearing. Data points presented as mean values; standard error bars are not included for clarity of viewing. No significant differences were found over time within groups.

Figure 2. Effect of exercise during partial weight bearing on proximal tibia metaphysis vBMD. Both resistance (G/6+CLB) and aerobic (G/6+RUN) exercise during reduced gravity loading mitigated total vBMD losses compared to G/6. Values presented as mean percent change ((pre-post)/pre·100%) ± SE. # indicates significantly different than G/6.

Figure 3. Effect of exercise during partial weight bearing on tibia mid-diaphysis cortical vBMD. Even in the presence of a reduced gravity environment, exercise (G/6+CLB and G/6+RUN) produced an anabolic response. Values presented as mean percent change ((pre-post)/pre·100%) ± SE. # indicates significantly different than G/6.

Figure 4: Effect of exercise during partial weight bearing on mineralizing surface (%MS/BS) of the tibia mid-diaphysis. A. Endocortical and B. Periosteal %MS/BS is increased with resistance exercise (G/6+CLB). Values presented as mean ± SE. # indicates significantly different than G/6.

Figure 1.

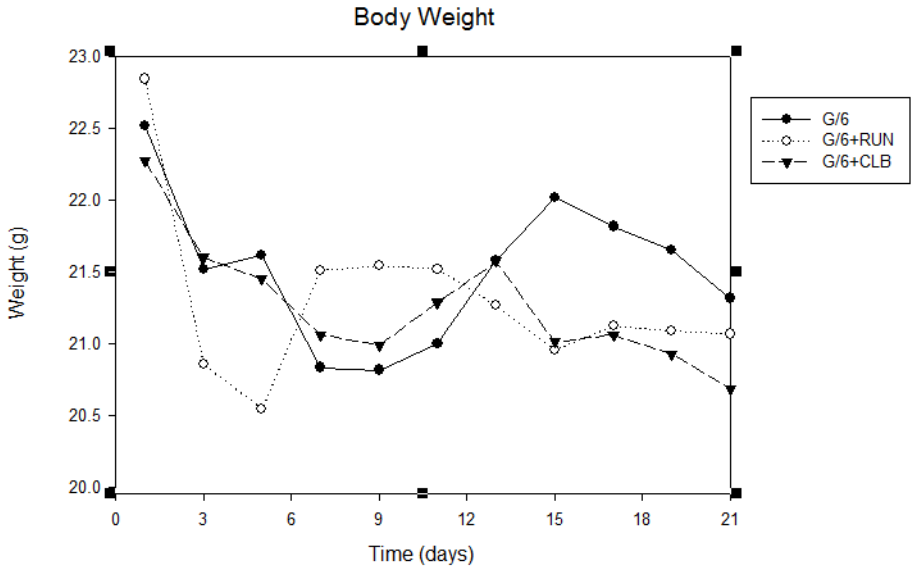
Body Weight
Weight (g)
23.0
22.5
22.0
21.5
21.0
20.5
20.0
0
3
6
9
12
15
18
21
Time (days)
G/6
G/6+RUN
G/6+CLB

Figure 2.

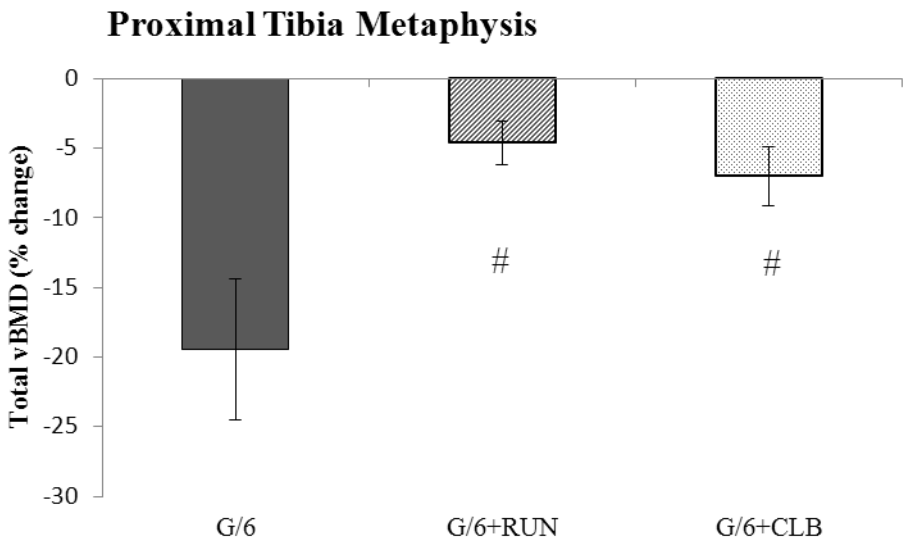
Proximal Tibia Metaphysis
Total vBMD (% change)
0
-5
-10
-15
-20
-25
-30
#
#
G/6
G/6+RUN
G/6+CLB

Figure 3.

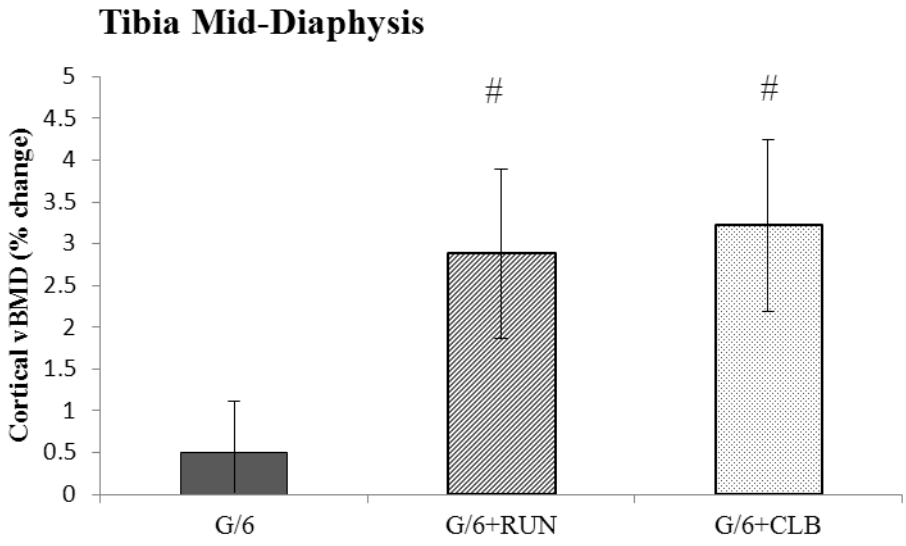
Tibia Mid-Diaphysis
Cortical vBMD (% change)
5
4.5
4
3.5
3
2.5
2
1.5
1
0.5
0
#
#
G/6
G/6+RUN
G/6+CLB

Figure 4.

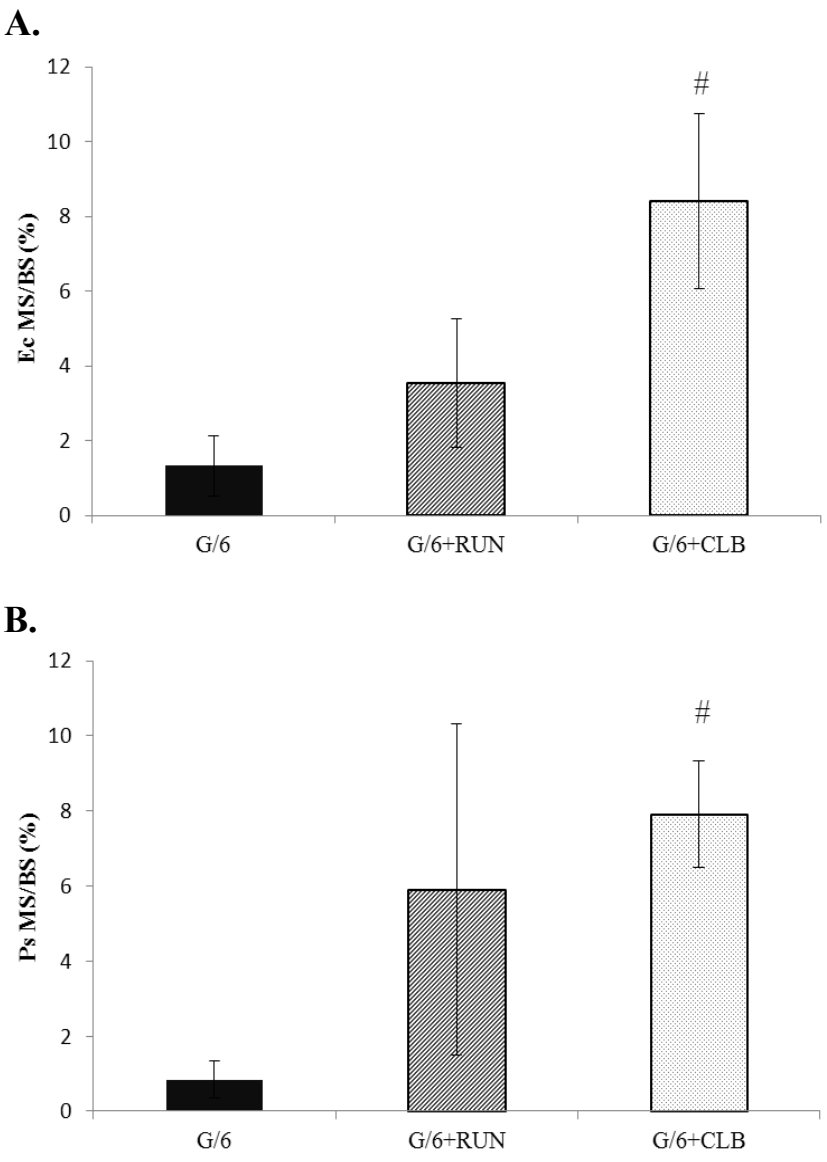
A.
12
10
8
6
4
2
0
Ec MS/BS (%)
#
G/6
G/6+RUN
G/6+CLB
B.
12
10
8
6
4
2
0
Ps MS/BS (%)
#
G/6
G/6+RUN
G/6+CLB